Pathogenesis of Myocarditis and Inflammatory Dilated Cardiomyopathy: the Sign of Four

By Lei Wu

A dissertation submitted to Johns Hopkins University in conformity with the requirements for the degree of Doctor of Philosophy

Baltimore, Maryland
April 2014

© 2014 Lei Wu
All Rights Reserved

Abstract

Myocarditis and inflammatory dilated cardiomyopathy (DCMi) are major causes of heart failure in individuals below the age of 40. In the work presented in this dissertation, using a model of mouse experimental autoimmune myocarditis (EAM) and DCMi, the roles of four pathogenic factors: CD4+ T lymphocytes, interleukin 23 (IL-23), interleukin 17A (IL-17A), and granulocyte macrophage colony-stimulating factor (GM-CSF), are investigated. With transgenic *IL-23a*$^{-/-}$ and *IL-17ra*$^{-/-}$ mice, we demonstrate that IL-23 drives the pathogenicity of CD4+ T cells and maintains their IL-17A production. IL-17A induces chemokine production by cardiac fibroblasts, resulting in an infiltrate rich in neutrophils and Ly6C^{hi} MO/MΦs in the heart, which aggravate disease and lead to worse prognosis. Furthermore, IL-17A directs monocytic infiltrates into an even more inflammatory phenotype by inducing GM-CSF production from cardiac fibroblasts. Taken together, this IL-23 – CD4+ T lymphocytes – IL-17A – GM-CSF axis provides a novel target for the treatment of DCMi and related inflammatory cardiac diseases.

Adviser: Noel R. Rose, M.D., Ph. D.

Readers: Daniela Čiháková, M.D., Ph.D., Fengyi Wan, Ph.D., Alan Scott, Ph.D., Patrizio Caturegli, M.D., Pierre A. Couloumbe, Ph.D., Jay H. Bream, Ph.D.

Preface

As a fan of detective fiction, I have always been fascinated by the similarities between biomedical research and the fictional world of detective mystery. In the world of fictional detectives, the likes of Sherlock Holmes encounter criminal cases, develop theories, interview witnesses, and collect evidence to uncover the truths behind crimes. In biomedical research, investigators design and conduct experiments, collect and analyze data to back up hypotheses, and discover the underlying mechanism of disease pathogenesis. Sherlock Holmes, the most famous fictional detective of all, is notorious for rarely showing empathy for the well being of victims of crime. Biomedical research, however, is fundamentally motivated by the welfare of the patients. Therefore, not only does biomedical research require exceptional reasoning skills, but it also bears a noble cause. The original Sherlock Holmes story of *the Sign of the Four* by Arthur Conan Doyle centered on a conspiracy involving a British soldier stationed in India and three local Sikhs. In this dissertation, the interactions between CD4+ T lymphocyte and three cytokines, interleukin 23, interleukin 17A and granulocyte macrophage colony-stimulating factors (GM-CSF), are investigated to reveal the pathogenesis of myocarditis and inflammatory dilated cardiomyopathy (DCMi).

This work would not be possible without the extraordinary guidance and professional support I received over my years at the Johns Hopkins University.

First and foremost, I would like to express my sincere gratitude to my mentors Drs. Noel R. Rose and Daniela Čiháková. They gave me the chance to explore the fascinating world of immunology. Over the years, they constantly supported my urge to learn and try new things, while teaching me the fundamental principles in biomedical research. Their work ethic exemplified the passion and persistence required to excel in science.

I would also like to thank Drs. Jobert Barin and Christian Baldeviano for their teaching. Their knowledge and advice helped me convert from a student into an investigator capable of independently designing and conducting my own research.

I am also immensely indebted to my dear colleagues: SuFey Ong, from whom I constantly asking for “small favors” to help with my experiments; Monica Talor, whose excellence keeps the lab running and keeps the lab from running into trouble; and Jillian Legault, Nicola Diny, Dr. Quan Nhu, Natalie Stickel, Ashley Cardamone, Elizabeth Gebremariam, Drs. Ping Chen, and Davinna Ligons, without whom it would be impossible to finish my projects.

My work was also made possible by professional help from collaborators and core facilities. I would like to acknowledge Drs. David Kass, Norimichi Koitabashi, and Djahida Bedja for their assistance in the isolation of cardiac cells and mouse echocardiography; Dr. Hao Zhang, Xiaoling Zhang, Tricia Nilles, and Lee Blosser for their support in flow cytometry; Drs. Jay Kolls, Yoichiro Iwakura, Amgen Inc., and Pfizer Inc. for providing transgenic mice. I would also like to acknowledge my neighbors in the Ross Research Building, Drs. Shey-Cherng Tzou, Alessandra De Remigis, AeRyon Kim, Samarjit Das, Peter Rainer, and Nianbin Song, for their help with reagents and instruments.

I would extend my gratitude to the professors who gave me valuable advice in the direction of my study: Dr. Alan Scott for his consultation with macrophages; Dr. Fengyi Wan for his assistance in cell signaling; Dr. Patrizio Caturegli for providing a clinical perspective; Dr. Jay Bream for his instructions in quantitative PCR; Dr. Jelena Levitskaya for her guidance in flow cytometry; Drs. Fidel Zavala, Dolores Njoku, Pien-Chien Huang, and Pierre Coulombe for serving in my exam committees. My work was partially supported financially by the O'Leary – Wilson Fellowship in Autoimmune Disease Research, the Katharine E. Welsh Fellowship in Immunology & Infectious Disease, and the Carlton and Estelle Herman Award, and I would express my appreciation to the kind donors to these awards.

Research being only part of my journey over the past five years, I would like to take this opportunity to express my ever-lasting appreciation for my classmates and friends, SuFey Ong, Jillian Legault, Stefanie Trop, Andrea Hodgson, Kyle Metz, Patricia Ferrer, Peter Dumoulin, Benjamin Blumberg, Kely Sheldon, Dr. Zhen Anjie, Liang Ou, Yang Xuan, Dr. Zhang Lili, Han Teng, Dr. Huang Yong, Feng Jianqiao, Ye Chuyang, Si Fangwei, Shou Haochang, Yu Tsung, Zhou Xianchong, Ma Qing, Li Yijie, Zhang Tianxiao, He Huan, Xiao Xiao, and Kinbo Lee, for helping me settling in a completely different world and sailing through challenges in my new life. I would also like to thank my old friends currently living in all corners of the world: Jia Xiaolei, Dr. Liu Xinran, Fei Xudong, Qian Yinuo, Dr. Liu Mengxi, Zhang Cheng, Sun Zhuo, Wang Jing, Zhang Hao, Gao Xiaojing, Dai Yun, Wang Nan for spending their precious time visiting me in Baltimore, or hosting me, the usually unusually annoying guest.

Finally, me being in a graduate school finishing my doctoral dissertation in scientific research, I fully attribute it to the teachings in life from my family, my parents and my late grandmother. It is their love and support, their belief in my potential, their nurturing of my curiosity, my confidence, and my independence from a very young age, which ultimately made me who I am.

Table of Contents

List of Tables

List of Figures

Chapter I Introduction

Myocarditis: Etiology

Myocarditis is the inflammation of myocardium, the cardiac muscle (Cooper, Leslie T., 2009). A broad range of immunopathologic processes may contribute to the development of disease; thus myocarditis is usually classified by cause and types of cardiac infiltrate determined by histology (Table I) (Sagar et al., 2011).

Myocarditis is usually induced by infection or cardiotoxic chemicals. Parvovirus B19, Coxsackie B virus, *Borrelia burgdorferi* and *Trypanosoma cruzi* are among the most common pathogens associated with human myocarditis (Kindermann et al., 2012). Viral infection is most frequently implicated in myocarditis cases in the industrialized world. Presently, Parvovirus B19 is among the most prevalent viruses found in the heart tissue of acute myocarditis patients (Breinholt et al., 2010). Myocarditis caused by *Trypanosoma cruzi* infection poses particular health threat in South and Central America (Bocchi et al., 2013). As the distribution of its vector *Reduviidae species* spreads due to a shifting global climate, *Trypanosoma cruzi* may spread to previously unaffected places, such as the southern United States (Nunes et al., 2013). Mouse models have been established to study the pathogenesis of myocarditis caused by Coxsackie B virus and *Trypanosoma cruzi* (RABIN et al., 1964; Cihakova and Rose, 2008; Bonney and Engman, 2008).

Regardless of the etiology, autoimmunity is involved in the pathogenesis of many myocarditis patients (Schultheiss et al., 2011). The involvement of autoimmunity usually leads to prolonged immunopathology and a poor prognosis. Giant cell myocarditis is strongly associated with autoimmunity due to its connection with a variety of autoimmune-related disorders, such as celiac disease and systemic lupus erythematosus (Chung et al., 2005; Frustaci et al., 2002). Patients with giant cell myocarditis bear high likelihood of heart failure (Cihakova and Rose, 2008), and immunosuppression has shown to be of benefit in the treatment of giant cell myocarditis (Kandolin et al., 2013). Anti-heart autoantibodies were found in the serum of many myocarditis patients (Caforio et al., 2008), further suggesting that autoimmunity may be important in human myocarditis. In addition, CD4+ T cells isolated from some myocarditis patients were reported to be activated by heart autoantigens (Kallwellis-Opara et al., 2007).

There are different theories regarding the initiation of autoimmunity in myocarditis patients. The exposure of otherwise secluded autoantigens and the activation of immune system during infection both contribute to the induction of autoimmunity (Kindermann et al., 2012). In addition, some pathogens, such as *Trypanosoma cruzi*, express immunologic epitopes mimicking cardiac autoantigens, thus may also contribute to the induction of autoimmunity (Cunha-Neto et al., 2006). In chapter II of

this dissertation, the detailed mechanism of the induction of autoreactive CD4+ T cells will be examined in an animal model of human myocarditis.

Myocarditis: Diagnosis

Myocarditis can present with a wide range of symptoms from fatigue and mild chest pain to cardiac shock and death (Cooper, Leslie T., 2009). Blood tests for cardiac troponin I and creatine kinase MB, echocardiography, and cardiac MRI are all used in the diagnosis of myocarditis (Kindermann et al., 2012). However, since myocarditis presents no characteristic symptoms, it is usually diagnosed after other causes are excluded (Sagar et al., 2011). The gold standard for diagnosis is endomyocardial biopsy. According to the Dallas Criteria, the diagnosis of myocarditis rest on the presence of mononuclear infiltration and cardiomyocyte necrosis upon histopathological examination (Aretz et al., 1987). However, because of the patchy nature of myocarditis, endomyocardial biopsy alone lacks sensitivity. Recently, cardiac MRI has been used to localize sites for endomyocardial biopsy in order to achieve higher sensitivity. In one study, MRI-guided biopsy was able to identify cardiac inflammation in 19 of 21 previously diagnosed myocarditis patients, while unguided endomyocardial biopsy alone only detected inflammation in less than 20% of the same patients (Abdel-Aty et al., 2005).

Since the prognosis of myocarditis varies drastically from patient to patient, there have been attempts to develop reliable biomarkers to indicate the disease outcome and develop strategies for treatment. For instance, patients with high serum levels of soluble fatty acid synthase (FAS) and interleukin 10 (IL-10) were found to have worse outcomes (Sheppard et al., 2005; Nishii et al., 2004). However, these assays are not readily available clinically. In Chapter III of this dissertation, the prospect of new biomarkers for predicting the disease outcome will also be discussed.

Inflammatory Dilated Cardiomyopathy

The short-term prognosis of myocarditis is usually good. However, myocarditis patients may progress to inflammatory dilated cardiomyopathy (DCMi) (Cooper, Leslie T., 2009). In one long-term follow-up study, 21% of acute myocarditis patients developed DCMi within 3 years (D'Ambrosio et al., 2001). In DCMi patients, the damaged cardiomyocytes are replaced by scar tissue and the myocardium undergoes irreversible fibrosis and remodeling, making DCMi among the most common causes of non-congenital heart failure in individuals under the age of 40 (Dimas et al., 2009). There has been limited success with symptomatic therapy in chronic DCMi patients, such as angiotensin converting enzyme (ACE) inhibitors and ß adrenergic receptor blockers

treatment, leaving cardiac transplantation the only cure for end stage heart failure secondary to DCMi (Pietra et al., 2012). Recently, immunosuppressive drugs azathioprine and prednisone have been tested to treat DCMi without active viral infection. Compared with placebo, immune suppression significantly improved cardiac function in patients (Cooper et al., 2008). This finding support the view that immune responses are vital in the development of DCMi. In Chapter III of this dissertation, a detailed mechanism of how cardiac inflammation leads to DCMi will be proposed, and the prospect of this pathway as a new target for immune modulation will be discussed.

Mouse Model of Experimental Autoimmune Myocarditis

To investigate the immunopathologic mechanism responsible for myocarditis and DCMi in humans, we have adopted a mouse model of experimental autoimmune myocarditis (EAM). In BALB/c mice, EAM is induced by immunization with a peptide derived from the cardiac myosin heavy chain alpha (MyHC$\alpha_{614\text{-}629}$). A/J, A.SW, C3H and FVB/NF are also good responders to EAM. Immunized mice develop myocarditis characterized by inflammatory infiltration. Heart inflammation in this murine model starts about day 10 and peaks about day 21. Immunized mice subsequently progress to DCMi around day 42 to day 63, which is

characterized by cardiac fibrosis and impaired cardiac function (Cihákova et al., 2004) (Figure 1).

EAM is a CD4+ T helper cell-dependent disease (Smith and Allen, 1991, 1993), as depletion of CD4+ T cells protects mice from EAM. CD4+ promotes the infiltration of other effector leukocytes populations, including $CD8^+$ T cells, natural killer (NK) cells, neutrophils, eosinophils, monocytes and macrophages (Barin et al., 2012). Chapter II and III of this dissertation will interrogate the initiation of autoreactive CD4+ T cell response, and describe how CD4+ T cells direct the augmentation of the immune response and determine the prognosis of EAM.

The Polarization of T Helper 17 Cells and Their Involvement in Experimental Autoimmune Myocarditis

CD4+ T cells undergo different differentiation programs upon stimulation from their microenvironment (Figure 2). For instance, interleukin 12 (IL-12) and interleukin 18 (IL-18) promote Th1 differentiation driven by transcription factor T-bet, while interleukin 4 (IL-4) and interleukin 33 (IL-33) promote Th2 differentiation driven by GATA3 (Mukasa et al., 2010). They play critical roles in immune responses against viral infections and during asthma (Maruyama et al., 2010).

The polarization of CD4+ T cells was believed to be stable; however, recent studies underscore the plasticity of their differentiation (McAleer

and Kolls, 2011). Rather than being rigidly committed, under certain stimulations, differentiated CD4+ T cells can convert into new phenotypes by activating other polarization programs. For instance, one fate mapping study showed that in the mouse model, experimental autoimmune encephalomyelitis (EAE), most IFN γ - producing CD4+ T cells in the CNS were originally IL-17A – producing cells (Hirota et al., 2011).

Early studies have shown that neither Th1 nor Th2 program is the driver of EAM disease. Mice with deficiencies in the Th1 program, such as *Ifng*$^{-/-}$ and *Tbx21*$^{-/-}$ mice, develop even severer disease than wild-type (WT) mice (Rangachari et al., 2006; Afanasyeva et al., 2004). In addition, *Il12a*$^{-/-}$ mice develop disease comparable with WT controls (Afanasyeva et al., 2001b). These results demonstrate that Th1 polarization is dispensable in the development of EAM, and may play a protective role in its pathogenesis. Th2 cytokines were found to aggravate EAM in A/J mice in an IL-4-dependent fashion (Afanasyeva et al., 2001a). However, they were protective in BALB/c mice by skewing the phenotype of macrophages (Cihakova et al., 2008). Thus, Th2 cells are not the primary driver of EAM.

In recent years, another CD4+ T helper cell subset, Th17 cells, has been characterized and discovered to be critical in autoimmunity (Korn et al., 2009). Th17 program is initiated by transforming growth factor ß (TGFß) and interleukin 6 (IL-6), and is further promoted by interleukin 1ß (IL-

1ß) and interleukin 23 (IL-23) (Figure 3) (Gaffen, 2011). This combination of stimuli activates the FOXO, NFκB and STAT3 pathways, leading to the expression of master transcription factor retinoic acid receptor-related orphan receptor γt (RORγt) encoded by gene *Rorc* (Yang et al., 2008). RORγt switches on multiple Th17 effector molecules that play critical roles in autoimmunity (Zúñiga et al., 2013). Mice with a deficiency in the *Rorc* gene were resistant to autoimmune diseases (Maddur et al., 2012), demonstrating the pivotal roles Th17 cells play in autoimmunity.

Th17 cells infiltrate the heart during EAM (Baldeviano et al., 2010). Furthermore, patients with DCMi have increased numbers of Th17 cells in their blood and elevated levels of Th17 cytokines in serum, suggesting that Th17 cells are involved in the pathogenesis of DCMi (Yuan et al., 2010; Ding et al., 2010). This dissertation will look into how Th17 program is induced during the induction of EAM, and the detailed downstream effector pathways that dictate disease outcomes.

Interleukin 23 and the Differentiation of Th17 Cells

IL-23 is critical in the maturation of Th17 cells. IL-23 is a heterodimer of subunits p19 and p40, encoded by genes *Il23a* and *Il12b*, respectively. It is recognized by IL-23 receptor (IL-23R) (Abraham and Cho, 2009). p19 subunit is unique to IL-23 and determines the binding of IL-23 to its receptor, while p40 subunit is shared with IL-12. Antigen presenting

cells (APCs) are the main source of IL-23 (Kinnebrew et al., 2012). Upon activation by TGFß and IL-6, usually expressed by injured tissue, CD4+ T cells upregulate IL-23R and react to IL-23 signal from APCs (Kurschus et al., 2010). IL-23 induces the activation of STAT3 pathway, which further stabilizes the Th17 program and enhances the expression of major Th17 effector molecules (El-Behi et al., 2011a). Deficiencies in the IL-23 gene ameliorate experimental autoimmune encephalomyelitis (EAE) in mice (Becher et al., 2003), suggesting IL-23 is critical in the pathogenicity of Th17 cells. In chapter II of this dissertation, *Il23a*$^{-/-}$ mice will be employed to study the role IL-23 plays in the induction of pathogenic CD4 T cells and the initiation of EAM.

Interleukin 17A: Signal Transduction and Roles in EAM

Interleukin 17A (IL-17A), one of the Th17 effector molecules, is the hallmark cytokine produced by Th17 cells. IL-17A functions as a homodimer of two subunits and is recognized by receptor complex consisting of interleukin 17 receptor A (IL-17RA) and receptor C (IL-17RC). IL-17RC dictates the affinity of IL-17RA/RC receptor complex to IL-17A, while IL-17RA is responsible for the signal transduction through its cytoplasmic tail. IL-17RA recruits the scaffold protein ACT1 via its SEFIR domain upon binding with ligands, and activates NFκB, MAPK and C/EBP pathways (Figure 4) (Ho et al., 2010).

IL-17A receptors are widely expressed among different cell types. However, stromal cells are found to be particularly sensitive to IL-17A stimulation (Gaffen, 2009). IL-17A induces the production of defensin ß2 and lipocalin 2, which are critical in innate defense against extracellular fungal and bacterial infections (McAleer and Kolls, 2011). Human and mouse studies show that deficiencies in IL-17A and its receptor impair protection against *Candida albicans* and *Staphylococcus aureus* infections (Cho et al., 2010; Puel et al., 2011). In humans, APECED patients with impaired IL-17A functions are highly susceptible to Candida and Staphylococcus infections (Ng et al., 2010).

Baldeviano et. al. reported that *Il17a*$^{-/-}$ mice were completely protected from the development of DCMi, although they had myocardial inflammation comparable in overall severity to wild-type (WT) controls (Baldeviano et al., 2010). Thus, IL-17A is dispensable for early stage myocarditis, but is required for the progression to DCMi. These results indicate a key role for IL-17A in driving cardiac damage and fibrosis during the development of DCMi. Similar profibrotic functions of IL-17A have been reported in cirrhosis (Lan et al., 2009) and fibrotic lung injury (Wilson et al., 2010) models. In Chapter III of this dissertation, a detailed mechanism by which IL-17A induces DCMi will be investigated.

Monocytes and Macrophages

Monocytes (MOs) and macrophages (MΦs) are key effector cells during inflammatory processes (Gordon and Taylor, 2005) including myocarditis and DCMi.

During embryonic development, cells originating in yolk sac, fetal liver, and bone marrow migrate into non-lymphoid organs and develop into stable populations of tissue resident macrophages (rMΦs) (Figure 5) (Epelman et al., 2014; Ginhoux et al., 2010; Guilliams et al., 2013). Tissue resident macrophages from different organs have unique characteristics and play critical roles in the homeostasis of their resident organs through adult life. Under normal conditions, tissue resident macrophages replenish themselves by local proliferation, with little contribution from the hematopoietic cells in the blood (Guilliams et al., 2013). However, animal studies have shown that cells originating from bone marrow are able to replenish tissue resident macrophages under extraordinary circumstances when the latter are depleted, such as after irradiation (Yona et al., 2013).

Monocytes arise from hematopoietic stem cells (HSCs) in the bone marrow. HSCs undergo several stages of development, through common myeloid progenitors (CMPs) and granulocyte/monocyte progenitors (GMPs), to differentiate into monocytes in the blood and lymphoid organs (Shi and Pamer, 2011). Some of these progenitor cells migrate from bone marrow to spleen and react rapidly to signals of inflammation, such as

myocardial infarction (MI), thereby replenishing the monocyte repository (Figure 5) (Leuschner et al., 2012).

Monocytes form distinct subpopulations in blood (Table II) (Auffray et al., 2009). In mouse, the two monocyte subsets, $CCR2^{hi}CX3CR1^{lo}Ly6C^{hi}$ and $CCR2^{lo}CX3CR1^{hi}Ly6C^{lo}$ monocytes, infiltrate sites of inflammation responding to different chemokine signals. There they differentiate into inflammatory macrophages (iMΦs) guided by local cytokine signals (Shi and Pamer, 2011) (Figure 5). Studies in MI and liver fibrosis models have shown that these two sub-populations have distinct properties and functions that may affect the progression and resolution of inflammation.

In EAM, MO/MΦs comprise about half of all heart-infiltrating inflammatory cells at the peak of inflammation and play important roles in pathogenesis (Barin et al., 2012; Cihakova et al., 2008). The balance between MO/MΦ subsets and their differentiation is critical in determining the pathogenic outcome in EAM. In Chapter III of this dissertation, the connection between Th17 program and the balance of MO/MΦ subsets will be examined.

Figures and Tables

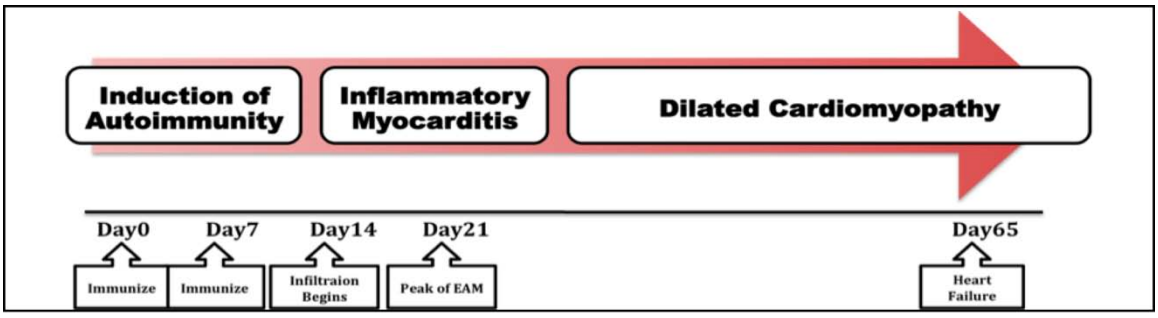

Figure 1 Mouse model of experimental autoimmune myocarditis (EAM) and inflammatory dilated cardiomyopathy

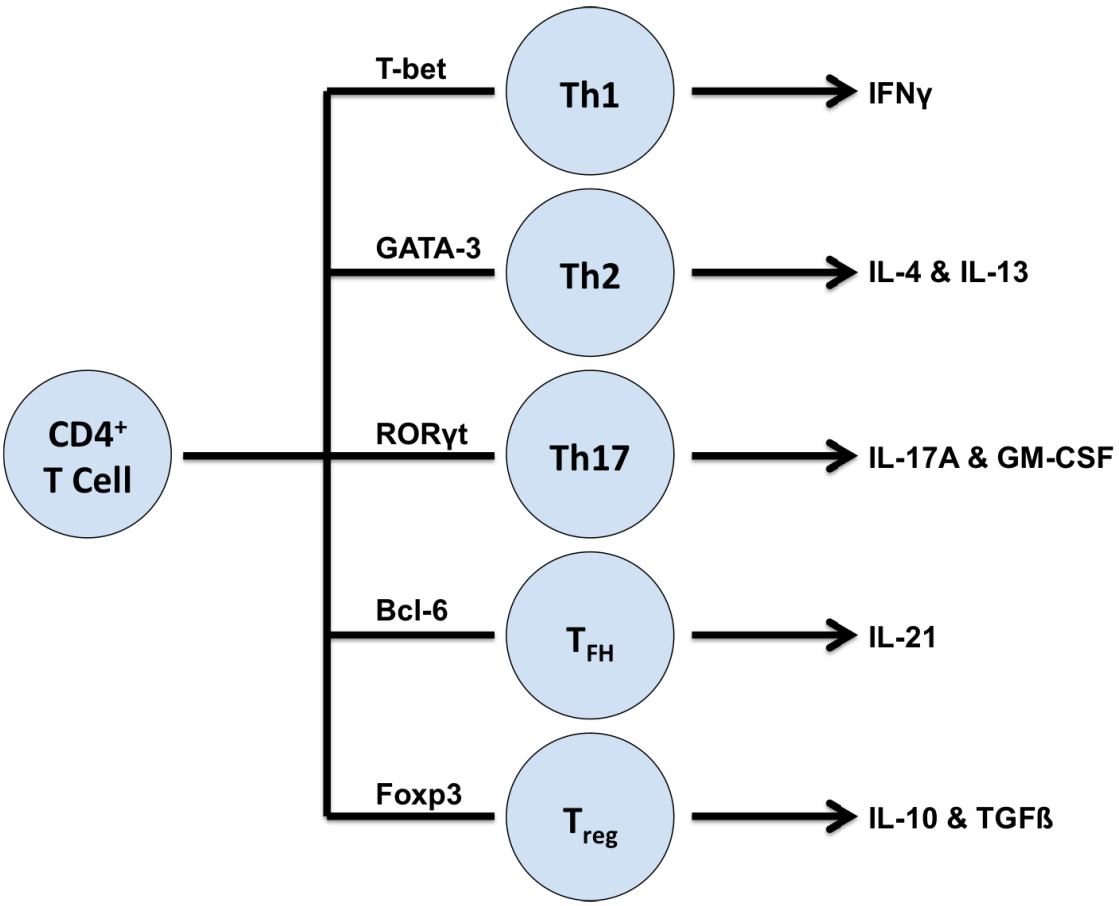

Figure 2 Differentiation of CD4+ T cells

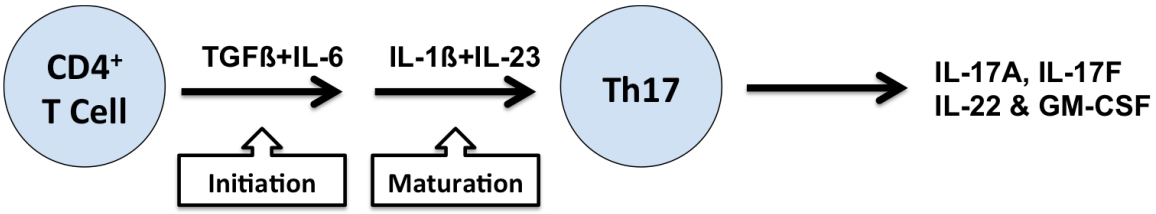

Figure 3 Th17 polarization of CD4+ T cells

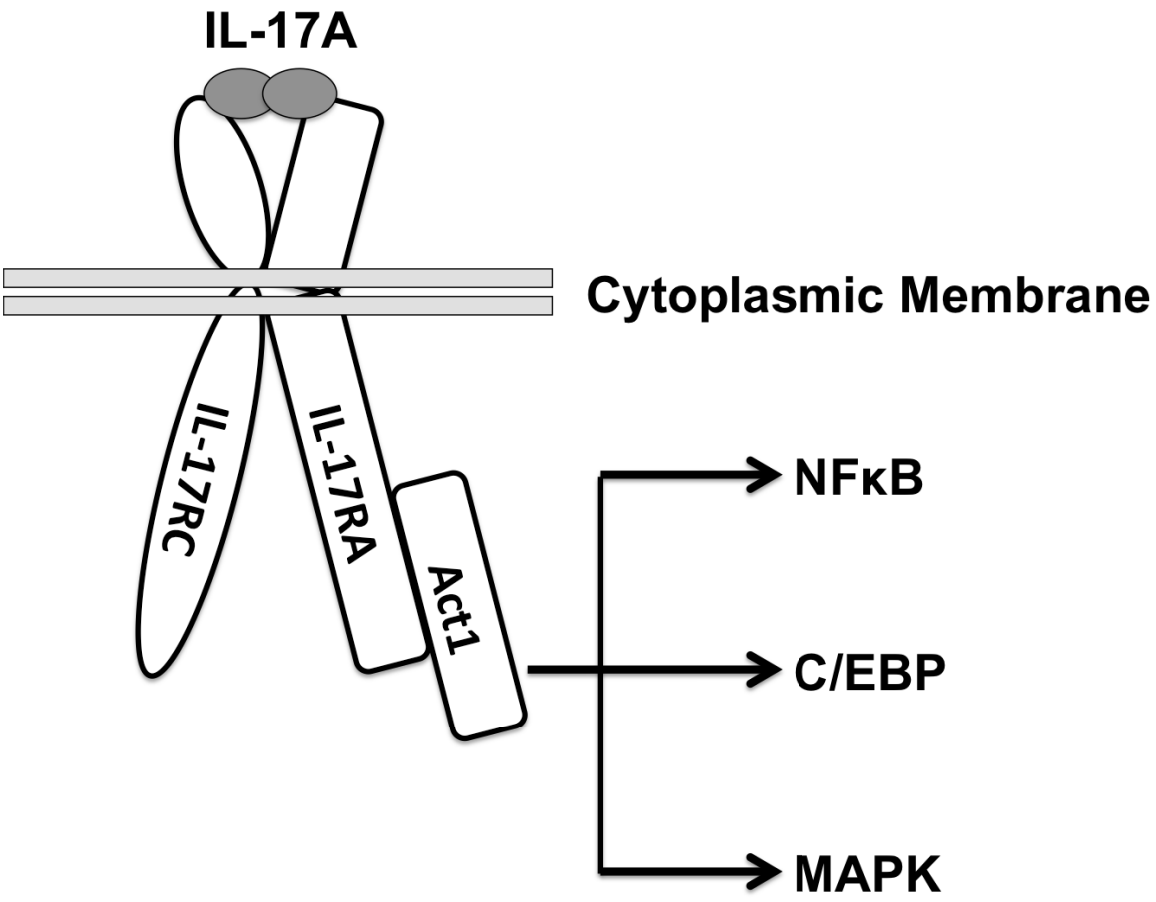

Figure 4 Signal transduction of IL-17A

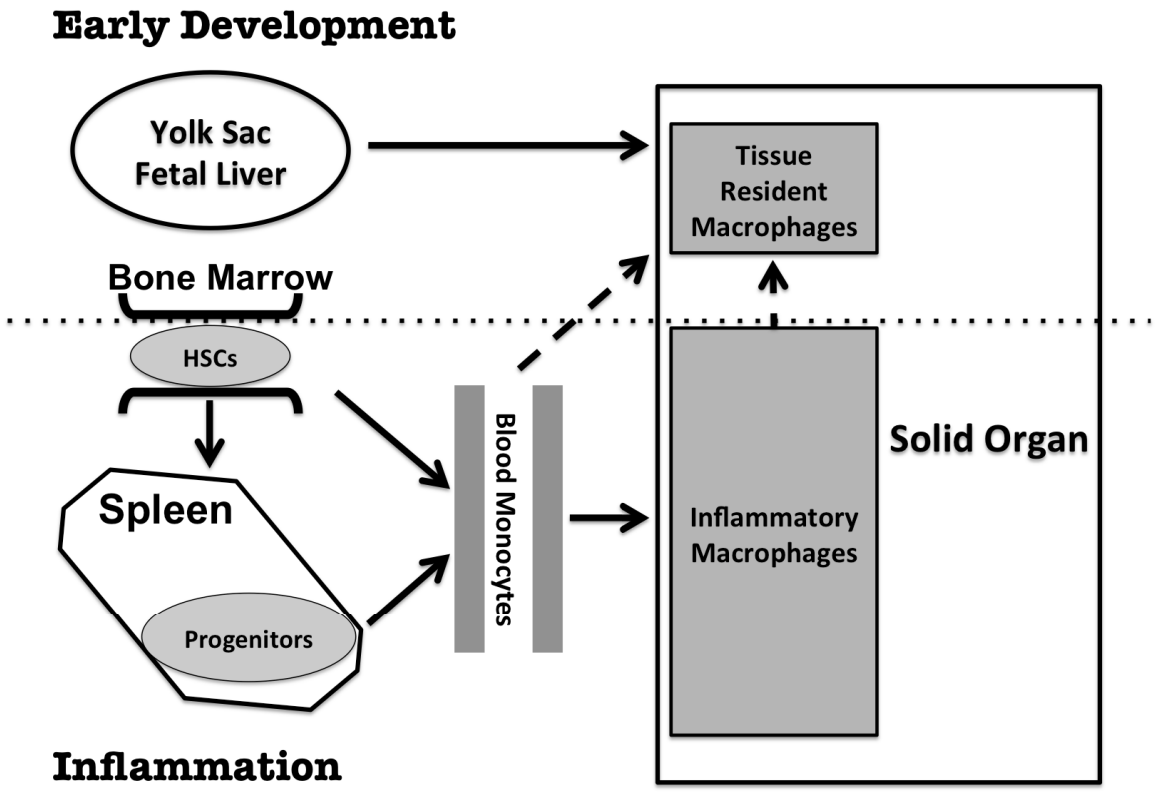

Figure 5 Origin of tissue resident and inflammatory macrophages

Table I Selected Classifications of Myocarditis

By Cause	
Viral	Parvovirus B19, Coxsakie B Virus, HIV, HSV, etc.
Bacterial	*Borrelia burgdorferi, Staphylococcus aureus, etc.*
Protozoal	*Trypanosoma cruzi, Toxoplasma gondii, Babesia, etc.*
Toxic	Alcohol, arsenic, antibiotics and doxorubicin, etc
By Types of Cardiac Infiltrate	
Lymphocytic	
Granulomatous	
Giant Cell	
Eosinophilic	

Modified from Sagar et. al. 2011

Table II Monocyte Heterogeneity

In Human	
$CD14^{hi}$ $CD16^{-}$	Pro-inflammatory “classical” monocytes Antimicrobial functions
$CD14^{lo}$ $CD16^{hi}$	“Non-classical” patrolling monocytes Homeostasis of blood vessel
$CD14^{hi}$ $CD16^{lo}$	Intermediate monocytes
In Mouse	
$Ly6C^{hi}$ $CCR2^{hi}$ $CX3CR1^{lo}$	Resemble human $CD14^{hi}$ $CD16^{-}$ monocytes Pro-inflammatory
$Ly6C^{lo}$ $CCR2^{lo}$ $CX3CR1^{hi}$	Resemble human $CD14^{lo}$ $CD16^{hi}$ monocytes Homeostatic

Modified from Gordon et. al. 2005

Chapter II Interleukin 23 Is Required in the Induction of Experimental Autoimmune Myocarditis

2.1 Results

Il23a$^{-/-}$ Mice Are Protected from EAM

IL-23 is a heterodimer of subunits p19 and p40, encoded by genes *Il23a* and *Il12b* respectively, and is recognized by the IL-23 receptor (IL-23R). p19 subunit is unique to IL-23 and determines the binding of IL-23 to its receptor, while p40 subunit is shared with IL-12. In order to study the roles IL-23 plays in the pathogenesis of EAM, we employed *Il23a*$^{-/-}$ mice.

Il23a$^{-/-}$, *Il23a*$^{+/-}$ and wild-type (WT) BALB/c mice were immunized with the MyHC$\alpha_{614\text{-}629}$ peptide and sacrificed 21days post immunization. Histopathology of mouse hearts showed that *Il23a*$^{-/-}$ mice were fully protected from heart inflammation, whereas WT and *Il23a*$^{+/-}$ controls developed EAM (Figure 6A). Flow cytometric analysis revealed extensive infiltration of CD45^{+} leukocytes in the hearts of WT and *Il23a*$^{+/-}$ but not *Il23a*$^{-/-}$ mice (Figure 6B). In addition, cardiac inflammation in WT and *Il23a*$^{+/-}$ mice was accompanied by substantial expansion of myeloid effector cells, including Ly6G^{hi} neutrophils and Ly6G^{-}CD11b^{+} monocytes in spleen and peripheral blood, while *Il23a*$^{-/-}$ mice were protected (Figure 7).

Interestingly, the ability of *IL23a*$^{-/-}$ mice to generate antibodies against MyHC$\alpha_{614\text{-}629}$ peptide used in immunization was not hampered by p19

deficiency, as their serum anti-MyHC$\alpha_{614\text{-}629}$ IgG titers were comparable with WT and *IL23a*$^{+/-}$ controls (Figure 8).

In summary, *Il23a*$^{-/-}$ mice were protected from cardiac inflammation, which demonstrated that IL-23 is indispensable in the induction of EAM.

IL-23 Deficiency Impairs Th17 Polarization during the Induction of EAM

Since IL-23 has been shown to be critical in Th17 differentiation, we interrogated if IL-23 deficiency had any effect in CD4+ T cell polarization in the induction phase of EAM.

Il23a$^{-/-}$ and *Il23a*$^{+/-}$ BALB/c mice were immunized in the hind limb and sacrificed 14 days post immunization. Flow cytometric analysis showed that *Il23a*$^{-/-}$ mice had significantly lower levels of IL-17A-producing CD4+ T cells in the draining lymph nodes of the sites of immunization (Figure 9A). In contrast, the levels of IFN γ and IL-13 producing CD4+ T cells are comparable in *Il23a*$^{-/-}$ and *Il23a*$^{+/-}$ mice (Figure 9B and 9C). Interestingly, the levels of IL-17A / GM-CSF double producer CD4+ T cells showed a greater difference between the two groups (Figure 9D). A similar pattern was observed in the spleens of *Il23a*$^{-/-}$ and *Il23a*$^{+/-}$ mice (Figure 10). In addition, *Il23a*$^{-/-}$ mice had significantly lower levels of IL-17A in the serum (Figure 11A), while the levels of IL-13 were comparable with

Il23a$^{+/-}$ mice (Figure 11C). *Il23a*$^{-/-}$ mice also had a trend of lower levels of IFN γ in the serum, albeit not statistically significant (Figure 11B), indicating that IFN γ production during EAM may reflect heart inflammation.

In summary, IL-23 deficiency impaired Th17 polarization program in the induction phase of EAM. These results indicate that Th17 polarization of CD4+ T cells is required for the induction of EAM.

IL-23 is Not Required in EAM after Autoreactive CD4+ T Cell Population Is Established

Previous results indicated that IL-23-dependent Th17 polarization was indispensable for the development of pathogenic autoreactive CD4+ T cells. In order to determine if IL-23 is still required to maintain the autoimmune response after pathogenic CD4+ T cells are generated, we used a CD4+ T cell transfer model of EAM disease. In this model, splenocytes were collected from immunized Thy1.1 donor mice 14 days post immunization, after the onset of cardiac inflammation. After culturing in a Th17 polarizing environment *ex vivo* for 4 days, CD4+ T cells were isolated and transferred intravenously into sublethally irradiated Thy1.2 recipients. Heart inflammation was examined 2 weeks after the transfer (Figure 12).

Histopathology showed that even without any IL-23 signal in the recipients, established autoreactive CD4+ T cells were able to induce heart inflammation in *Il23a*$^{-/-}$ mice comparable to WT recipients (Figure 13A). Flow cytometric analysis showed that *Il23a*$^{-/-}$ recipients had levels of CD45^{+} cell infiltration comparable to WT controls (Figure 13B), and the compositions of infiltration cells were similar between two groups (Figure 14).

We next investigated the polarization of CD4+ T cells in different recipients. The vast majority of the heart-infiltrating CD4+ T cells were transferred Thy1.1^{+} donor cells (Figure 15A). Moreover, cytokine producing CD4+ T cells were almost exclusively of donor origin (Figure 15B, 15C and 15D). These suggested that autoreactive CD4+ T cells used in transfer were highly pathogenic. Although transferred autoreactive CD4+ T cells were able to initiate cardiac inflammation in both WT and *Il23a*$^{-/-}$ mice, the cytokine production profiles were different between two groups. CD4+ T cells in *Il23a*$^{-/-}$ recipients produced significantly lower levels of IL-17A (Figure 16A) but higher levels of IFNγ (Figure 16B). These results suggested that although IL-23 was not required for the development of cardiac inflammation once autoreactive CD4+ T cell population was established, it was crucial in maintaining IL-17A production in pathogenic CD4+ T cells. Pathogenic CD4+ T cells would otherwise convert from IL-17A producers to IFNγ producers. However, these results also indicated that IL-17A and IFNγ production did not

affect EAM development once pathogenicity was already established, thus IL-17A and IFNγ may not be the "pathogenic" factor that donor CD4+ T cells produced during EAM.

Although CD4+ T cells in the hearts of WT and *Il23a*$^{-/-}$ recipients differed in IL-17A and IFNγ production, the levels of GM-CSF producers were comparable in the two groups (Figure 16C), indicating that GM-CSF may play an important role in the development of cardiac inflammation during EAM.

IL-23 from Various Sources Induces Pathogenicity in CD4+ T Cells

We next used a dendritic cell (DC) transfer model to study the roles IL-23 plays in the induction of pathogenic autoreactive CD4+ T cells. Bone marrow derived DCs (BMDCs) from WT or *Il23a*$^{-/-}$ donors were matured with LPS and loaded with MyHC$\alpha_{614\text{-}629}$ peptide. Loaded BMDCs, $0.1\text{x}10^6$, were then subcutaneously injected in the hind limb of *Il23a*$^{-/-}$ or WT recipients. Heart inflammation was examined 2 weeks after transfer (Figure 17).

Histopathology showed that WT BMDCs induced EAM in *Il23a*$^{-/-}$ recipients as well as *Il23a*$^{-/-}$ BMDCs in WT recipients (Figure 18). However, compared with *Il23a*$^{-/-}$ BMDCs in WT recipients, WT BMDCs were able to inducing higher levels of IL-17A-producing and IFNγ-producing CD4+ T cells in the draining lymph nodes of the site of

injection (Figure 19). The difference in IL-17A and IFNγ production was not detected in the spleen (Figure 15).

We conclude that these results indicate that transient IL-23 stimulation during the antigen presentation process is sufficient to induce autoreactive CD4+ T cells, as a small number of WT BMDCs were able to reinstate pathogenicity in *Il23a*$^{-/-}$ recipients. Second, IL-23 stimulation and antigen presentation could be separated in the induction of pathogenicity in CD4+ T cells, as *Il23a*$^{-/-}$ BMDCs were able to induce disease in WT recipients, and the difference in IL-17A production in draining lymph nodes disappeared once CD4+ T cells reached the spleen.

2.2 Discussion

In this series of experiments we employed *Il23a*$^{-/-}$ BALB/c mice and demonstrated the requirement of IL-23 in the induction of cardiac inflammation in EAM. Deficiency of IL-23 impaired Th17 polarization, which was associated with resistance to EAM in *Il23a*$^{-/-}$ mice. The BMDC transfer model showed that transient IL-23 stimulation from a small number of antigen presenting cells was sufficient to generate pathogenic CD4+ T cells. However, IL-23 from other sources compensated for the lack of IL-23 during antigen presentation. Furthermore, IL-23 was dispensable in EAM once a pathogenic autoreactive CD4+ T cell population was established, whereas the ability of CD4+ T cells to continue producing IL-17A relied upon IL-23.

These results confirmed previous findings that *Il12b*$^{-/-}$ but not *Il12a*$^{-/-}$ mice were protected from EAM (Afanasyeva et al., 2001b, Baldeviano, 2010). Since p19 subunit is unique to IL-23, these results provided direct evidence that IL-23 is required in the induction of cardiac autoimmunity in EAM, adding to the increasing list of IL-23-dependent autoimmune disease models (Izcue et al., 2008; El-Behi et al., 2011b; Poppensieker et al., 2012). Since IL-23 deficiency directly impaired Th17 polarization program in CD4+ T cells, these results also strongly indicated that Th17 cells drive the pathogenesis of EAM.

However, it is still unclear what factor produced by Th17 cells is responsible for the pathogenesis of EAM. The CD4+ T cell transfer experiments illustrated that although IL-23 was required in maintaining IL-17A production in autoreactive CD4+ T cells, the lack of it had no significant effect on pathogenicity, as *Il23a*$^{-/-}$ recipients developed disease comparable with WT controls. As will be demonstrated in Chapter III of this dissertation, IL-17A is dispensable in the development of EAM as well, further indicating that the pathogenicity of EAM does not rely on IL-17A production.

Resent studies in mouse EAE model have implicated that GM-CSF production by Th17 polarized CD4+ T cells is crucial in their pathogenicity (El-Behi et al., 2011a). The results above further indicated that GM-CSF production determines the pathogenicity of CD4+ T cells in EAM model as well. First, in the active immunization model of EAM, IL-23 deficiency significantly impaired GM-CSF production in CD4+ T cells, concurrent with decreased heart pathology. Second, in the CD4+ T cell transfer model of EAM, although lack of IL-23 in recipients lowered IL-17A production in CD4+ T cells, GM-CSF production remained the same, consistent with the unaffected disease outcome.

Although IL-23 is not required once pathogenicity of autoreactive CD4+ T cells is established, IL-23 is indispensable in establishing pathogenicity. Therefore, it is possible that in order for CD4+ T cells to become a GM-CSF producer and gain pathogenicity, they first have to undergo IL-23-

dependent Th17 polarization program. Once GM-CSF production is established, IL-23 signaling is no longer required for pathogenicity.

As suggested in CD4+ T cell transfer model of disease, Th17 polarized cells may convert from a IL-17A-producing phenotype towards a IFNγ-producing phenotype. However, their pathogenicity was not significantly affected. Recent studies in the mouse EAE model discovered similar pattern (Annunziato and Romagnani, 2010). With the help of YFP reporter mice, it was reported that the majority of IFNγ-producing CD4+ T cells are converted from IL-17A producers (Hirota et al., 2011). All of these findings support the promise that the Th17 program plays a critical role in the initiation of pathogenic autoimmunity.

2.3 Figures

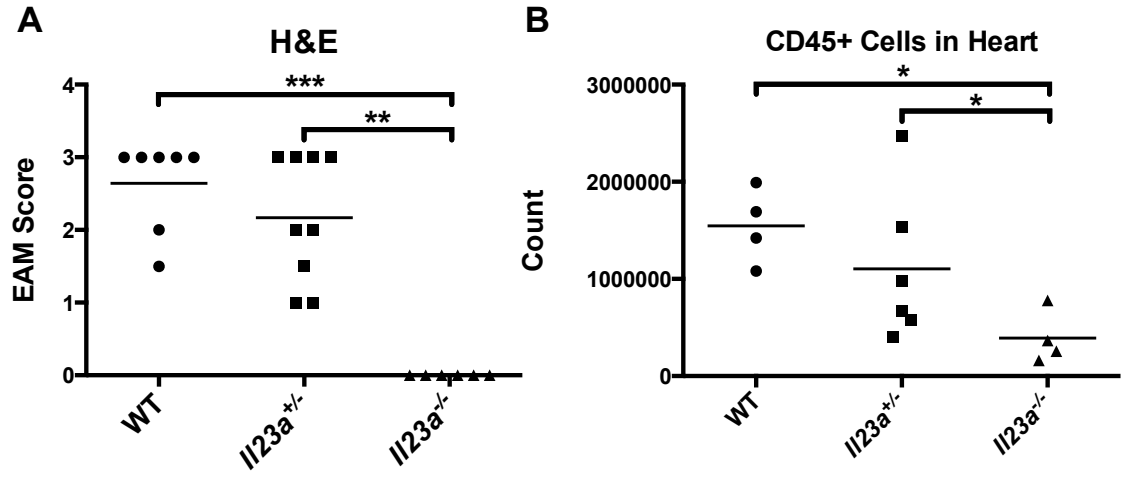

Figure 6. *Il23a*$^{-/-}$ mice were protected from EAM

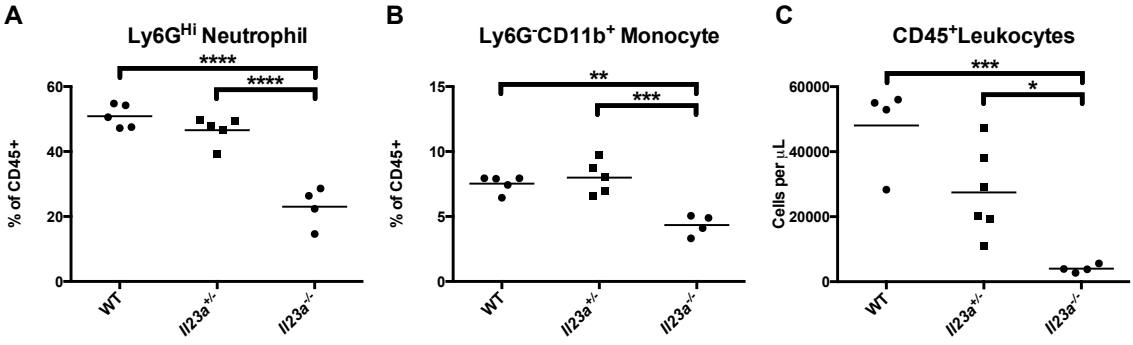

Figure 7. *Il23a*$^{-/-}$ mice were protected from myeloid expansion during EAM

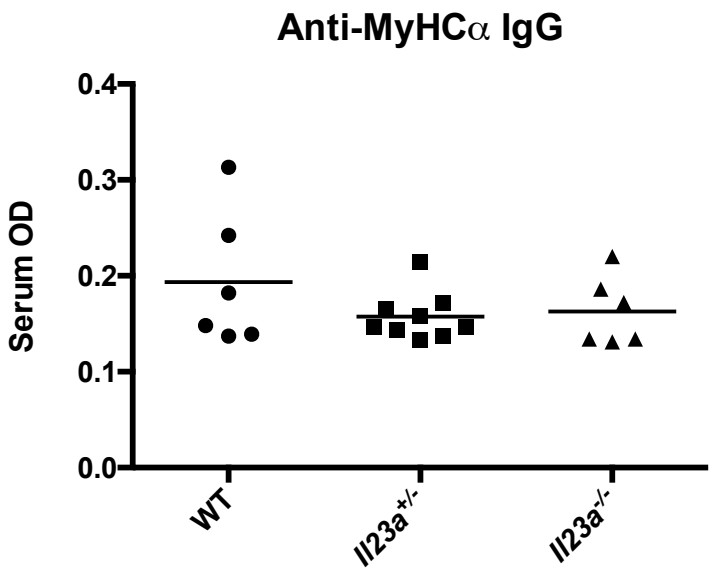

Figure 8. Ability to generate antibodies was not impaired by IL-23 deficiency

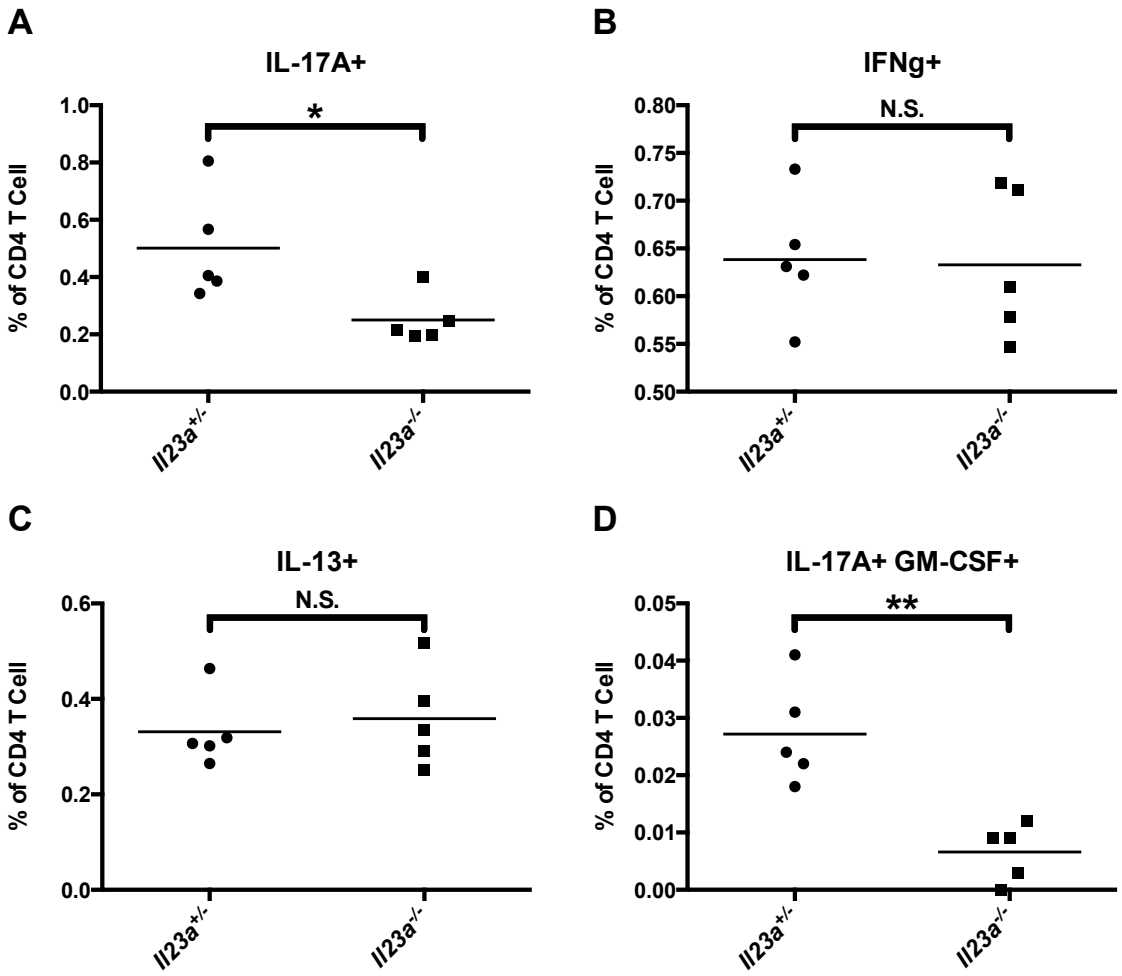

Figure 9. IL-23 deficiency impaired Th17 polarization in draining lymph nodes

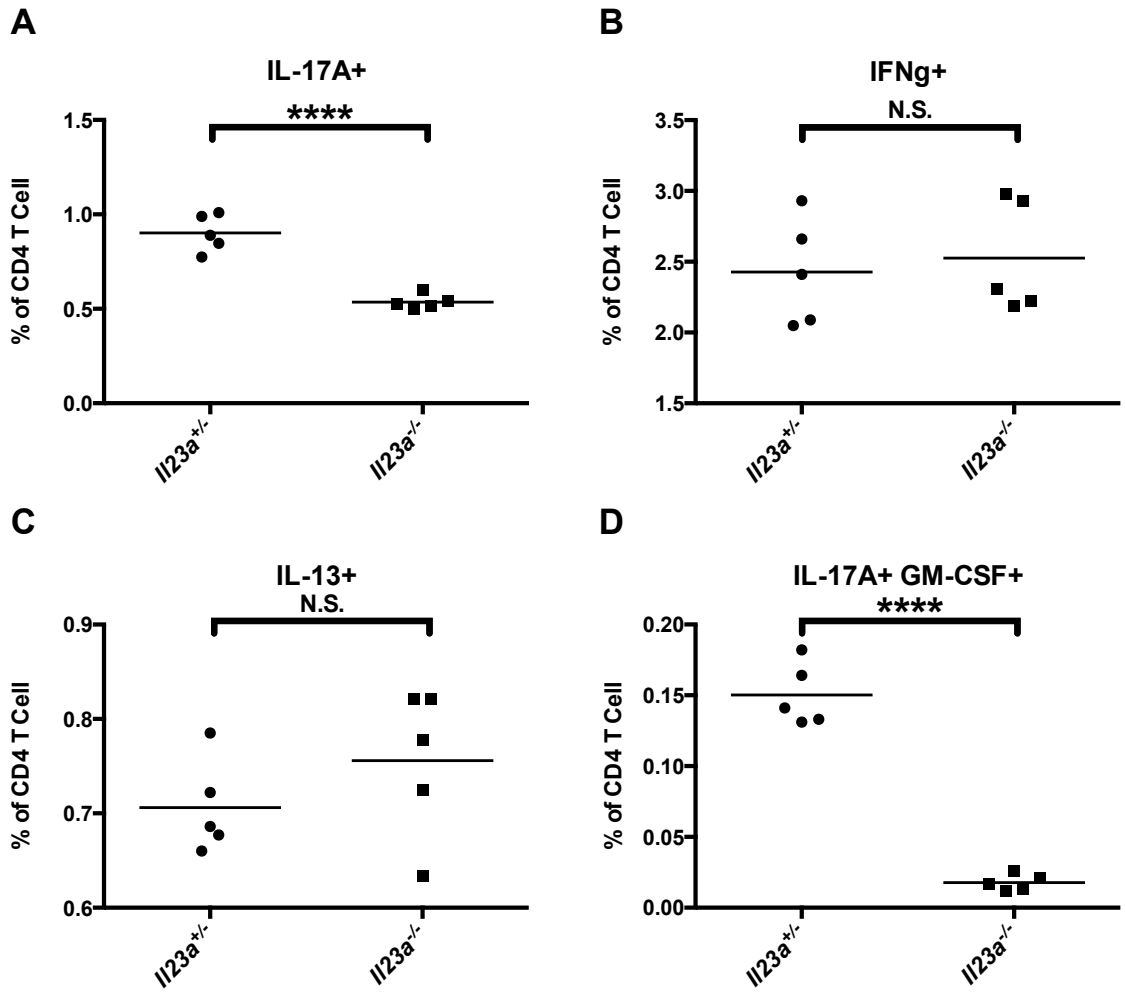

Figure 10. IL-23 deficiency impaired Th17 polarization in spleen

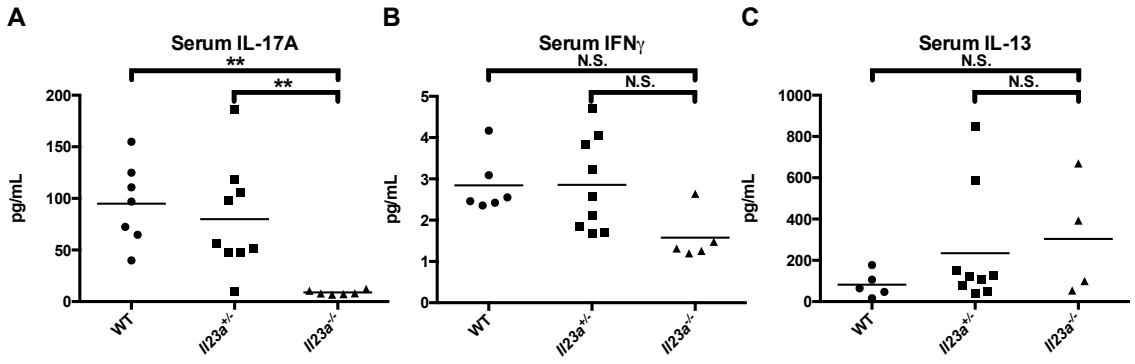

Figure 11. IL-23 deficiency affected cytokine production

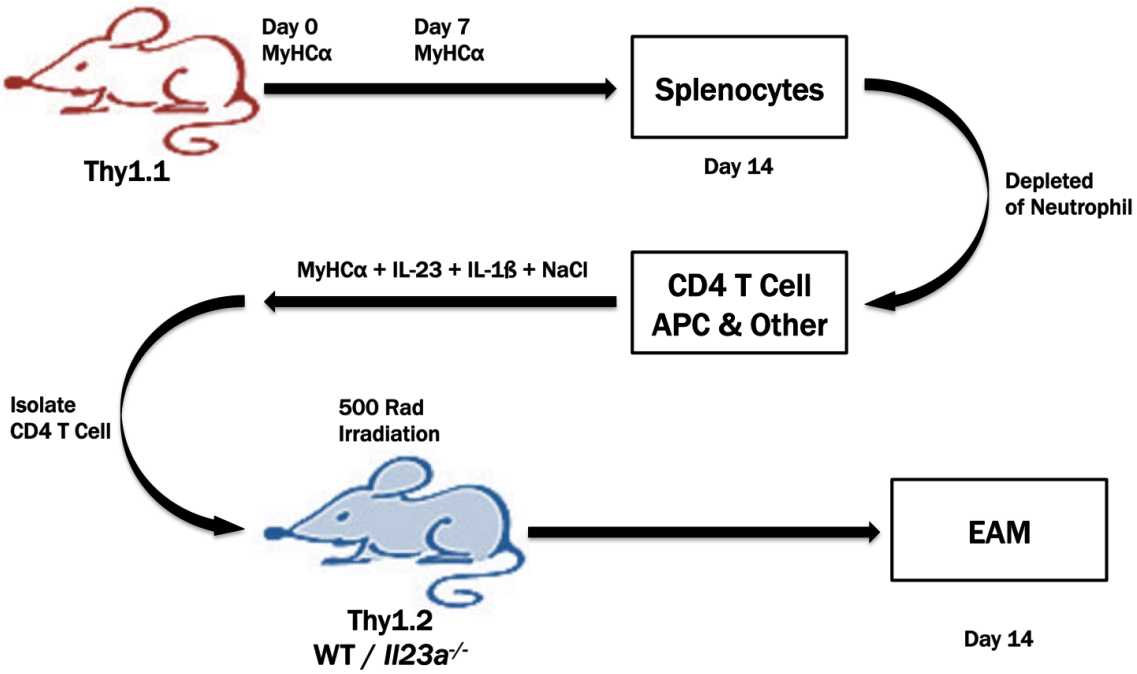

Figure 12. Schematic illustration of CD4+ T cell transfer model of EAM

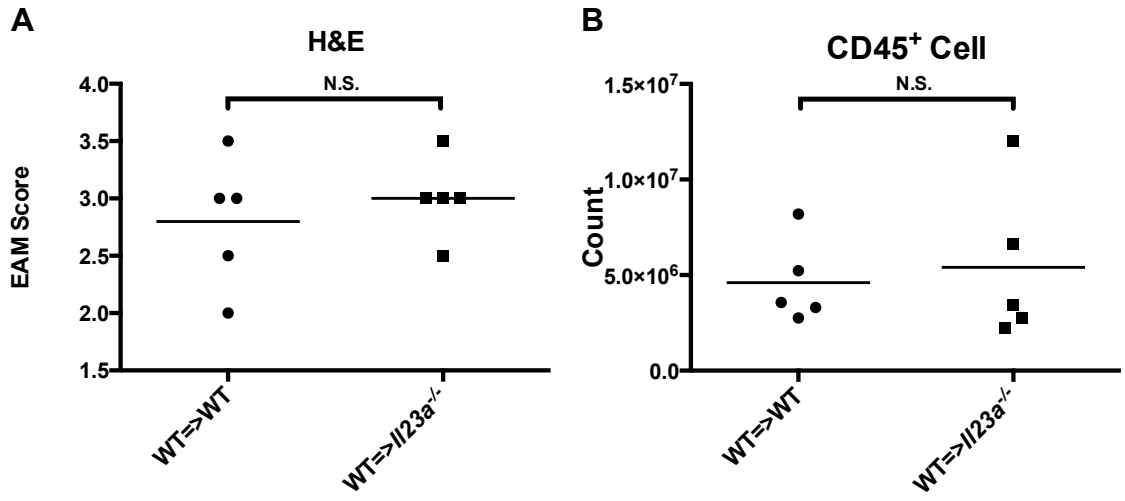

Figure 13. IL-23 was not required for EAM after the establishment of pathogenic autoreactive CD4+ T cells

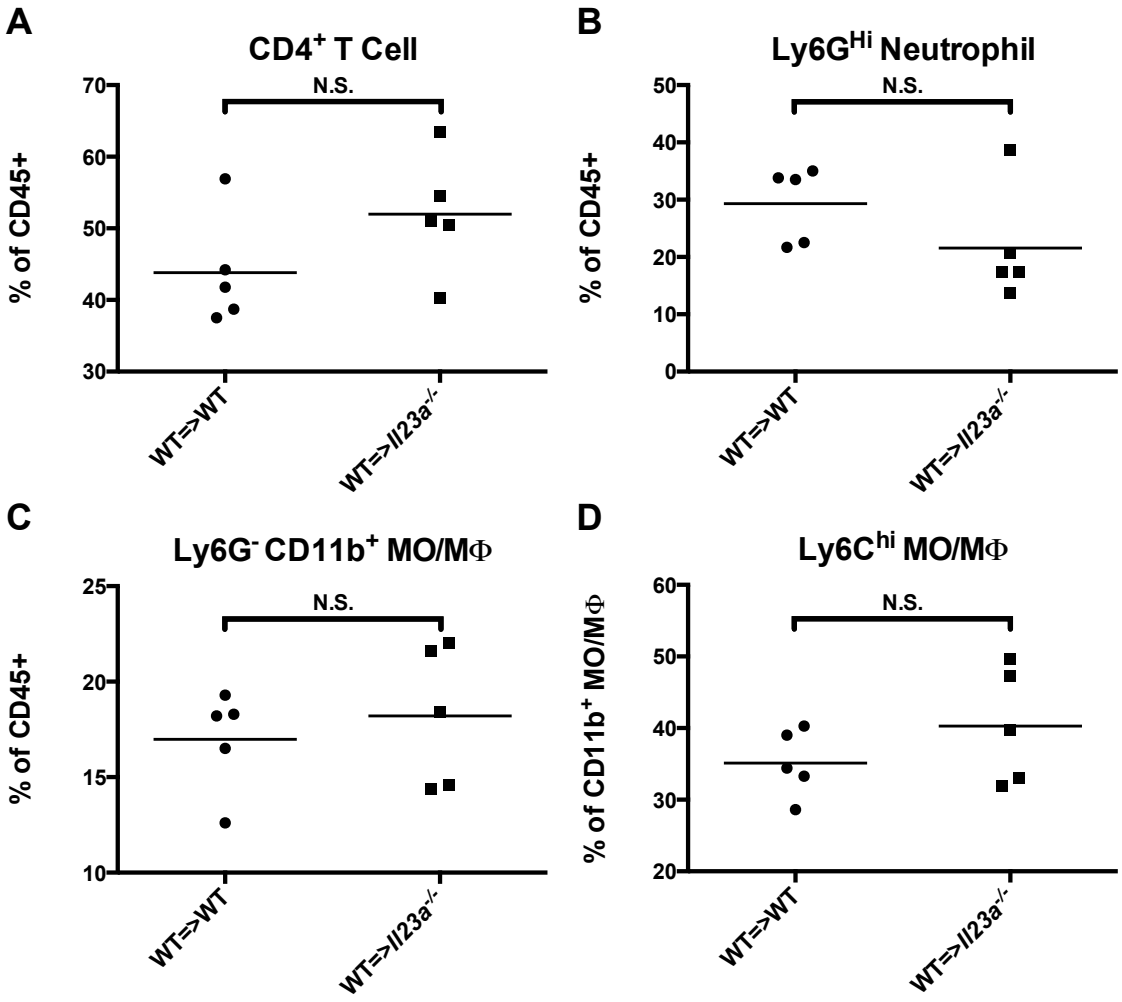

Figure 14. IL-23 had no effect on the composition of heart-infiltrating cells once pathogenic autoreactive CD4+ T cell population was established

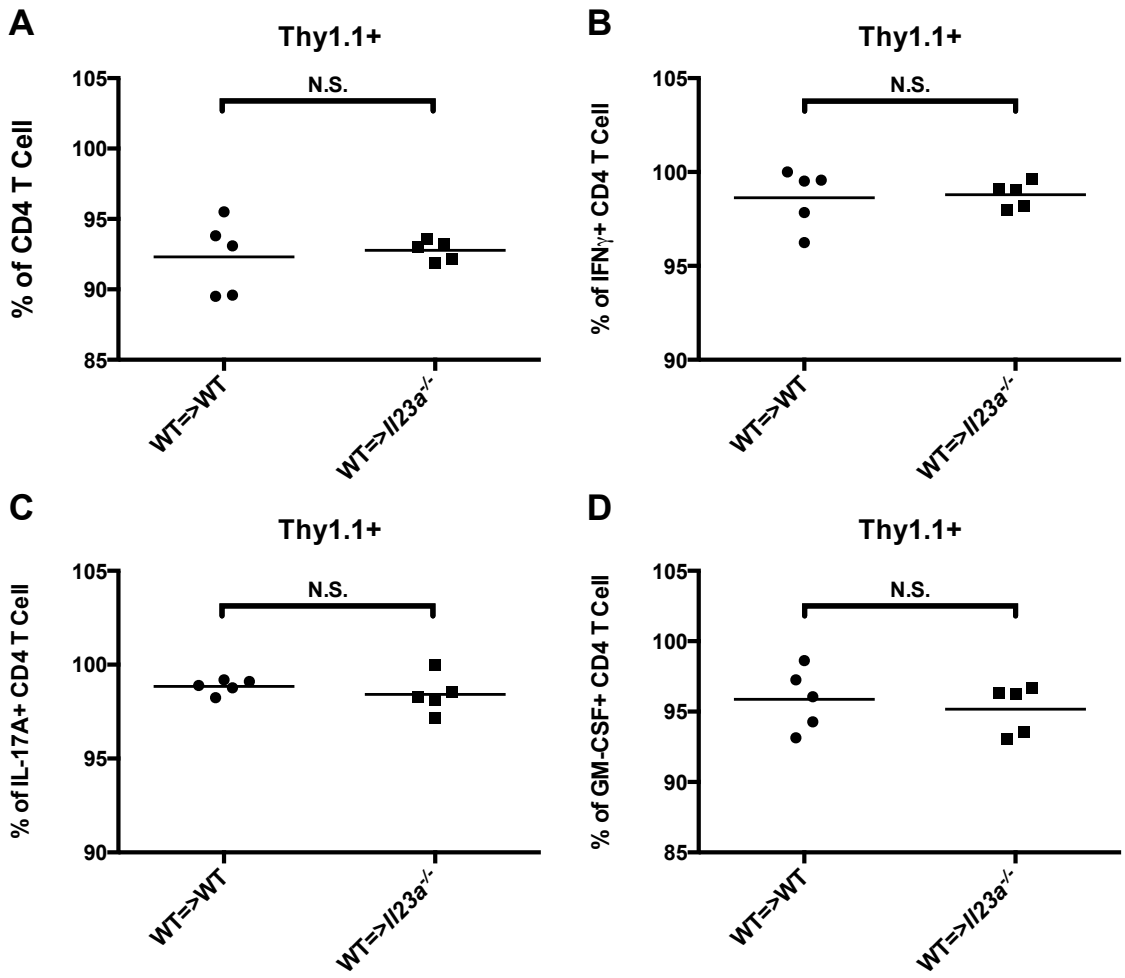

Figure 15. Heart-infiltrating CD4+ T cells were predominantly of donor origin

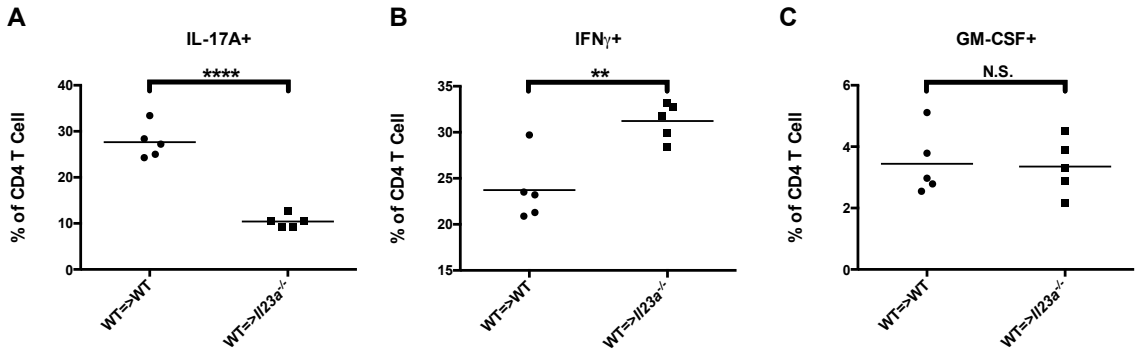

Figure 16. IL-23 was critical in directing cytokine production in autoreactive CD4+ T cells

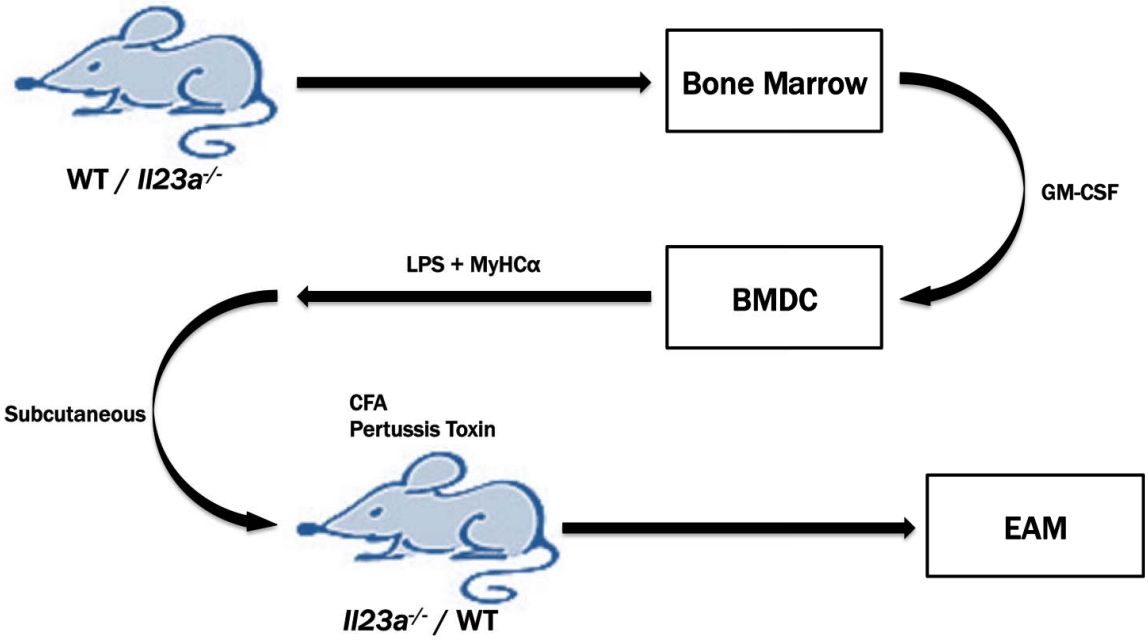

Figure 17. Schematic illustration of BMDC transfer model of EAM

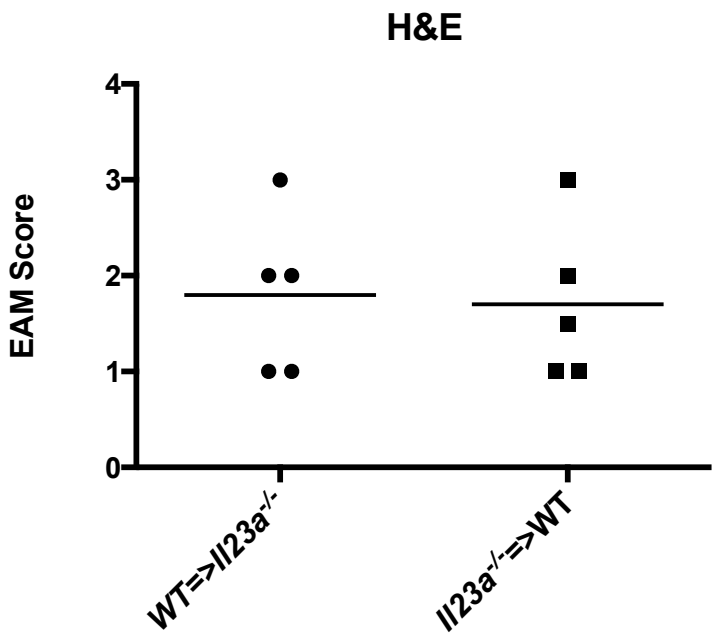

Figure 18. IL-23 from various sources induced pathogenicity

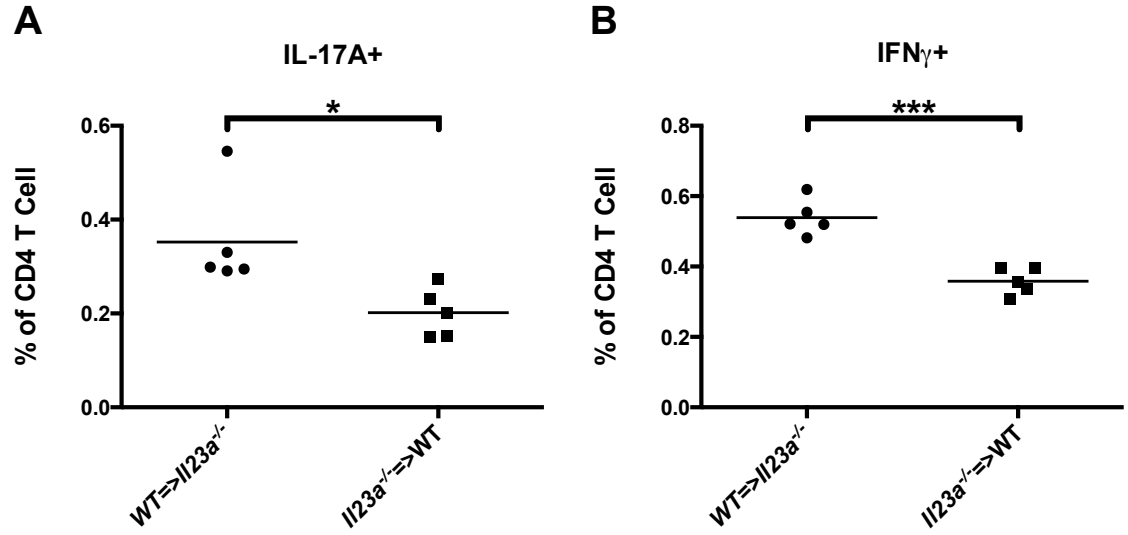

Figure 19. IL-23 from APC was critical in directing cytokine production in CD4+ T cells locally

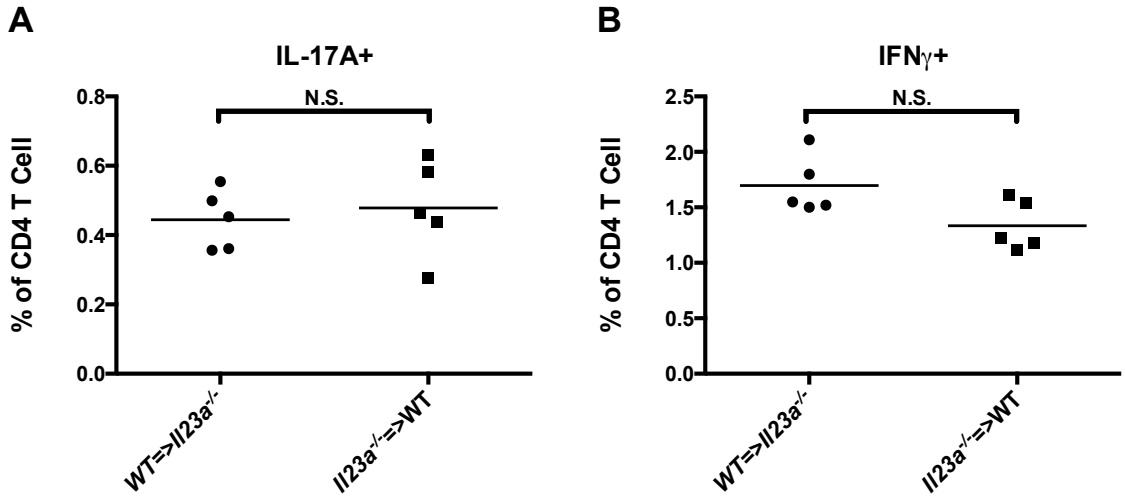

Figure 20. IL-23 from other sources was able to compensate deficiency in APCs

2.4 Figure Legends

Figure 6. *Il23a*$^{-/-}$ mice were protected from EAM

EAM was induced in WT, *Il23a*$^{+/-}$ and *Il23a*$^{-/-}$ mice. Mice were sacrificed 21 days post-immunization. The composition of heart-infiltrating cells was analyzed by flow cytometry.

(A) EAM in WT, *Il23a*$^{+/-}$ and *Il23a*$^{-/-}$ mice scored using H&E staining. Data points represent individual mice. Bars represent mean. Data are analyzed by Kruskal-Wallis test followed by Dunn's procedure.

(B) Total intracardiac CD45^{+} leukocytes in WT, *Il23a*$^{+/-}$ and *Il23a*$^{-/-}$ mice. Data points represent individual mice. Bars represent mean. Data are analyzed by one-way ANOVA followed by Tukey's post-test. *, $p<0.05$.

Figure 7. *Il23a*$^{-/-}$ mice were protected from myeloid expansion during EAM

EAM was induced in WT, *Il23a*$^{+/-}$ and *Il23a*$^{-/-}$ mice. Mice were sacrificed 21 days post-immunization. The composition of splenocytes and blood leukocyte count were analyzed by flow cytometry.

(A) Ly6G^{hi} neutrophils as a proportion of total CD45^{+} leukocytes in in the spleen of WT, *Il23a*$^{+/-}$ and *Il23a*$^{-/-}$ mice.

(B) Ly6G^{-}CD11b^{+} MO/MΦs as a proportion of total CD45^{+} leukocytes in the spleen of WT, *Il23a*$^{+/-}$ and *Il23a*$^{-/-}$ mice.

(C) Blood leukocyte count in WT, *Il23a*$^{+/-}$ and *Il23a*$^{-/-}$ mice

(A) ~ (C) Data points represent individual mice. Bars represent mean. Data are analyzed by one-way ANOVA followed by Tukey's post-test. *, $p<0.05$; **, $p<0.01$; ***, $p<0.001$; ****, $p<0.0001$.

Figure 8. Ability to generate antibodies was not impaired by IL-23 deficiency

EAM was induced in WT, *Il23a*$^{+/-}$ and *Il23a*$^{-/-}$ mice. Mice were sacrificed 21 days post-immunization. The titer of anti-MyHC $\alpha_{614\sim629}$ in the serum was measured by ELISA. Data points represent individual mice. Bars represent mean. Data are analyzed by one-way ANOVA followed by Tukey's post-test.

Figure 9. IL-23 deficiency impaired Th17 polarization in draining lymph nodes

EAM was induced in *Il23a*$^{+/-}$ and *Il23a*$^{-/-}$ mice by immunization at the hind limb. Mice were sacrificed 14 days post-immunization. Lymphoid cells were collected from the inguinal lymph nodes and stimulated with PMA (50ng/mL) and ionomycin (500ng/mL). Cytokine production in CD4+ T cells was analyzed by flow cytometry.

(A) IL-17A producer as a proportion of total CD4+ T cells.

(B) IFN γ producer as a proportion of total CD4+ T cells.

(C) IL-13 producer as a proportion of total CD4+ T cells.

(D) IL-17A and GM-CSF double producer as a proportion of total CD4+ T cells.

(A) ~ (D) Data points represent individual mice. Bars represent mean. Data are analyzed by unpaired two-tailed Student's t test. *, $p<0.05$; **, $p<0.01$.

Figure 10. IL-23 deficiency impaired Th17 polarization in spleen

EAM was induced in *Il23a*$^{+/-}$ and *Il23a*$^{-/-}$ mice by immunization at the hind limb. Mice were sacrificed 14 days post-immunization. Splenocytes were collected and stimulated with PMA (50ng/mL) and ionomycin (500ng/mL). Cytokine production in CD4+ T cells was analyzed by flow cytometry.

(A) IL-17A producer as a proportion of total CD4+ T cells.

(B) IFN γ producer as a proportion of total CD4+ T cells.

(C) GM-CSF producer as a proportion of total CD4+ T cells.

(D) IL-17A and GM-CSF double producer as a proportion of total CD4+ T cells.

(A) ~ (D) Data points represent individual mice. Bars represent mean. Data are analyzed by unpaired two-tailed Student's t test. ****, $p<0.0001$.

Figure 11. IL-23 deficiency affected cytokine production

EAM was induced in WT, *Il23a*$^{+/-}$ and *Il23a*$^{-/-}$ mice. Mice were sacrificed 21 days post-immunization. The levels of cytokines (A) IL-17A, (B) IFNγ and (C) IL-13 in the serum were measured by ELISA. Data points represent individual mice. Bars represent mean. Data are analyzed by one-way ANOVA followed by Tukey's post-test. **, $p<0.01$.

Figure 12. Schematic illustration of CD4+ T cell transfer model of EAM

Thy1.1 donor mice were immunized with MyHC $\alpha_{614\sim629}$ peptide. Splenocytes were collected from donor mice 14 days post immunization and cultured *ex vivo* with 50μg/mL MyHC $\alpha_{614\sim629}$, 20ng/mL rIL-23, 10ng/mL rIL-1ß and 40mmol NaCl for 4 days. CD4+ T cells were isolated and transferred intravenously into WT or *Il23a*$^{-/-}$ Thy1.2 recipients irradiated by 500 Rad γ-radiation. Heart inflammation was examined 2 weeks after the transfer.

Figure 13. IL-23 was not required for EAM after the establishment of pathogenic autoreactive CD4+ T cells

Thy1.1 donor mice were immunized with MyHC $\alpha_{614\sim629}$ peptide. Splenocytes were collected from donor mice 14 days post immunization and cultured *ex vivo* with 50 μg/mL MyHC $\alpha_{614\sim629}$, 20ng/mL rIL-23, 10ng/mL rIL-1ß and 40mmol NaCl for 4 days. CD4+ T cells were isolated and transferred intravenously into WT or *Il23a*$^{-/-}$ Thy1.2 recipients irradiated by 500 Rad γ-radiation. Heart inflammation in recipient mice was examined 2 weeks after the transfer by histopathology and flow cytometry.

(A) EAM in WT and *Il23a*$^{-/-}$ recipients scored using H&E staining. Data points represent individual mice. Bars represent mean. Data are analyzed by Mann-Whitney U test.

(B) Total intracardiac CD45^{+} leukocytes in WT and *Il23a*$^{-/-}$ recipients. Data points represent individual mice. Bars represent mean. Data are analyzed by unpaired two-tailed Student's t-test.

Figure 14. IL-23 had no effect on the composition of heart-infiltrating cells once pathogenic autoreactive CD4+ T cell population was established

Thy1.1 donor mice were immunized with MyHC $\alpha_{614\sim629}$ peptide. Splenocytes were collected from donor mice 14 days post immunization and cultured *ex vivo* with 50 μg/mL MyHC $\alpha_{614\sim629}$, 20ng/mL rIL-23, 10ng/mL rIL-1ß and 40mmol NaCl for 4 days. CD4+ T cells were isolated and transferred intravenously into WT or *Il23a*$^{-/-}$ Thy1.2 recipients irradiated by 500 Rad γ-radiation. Heart inflammation was examined 2 weeks after the transfer. The composition of heart-infiltrating CD45^{+} leukocytes was analyzed by flow cytometry.

(A) CD4+ T cell as a proportion of total CD45^{+} leukocytes.

(B) Ly6G^{hi} neutrophils as a proportion of total CD45^{+} leukocytes.

(C) Ly6G^{-}CD11b^{+} MO/MΦs as a proportion of total CD45^{+} leukocytes.

(D) Ly6C^{hi} MO/MΦs as a proportion of Ly6G^{-}CD11b^{+} MO/MΦs.

(A) ~ (D) Data points represent individual mice. Bars represent mean. Data are analyzed by unpaired two-tailed Student's t-test.

Figure 15. Heart-infiltrating CD4+ T cells were predominantly of donor origin

Thy1.1 donor mice were immunized with MyHC $\alpha_{614\sim629}$ peptide. Splenocytes were collected from donor mice 14 days post immunization and cultured *ex vivo* with 50 μg/mL MyHC $\alpha_{614\sim629}$, 20ng/mL rIL-23, 10ng/mL rIL-1ß and 40mmol NaCl for 4 days. CD4+ T cells were isolated

and transferred intravenously into WT or *Il23a*$^{-/-}$ Thy1.2 recipients irradiated by 500 Rad γ-radiation. Heart inflammation was examined 2 weeks after the transfer. The origin of heart-infiltrating CD4+ T cells was examined by flow cytometry analysis of surface marker Thy1.

(A) Thy1.1^{+} donor cells as a proportion of total CD4+ T cell.

(B) Thy1.1^{+} donor cells as a proportion of IFNγ^{+} CD4+ T cell.

(C) Thy1.1^{+} donor cells as a proportion of IL-17A^{+} CD4+ T cell.

(D) Thy1.1^{+} donor cells as a proportion of GM-CSF^{+} CD4+ T cell.

(A) ~ (D) Data points represent individual mice. Bars represent mean. Data are analyzed by unpaired two-tailed Student's t-test.

Figure 16. IL-23 was critical in directing cytokine production in autoreactive CD4+ T cells

Thy1.1 donor mice were immunized with MyHC $\alpha_{614\sim629}$ peptide. Splenocytes were collected from donor mice 14 days post immunization and cultured *ex vivo* with 50μg/mL MyHC $\alpha_{614\sim629}$, 20ng/mL rIL-23, 10ng/mL rIL-1ß and 40mmol NaCl for 4 days. CD4+ T cells were isolated and transferred intravenously into WT or *Il23a*$^{-/-}$ Thy1.2 recipients irradiated by 500 Rad γ-radiation. Heart inflammation was examined 2 weeks after the transfer. Single cell suspension of mouse hearts was stimulated with PMA (50ng/mL) and ionomycin (500ng/mL). The

cytokine production profile of heart-infiltrating CD4+ T cells was analyzed by flow cytometry.

(A) IL-17A producers as a proportion of total CD4+ T cell.

(B) IFN γ producers as a proportion of total CD4+ T cell.

(C) GM-CSF producers as a proportion of total CD4+ T cell.

(A) ~ (C) Data points represent individual mice. Bars represent mean. Data are analyzed by unpaired two-tailed Student's t-test. **, $p<0.01$; ****, $p<0.0001$.

Figure 17. Schematic illustration of BMDC transfer model of EAM

Bone marrow derived DCs (BMDCs) from WT or *Il23a*$^{-/-}$ donors were matured with LPS and loaded with MyHC$\alpha_{614-629}$ peptide. $0.1x10^6$ loaded BMDCs were then subcutaneously injected under the skin of hind limb of *Il23a*$^{-/-}$ or WT recipients. Heart inflammation was examined 2 weeks after transfer.

Figure 18. IL-23 from various sources induced pathogenicity

Bone marrow derived DCs (BMDCs) from WT or *Il23a*$^{-/-}$ donors were matured with LPS and loaded with MyHC$\alpha_{614-629}$ peptide. $0.1x10^6$ loaded BMDCs were then subcutaneously injected under the skin of hind limb of *Il23a*$^{-/-}$ or WT recipients. Heart inflammation was examined 2 weeks

after transfer by H&E staining. Data points represent individual mice. Bars represent mean. Data are analyzed by Mann-Whitney U test.

Figure 19. IL-23 from APC was critical in directing cytokine production in CD4+ T cells locally

Bone marrow derived DCs (BMDCs) from WT or *Il23a*$^{-/-}$ donors were matured with LPS and loaded with MyHC$\alpha_{614\text{-}629}$ peptide. 0.1x10^6 loaded BMDCs were then subcutaneously injected under the skin of hind limb of *Il23a*$^{-/-}$ or WT recipients, repeated twice subsequently. Recipient mice were sacrificed 14 days after the last transfer. Lymphoid cells were collected from the inguinal lymph nodes and stimulated with PMA (50ng/mL) and ionomycin (500ng/mL). Cytokine production in CD4+ T cells was analyzed by flow cytometry.

(A) IL-17A producer as a proportion of total CD4+ T cells.

(B) IFNγ producer as a proportion of total CD4+ T cells.

(A) and (B) Data points represent individual mice. Bars represent mean. Data are analyzed by unpaired two-tailed Student's t test. *, $p<0.05$; ***, $p<0.001$

Figure 20. IL-23 from other sources was able to compensate deficiency in APCs

Bone marrow derived DCs (BMDCs) from WT or *Il23a*$^{-/-}$ donors were matured with LPS and loaded with MyHC$\alpha_{614\text{-}629}$ peptide. 0.1x10^6 loaded BMDCs were then subcutaneously injected under the skin of hind limb of *Il23a*$^{-/-}$ or WT recipients, repeated twice subsequently. Recipient mice were sacrificed 14 days after the last transfer. Splenocytes were stimulated with PMA (50ng/mL) and ionomycin (500ng/mL). Cytokine production in CD4+ T cells was analyzed by flow cytometry.

(A) IL-17A producer as a proportion of total CD4+ T cells.

(B) IFN γ producer as a proportion of total CD4+ T cells.

(A) and (B) Data points represent individual mice. Bars represent mean. Data are analyzed by unpaired two-tailed Student's t test.

2.5 Materials and Methods

Mice

Il23a$^{-/-}$ founder mice were provided by Wyeth Inc and backcrossed with BALB/c for 10 generations. WT BALB/cJ and CBy.PL(B6)-Thy1a/ScrJ (Thy1.1) mice were purchased from the Jackson Laboratory. All mice were maintained in the Johns Hopkins University School of Medicine specific-pathogen free vivarium. Experiments were conducted on 6-10 week old male mice, in compliance with the Animal Welfare Act and the principles set forth in the Guide for the Care and Use of Laboratory Animals. All methods and protocols are approved by the Animal Care and Use Committee of The Johns Hopkins University.

Induction of EAM

We employed the myocarditogenic peptide of cardiac myosin heavy chain, MyHC$\alpha_{614\text{-}629}$ (Ac-SLKLMATLFSTYASAD), commercially synthesized by fMOC chemistry and purified to a minimum of 90% by HPLC (Genscript). On days 0 and 7, mice received an axillary subcutaneous immunization of 100 μg of MyHC$\alpha_{614\text{-}629}$ peptide emulsified in complete Freund's adjuvant (CFA) (Sigma) supplemented to 5 mg/mL of heat-killed *Mycobacterium tuberculosis* strain H37Ra (Difco). On day 0, mice also received 500 ng of pertussis toxin *intraperitoneally.* (List Biologicals).

For CD4+T cell transfer of EAM, Thy1.1 donor mice were immunized with MyHC $\alpha_{614\text{~}629}$ peptide. Splenocytes were collected from donor mice 14

days post immunization and cultured *ex vivo* in Dulbecco's modified Eagle's medium (DMEM) with 4.5g/L glucose, 2mM L-Glutamine, 1mM sodium pyruvate, 25mM HEPES, 100U/mL penicillin G, 100μg/mL streptomycin, 55μM 2-mercaptoethanol and 10% fetal bovine serum (FBS) supplemented with 50 μ g/mL MyHC $\alpha_{614\sim629}$, 20ng/mL rIL-23, 10ng/mL rIL-1ß and 40mmol NaCl for 4 days. CD4+ T cells were isolated and transferred intravenously into WT or *Il23a*$^{-/-}$ Thy1.2 recipients irradiated by 500 Rad γ-radiation. Heart inflammation was examined 2 weeks after the transfer.

Assessment of EAM Histopathology

Mice were evaluated for the development of EAM on day 21. Heart tissues were fixed in SafeFix solution (Fisher Scientific). Tissues were embedded longitudinally, and 5 μm serial sections were cut and stained with hematoxylin and eosin (H&E) (HistoServ, Gaithersburg, MD). Myocarditis severity was evaluated by H&E staining of myocardium area infiltrated with hematopoietic cells, according to the following scoring system: grade 0, no inflammation; grade 1, less than 10% of the heart section is involved; grade 2, 10-25%; grade 3, 25-50%; grade 4, 50-75%; grade 5, more than 75%. Grading was performed by grading five sections per heart by two independent, blinded investigators and averaged.

Flow Cytometry Analysis and FACS Isolation of Heart Infiltrating Cells

For Flow cytometry analysis, single cell suspension were made from mice hearts perfused for 3 min with 1x phosphate buffered saline (PBS) + 0.5% FBS, and digested in GentleMACS C Tubes according to manufacturer's instructions (Miltenyi Biotec). Viability was determined by LIVE/DEAD staining according to manufacturer's instructions (Life Techonologies). Cells were blocked with αCD16/32 (eBiosciences), and surface markers were stained with fluorochrome-conjugated mAbs (eBioscience, BD Pharmingen, BioLegend). Samples were acquired on the LSR II cytometer running FACSDiva 6 (BD Immunocytometry). Data were analyzed with FlowJo 7.6 (Treestar Software).

Real-Time Quantitative PCR

Tissue total RNA was extracted in TRIZOL (Life Technologies). cDNA were synthesized with High Capacity cDNA Reverse Transcription Kit (Life Technologies) and amplified with Power SYBR Green Mastermix (Life Technologies) in MyiQ2 thermocycler (Bio-Rad) running iQ5 software (Bio-Rad). Primer sequences are detailed in Supplemental Data. Data were analyzed by the 2–ΔΔCt method of Livak, et al., comparing threshold cycles first to *Hprt* expression, then ΔCt of target genes in controls.

EAM Induction by Bone Marrow Derived Dendritic Cells

Bone marrow cells from femur and tibia were isolated from adult wild-type (WT) or *Il23a*$^{-/-}$ BALB/cJ mice and cultured in DMEM with 4.5g/L

glucose, 2mM L-Glutamine, 1mM sodium pyruvate, 25mM HEPES, 100U/mL penicillin G, 100μg/mL streptomycin, 55μM 2-mercaptoethanol and 10% FBS supplemented with 10ng/mL recombinant GM-CSF (R&D Systems) for 8 days.

Bone marrow derived DCs (BMDCs) were matured with LPS and loaded with MyHC$\alpha_{614\text{-}629}$ peptide. Loaded BMDCs, $0.1x10^6$, were then subcutaneously injected in the hind limb of *Il23a*$^{-/-}$ or WT recipients. A total of 3 injections were performed with a 2-day interval. Heart inflammation was examined 2 weeks after transfer.

ELISA

Quantitative sandwich ELISA for cell culture supernatants were determined by colorimetric ELISA kits according to manufacturers' recommended protocols (R&D Systems).

Statistics

Normally distributed data were analyzed by two-tailed Student's t-test (up to two groups) or one-way ANOVA followed by Tukey's post-test. EAM severity scores were analyzed by Mann-Whitney U test (up to two groups) or Kruskal-Wallis test followed by Dunn's procedure. Values of $p < 0.05$ were considered statistically significant.

Chapter III Cardiac Fibroblasts Mediate Interleukin 17A – Driven Inflammatory Dilated Cardiomyopathy

3.1 Results

IL-17A/IL-17RA Signaling Is Required for the Development of DCMi

We previously demonstrated that *Il17a*$^{-/-}$ mice are susceptible to EAM but are protected from DCMi (Baldeviano et al., 2010). In order to investigate the downstream functions of IL-17A in the development of DCMi, we first excluded the possibility that other IL-17 family cytokines signaling though the IL-17 receptor contributed to the DCMi phenotype by comparing disease in *Il17ra*$^{-/-}$ and *Il17a*$^{-/-}$ mice. Similar to *Il17a*$^{-/-}$ mice, *Il17ra*$^{-/-}$ mice were fully protected from DCMi after immunization with myocarditogenic peptide MyHCα$_{614\text{-}629}$ (Figure 21), although they developed myocarditis histologically comparable to WT controls (Figure 22). *Il17ra*$^{-/-}$ mice developed limited cardiac fibrosis while WT mice hearts had significant fibrosis as determined by Mason's Trichrome staining (Figure 21A, 21B) and hydroxyproline assay (Figure 21C). In addition, *Il17ra*$^{-/-}$ mice retained normal heart function and were protected from ventricular dilation (Figure 21D, 21E and 23). Thus, we established that the IL-17A/IL-17RA signaling pathway is required for the development of DCMi. Moreover, since *Il17ra*$^{-/-}$ mice had disease similar to *Il17a*$^{-/-}$ mice, it is unlikely that other cytokines of the IL-17 family are critical in the pathogenesis of DCMi.

IL-17RA Deficiency Alters the Composition of Heart-Infiltrating Myeloid Populations during EAM

Histopathologic and flow cytometric analyses (Figure 24A) revealed that *Il17ra*$^{-/-}$ mice had a similar degree of inflammation and quantitatively comparable numbers of heart-infiltrating CD45^{+} cells as WT controls (Figure 24B). There was no significant difference in the percentages of infiltrating CD4^{+} T cells or SiglecF^{+} eosinophils (Figure 25A, 25B). However, IL-17RA deficiency led to profound changes in the composition of infiltrating myeloid cells. Specifically, *Il17ra*$^{-/-}$ mice had significantly diminished Ly6G^{hi} neutrophil infiltration in their hearts (Figure 24C). Moreover, even though the proportion of total Ly6G^{-}CD11b^{+} monocyte/macrophage (MO/MΦ) population in CD45^{+} cells was comparable (Figure 24D), *Il17ra*$^{-/-}$ mice had significantly lower levels of Ly6C^{hi} population and higher levels of Ly6C^{lo} population within the Ly6G^{-}CD11b^{+} MO/MΦ compartment (Figure 24E, 24F). Importantly, this shift in MO/MΦ populations was restricted to the heart, as the levels of Ly6C^{hi} and Ly6C^{lo} monocytes in the spleen were comparable between WT and *Il17ra*$^{-/-}$ mice (Figure 25C and data not shown). This was dissimilar to the reduction in cardiac infiltration of Ly6G^{hi} neutrophils, which was also detected in the spleen (Figure 25D). The specificity of the difference in the ratio of Ly6C^{hi} to Ly6C^{lo} MO/MΦs in the heart indicates that local but not systemic signals drive this change. In summary, protection from DCMi in *Il17ra*$^{-/-}$ mice is closely associated with the composition of myeloid

populations in the heart, particularly with a significant diminution of neutrophils and Ly6C^{hi} monocytes.

Intracardiac Ly6C^{hi} MO/MΦs Have Proinflammatory and Profibrotic Phenotype while Ly6C^{lo} MO/MΦs Upregulate IGF-1 and MMP Production

The striking decrease in the ratio of Ly6C^{hi} to Ly6C^{lo} MO/MΦs in the absence of IL-17RA signaling led us to examine the contribution of these cell subsets to cardiac damage and fibrosis during DCMi development. Using FACS, we isolated CD45^{+}Ly6G^{-}CD11b^{+}Ly6C^{hi} and CD45^{+}Ly6G^{-}CD11b^{+}Ly6C^{lo} MO/MΦs separately from WT mouse hearts at the peak of inflammation on day 21. Transcriptome profiles were generated by real-time quantitative PCR (qPCR) analysis of these two populations (Figure 26A, Table III).

Ly6C^{hi} MO/MΦs were characterized by higher *Ccr2* expression. Compared to the Ly6C^{lo} pupulation, Ly6C^{hi} MO/MΦs produced higher levels of several proinflammatory cytokines and enzymes (*Il1b*, *Il6*, *Il12a*, *Tnf* and *Nos2*). In addition, Ly6C^{hi} MO/MΦs upregulated thrombospondin-1 (*Thbs1*), which activates latent TGFβ trapped in the extracellular matrix (ECM) and initiates TGFβ-dependent fibrosis pathways (Frangogiannis, 2012). Ly6C^{hi} MO/MΦs also produced more arginase 2 (*Arg2*) and YM1 (*Chi3l3*), which are traditionally associated with M2 tissue-repair macrophages, indicating that the classic M1/M2

dichotomy does not perfectly fit with Ly6C^{hi}/Ly6C^{lo} MO/MΦ phenotypes in the cardiac inflammation scenario during EAM and DCMi. Conversely, Ly6C^{lo} MO/MΦs are characterized by greater expression of *Cx3cr1*, and they produced higher levels of matrix metalloproteinases (*Mmp9* and *Mmp12*) and Insulin-like Growth Factor-1 (*Igf1*) (Figure 26A). These molecules have been implicated in protecting against tissue fibrosis by breaking down excessive ECM (Ramachandran et al., 2012) as well as by other mechanisms (Bessich et al., 2013).

To summarize, heart-infiltrating Ly6C^{hi} MO/MΦs display a proinflammatory and profibrotic phenotype indicating a pathogenic role, while Ly6C^{lo} MO/MΦs produced high level of MMPs and IGF-1 suggesting a protective role. Therefore, *Il17ra*$^{-/-}$ mice had significantly less inflammatory monocytic infiltration in their hearts during the peak of inflammation, which helps to explain their resistance to DCMi.

Ly6C^{hi} MO/MΦs Aggravate DCMi

In order to test the hypothesis that Ly6C^{hi} MO/MΦs directly promote DCMi, we manipulated the balance of Ly6C^{hi} and Ly6C^{lo} MO/MΦs *in vivo* using two previously published methods. First, we injected mice with clodronate-loaded liposomes, which have been shown to induce apoptosis in MO/MΦs (van Rooijen et al., 1996). Second, we injected mice with PBS-loaded liposomes, which have been reported to induce a

phenotypic switch from $Ly6C^{hi}$ to $Ly6C^{lo}$ MO/MΦs through the phagocytosis of the liposomes (Ramachandran et al., 2012).

To assess how these treatments affect the myocarditis phase of EAM, we injected PBS-loaded or clodronate-loaded liposomes on days 14, 16, 18, and 20 of EAM, and sacrificed the mice on day 21. PBS-loaded liposomes significantly reduced the proportion of $Ly6C^{hi}$ MO/MΦs among all $Ly6G^{-}$ $CD11b^{+}$ MO/MΦs (Figure 26B) and dramatically lowered the ratio of $Ly6C^{hi}$ to $Ly6C^{lo}$ MO/MΦs (Figure 26C), while not affecting the total number of $Ly6G^{-}CD11b^{+}$ MO/MΦs among heart-infiltrating $CD45^{+}$ cells (Figure 26D). Clodronate-loaded liposomes, however, significantly decreased the total number of $Ly6G^{-}CD11b^{+}$ MO/MΦs in the hearts (Figure 26D), but also disproportionately reduced the proportion of $Ly6C^{hi}$ MO/MΦs among MO/MΦs (Figure 26B) and lowered the $Ly6C^{hi}$ to $Ly6C^{lo}$ MO/MΦ ratio (Figure 26C). Both PBS-loaded and clodronate-loaded liposome treatments had no significant effect on the severity of EAM on day 21 (Figure 27A), and the levels of $Ly6G^{hi}$ neutrophil infiltration in the heart were not affected (Figure 27B).

We next administered PBS- or clodronate-loaded liposomes intravenously every other day from day 14 to day 35 of EAM, through the peak of cardiac inflammation, and assessed the severity of DCMi at day 63. Clodronate-loaded liposomes protected mice from the deterioration of cardiac function (Figure 26E, 27C and 27D). PBS-loaded liposomes also showed promising effects (Figure 26E, 27C and 27D), as none of the

PBS-loaded liposome treated mice developed severe DCMi defined by an ejection fraction lower than 60% (Figure 26E). Furthermore, mice treated with PBS-loaded or clodronate-loaded liposomes had significantly reduced cardiac enlargement (Figure 26F) and fibrosis (Figure 26G). These results illustrate that while Ly6C^{hi} MO/MΦs are not required in the pathogenesis of acute myocarditis, they play critical roles in cardiac fibrosis and the development of DCMi.

IL-17A/IL-17RA Signaling to Cardiac-Resident Cells Is Required for the Development of DCMi

Protection of *Il17ra*$^{-/-}$ mice against DCMi is associated with significant diminution in neutrophil and Ly6C^{hi} monocyte infiltration. In the inflamed heart, IL-17A receptors are expressed by both infiltrating hematopoietic cells (Gaffen, 2009) and cardiac resident cells (Figure 29A). To determine whether IL-17A drives DCMi by directly signaling to infiltrating hematopoietic cells or indirectly through cardiac-resident cells, we generated bone marrow chimeras. WT or *Il17ra*$^{-/-}$ bone marrows were transferred into lethally irradiated *Il17ra*$^{-/-}$ or WT recipients to generate bone marrow chimeras with IL-17RA signaling ablated in either hematopoietic or non-hematopoietic compartments (Figure 28A). Syngeneic transfers were performed as controls to exclude the effects of the bone marrow reconstruction itself. Chimeras lacking IL-17RA on their cardiac resident cells were protected from DCMi, regardless of the

genotype of their bone marrow donors. Their hearts retained normal function (Figure 28B, 29B, 29C) with lower levels of collagen deposition in their hearts (Figure 28C). Two-way ANOVA (genotype of recipients vs genotype of donors) confirmed the genotype of recipient mice as the primary source of variance. Chimeras lacking IL-17RA signaling in their hematopoietic compartment showed partially mitigated DCMi compared with WT syngeneic transfer controls; however, they were not fully protected from DCMi as the chimeras with *Il17ra*$^{-/-}$ bone marrows (Figure 28B, 28C), suggesting IL-17RA signaling to hematopoietic cells is dispensable in the development of DCMi.

IL-17A/IL-17RA Signaling to Cardiac-Resident Cells Results in Neutrophil and Ly6C^{hi} MO/MΦ - Rich Infiltrate

We observed that protection from DCMi in *Il17ra*$^{-/-}$ mice was associated with diminished neutrophils and Ly6C^{hi} monocyte infiltration (Figure 24). To examine if this alteration in the cardiac infiltrate is due to IL-17A signaling to cardiac resident cells, we analyzed the composition of heart infiltrating cells in chimeras at the peak of inflammation on day 21. Flow cytometric analysis showed that lack of IL-17RA signaling in non-hematopoietic cardiac residents cells diminished neutrophil and Ly6C^{hi} MO/MΦ infiltration, mirroring our finding in *Il17ra*$^{-/-}$ mice hearts (Figure 28D, 28E). Thus, IL-17RA signaling in cardiac-resident cells is mainly

responsible for regulating the composition of myeloid cells in the cardiac infiltrate, and is required for cardiac fibrosis during DCMi pathogenesis.

IL-17A Fails to Induce Apoptosis in Adult Mouse Cardiomyocytes

Having established that IL-17A signaling to cardiac resident cells is essential in driving cardiac damage and fibrosis during DCMi, we sought to identify the specific cell target of IL-17A. We isolated primary cardiomyocytes (CMs) from adult WT mice and stimulated them with recombinant IL-17A (rIL-17A) *in vitro*. After 24 hours, we assessed CM viability and morphology. A recent study found that IL-17A was able to induce apoptosis in neonatal CMs *in vitro*, and the authors suggested that this effect contributed to CM death during myocardial infarction in adults (Liao et al., 2012). However, adult CMs stimulated with rIL-17A retained their viability and morphology when compared to unstimulated CM culture (Figure 30A, 30B). Thus, IL-17A does not induce apoptosis in primary adult CMs *in vitro*. In addition, qPCR assay of CM mRNA did not detect any induction of classic IL-17A targets, including *Il6* and *Cxcl1* (data not shown). Previous studies suggested that TNFα synergizes with IL-17A by stabilizing mRNA of IL-17A targets (Ruddy et al., 2004). However, addition of rTNFα to the culture did not induce activation of IL-17A targets either (data not shown). IL-17A signals through the classical NF-κB pathway, which requires the degradation of NF-κB inhibitor IκBα (Gaffen, 2009). Yet, western blot showed that IL-17A failed to induce IκBα

degradation in CMs (Figure 30C). To summarize, IL-17A does not appear to have any significant effects on CMs *in vitro*, indicating CMs are not the primary IL-17A target during DCMi.

IL-17A Induces Myeloid Chemokines and Cytokines Production from Cardiac Fibroblasts

Next, we assessed the effect of IL-17A signaling to cardiac fibroblasts (CFs). We isolated primary CFs from WT adult mice and tested the purity of CF culture to rule out the possibility of contamination by macrophages and other cells. Bone marrow-derived macrophages (BMDMs) were used as a positive control. First, using immunofluorescence microscopy, we found that cells in our CF culture expressed α-smooth muscle actin (αSMA) but not myeloid marker CD11b (Figure 31A). Second, by flow cytometry, we did not detect any $CD45^+$ leukocytes in our culture contaminating the $CD44^+$ CF population (Figure 31B). Third, by qPCR, we detected the expression of fibroblast-specific genes *Agtr1a* (angiotensin II receptor, type 1a) and *Ddr2* (discoidin domain receptor family member 2) in CF culture, but not myeloid-specific genes *Ccr2*, *Cx3cr1*, *Mpo* or *Pgcd1lg2* (PD-L2) (Table S2). Based on the sensitivity of qPCR assay and the number of cells in the culture, macrophage contamination in CF culture, if any, is extremely low.

To assess the effect of IL-17A on CFs, we isolated primary CFs from adult WT mice and stimulated with IL-17A for 24 hours. IL-17A was able to

induce the production of CXCL1, CCL2, GM-CSF, G-CSF, IL-6 and leukemia inhibitory factor (LIF) (Figure 31C), but not IL-1β, IL-33, TNFα, TGFβ, CCL8 and CCL11 (data not shown). Addition of TNFα further enhanced the stimulatory effects of IL-17A (Figure 31C). Interrogation of mRNA levels by qPCR confirmed these effects (Figure 32A). However, IL-17A failed to directly stimulate the production of collagen in CFs (Figure 32B), indicating that a more complex mechanism was involved in regulating fibrosis during IL-17A-driven DCMi.

To confirm these results *in vivo*, we next isolated $CD45^{-}CD34^{+}CD146^{+}CD44^{hi}CD31^{-}$ CFs from the hearts of immunized WT and *Il17ra*$^{-/-}$ mice by FACS (Figure 33A). qPCR analysis showed that CFs from *Il17ra*$^{-/-}$ mice expressed significantly lower levels of *Cxcl1*, *Csf2*, *Csf3*, and *Il6* compared with CFs from WT mice (Figure 33B), confirming our *in vitro* findings that IL-17A stimulated the production of proinflammatory cytokines and chemokines in CFs. However, the levels of *Ccl2* and *Lif* were comparable between CFs from WT and *Il17ra*$^{-/-}$ mice (Figure 34A), indicating more complex pathways were involved. Endothelial cells (ECs) have also been reported to respond to IL-17A signals. We therefore also isolated $CD45^{-}CD34^{+}CD146^{+}CD44^{lo}CD31^{hi}$ ECs by FACS from the hearts of WT mice on day 21 of EAM (Figure 33A). qPCR analysis showed that the mRNA levels of proinflammatory cytokines and chemokines of interest were dramatically higher in CFs than ECs, with the exception of *Csf3* (Figure 34B), indicating that, among cardiac resident cells, CFs are

the dominant source of proinflammatory cytokines and chemokines upon IL-17A stimulation during EAM and DCMi.

CXCL1 is a major chemokine for neutrophil chemotaxis, and the induction of CXCL1 in CFs by IL-17A helps explain the differences in the composition of heart-infiltrating myeloid cells between *Il17ra*$^{-/-}$ and WT mice. IL-17A however did not have a significant effect on CX3CL1 expression (Figure 32C), indicating that other mechanisms are involved in the accumulation of Ly6C^{lo} monocytes in *Il17ra*$^{-/-}$ hearts. Moreover, GM-CSF, G-CSF and IL-6 play important roles in the differentiation and activation of myeloid cells, suggesting further interactions of CFs and inflammatory cells under IL-17A stimulation.

IL-17A Is Able to Drive the Differentiation of Monocytes *in trans* through Cardiac Fibroblasts

To determine whether IL-17A is able to instruct the differentiation of monocytes by inducing cytokine production from CFs, we designed an *in vitro* fibroblast - monocyte co-culture system. Since spleen is the major reservoir of monocytes during cardiac inflammation (Swirski et al., 2009), Ly6G^{-}CD11c^{-}CD11b^{+}F4/80^{-}Ly6C^{hi} monocytes were FACS sorted from naïve *Il17ra*$^{-/-}$ mouse spleen and co-cultured with primary adult mouse CFs. In order to exclude direct signaling of IL-17A to monocytes, we used *Il17ra*$^{-/-}$ mice as monocyte donors. *Il17ra*$^{-/-}$ Ly6C^{hi} monocytes were co-cultured with WT CFs for 48 hours with or without rIL-17A stimulation.

Since monocytes themselves produce TNFα, no rTNFα was added to the cultures. After 48 hours of co-culture, monocytes were separated from CFs by FACS. qPCR assay of monocytes showed that, through its effects on CFs, IL-17A was able to indirectly upregulate proinflammatory genes *Il1b*, *Il6*, *Il12a* and *Nos2*, while downregulating suppressive gene *Il10* (Figure 35A). We repeated the experiment with *Il17ra*$^{-/-}$ CFs. rIL-17A failed to induce significant difference in *Il17ra*$^{-/-}$ monocytes (Figure 36) without responding CFs, demonstrating that these effects were IL-17A-specific. IL-17A however could not induce *de novo* conversion of Ly6C^{lo} MO/MΦs to Ly6C^{hi} MO/MΦs either directly or indirectly through CFs. rIL-17 failed to affect Ly6C^{hi} to Ly6C^{lo} ratio in Ly6G^{-}CD11c^{-} CD11b^{+}F4/80^{-} monocytes isolated from the spleen of WT mice (Figure 35B). Co-culture of splenic Ly6G^{-}CD11c^{-}CD11b^{+}F4/80^{-} monocytes from *Il17ra*$^{-/-}$ mice with WT CFs resulted in lower level of Ly6C^{hi} MO/MΦs, likely due to phagocytosis-induced conversion. However, addition of rIL-17A had no additional effects (Figure 35C).

Thus, IL-17A induced proinflammatory changes in Ly6C^{hi} monocytes indirectly through CFs, suggesting that CFs actively participate in immune response and serve as a mediator between IL-17A and Ly6C^{hi} monocytes.

IL-17A Drives the Differentiation of Monocytes by Inducing GM-CSF Production in Cardiac Fibroblasts

We have shown that IL-17A induces the production of IL-6, G-CSF and GM-CSF from CFs (Figure 31C and 33B), which are all potent drivers of myeloid cells differentiation and activation. We therefore blocked these cytokines with neutralizing antibodies in our CF/monocyte co-culture system to determine which cytokine is the main transducer of the IL-17A signals to monocytes. Anti-IL-6RA monoclonal antibody (mAb) and anti-G-CSF mAb both failed to reverse the effect of IL-17A (data not shown). However, anti-GM-CSF mAb strongly suppressed the indirect effect of IL-17A on Ly6C^{hi} monocytes (Figure 35A). Moreover, the phenotype of monocytes co-cultured with rGM-CSF resembled monocytes from the rIL17A-stimulated co-culture (Figure 35A). Therefore, IL-17A induces GM-CSF production from cardiac fibroblasts, which mediates the proinflammatory differentiation of Ly6C^{hi} monocytes.

Il17ra*$^{-/-}$ Mice Have Less Proinflammatory Ly6C^{hi} MO/MΦs Infiltration *in vivo

We have shown that IL-17A instructs proinflammatory differentiation of Ly6C^{hi} monocytes by inducing GM-CSF production *in vitro* (Figure 35A). To investigate whether IL-17A drives MO/MΦs into a proinflammatory phenotype in the heart, we isolated Ly6C^{hi} MO/MΦs from the hearts of WT or *Il17ra*$^{-/-}$ mice at the peak of inflammation (day 21). Since IL-17A

directs proinflammatory changes in monocytes *in vitro*, we expected that Ly6C^{hi} MO/MΦs from *Il17ra*$^{-/-}$ mice hearts would possess a less inflammatory phenotype due to lack of IL-17RA signaling. qPCR assay showed that Ly6C^{hi} MO/MΦs from *Il17ra*$^{-/-}$ mice hearts produced lower levels of proinflammatory cytokines *Il1b*, *Il6* (Figure 37A), mirroring the phenotype observed from *in vitro* co-culture experiments. Importantly, Ly6C^{hi} monocytes isolated from the spleens of *Il17ra*$^{-/-}$ mice had expression of *Il1b* and *Il6* comparable to WT splenic Ly6C^{hi} monocytes (Figure 38), demonstrating that the effects of IL-17A on MO/MΦs was a local phenomenon specific to the heart during EAM.

To confirm the *in vitro* results that GM-CSF mediates these effects, we injected immunized WT mice with rGM-CSF 36 hours and 12 hours before sacrifice on day 21 of EAM, and isolated Ly6C^{hi} MO/MΦs from the hearts by FACS. qPCR analysis showed that Ly6C^{hi} MO/MΦs from the hearts of rGM-CSF treated mice had higher levels of *Il1b* and *Il6* expression compared to controls injected with PBS (Figure 37B), illustrating that GM-CSF elicits proinflammatory polarization of Ly6C^{hi} MO/MΦs MO/MΦs during EAM and DCMi.

Thus, we confirmed our previous *in vitro* results *in vivo*, underscoring that this IL-17A → cardiac fibroblast → GM-CSF → monocyte pathway directs the development of DCMi after EAM. However, Ly6C^{hi} MO/MΦs from *Il17ra*$^{-/-}$ mice expressed comparable levels of *Il12a*, *Nos2* and *Il10* (not shown), which is not consistent with the findings from *in vitro* co-

culture experiment. This difference highlights the complexity of the *in vivo* inflammatory environment and suggests that other pathways play a role in the programing of MO/MΦs at the site of inflammation.

3.2 Discussion

About 9-16% of patients with myocarditis progress to dilated cardiomyopathy (Herskowitz et al., 1993; Sagar et al., 2011), but there are no reliable biological markers that would help identify myocarditis patients with high risk of progressing to DCMi (Cooper, 2009). Currently, a definitive diagnosis of myocarditis depends upon a biopsy of the myocardium. Based on the Dallas criteria, the heart is evaluated based on the presence and density of inflammatory infiltration and cardiomyocyte death (Aretz et al., 1987). However, our study clearly shows that not only the quantity, but also the quality of these infiltrating cells is critical in predicting the development of DCMi. Similar to *Il17a*$^{-/-}$ mice, *Il17ra*$^{-/-}$ mice developed myocarditis and had overall CD45^{+} cell infiltration comparable to WT, but were nonetheless not susceptible to DCMi. This protection is associated with a different infiltration profile. *Il17ra*$^{-/-}$ mice had diminished infiltration of neutrophils, which have been implicated in inducing cardiac damage and rupture in a myocardial infarction model (Hiroi et al., 2013; Vinten-Johansen, 2004). In addition, *Il17ra*$^{-/-}$ mice had significantly less infiltration of proinflammatory monocytes and lower Ly6C^{hi} to Ly6C^{lo} MO/MΦ ratios specifically in their heart, which represents a potentially useful biomarker for DCMi risk in myocarditis patients.

Monocytes and macrophages are key effector cells in EAM (Barin et al., 2012) as well as in human giant cell myocarditis (Cooper et al., 2007).

MO/MΦs are not a homogeneous population (Hashimoto et al., 2011). However, cardiac disease literature tended to ignore their heterogeneity until recently, leading to substantial disagreement in reported findings. During early development, progenitor cells migrate into solid organs and develop into tissue resident macrophages, which are maintained by local proliferation with minimal replenishment from blood monocytes (Hashimoto et al., 2013; Yona et al., 2013). During an inflammatory process, blood monocytes rapidly migrate to the site of inflammation, where they mature into macrophages in response to local stimulating signals (Sica and Mantovani, 2012). In mouse, monocytes forms two major subsets in blood, $CCR2^{hi}CX3CR1^{lo}Ly6C^{hi}$ (resembling human $CD14^{hi}CD16^{-}$ monocytes) and $CCR2^{lo}CX3CR1^{hi}Ly6C^{lo}$ (resembling human $CD14^{lo}CD16^{+}$ monocytes) (Geissmann et al., 2003; Shi and Pamer, 2011). In our study, the balance of these two MO/MΦs subsets in the heart determines the outcome of inflammation. Thus IL-17RA deficiency leads to a lower $Ly6C^{hi}/Ly6C^{lo}$ ratio and protection from DCMi. We found that heart-infiltrating $Ly6C^{hi}$ MO/MΦs had a proinflammatory and profibrotic phenotype. The proinflammatory cytokines and TGFβ activators they produce are likely to play critical roles in cardiac remodeling. $Ly6C^{lo}$ monocytes in heart produced high levels of MMPs and IGF-1, which have been described as protective in fibrosis (Ramachandran et al., 2012; Bessich et al., 2013). We used two methods to manipulate the balance of $Ly6C^{hi}$ and $Ly6C^{lo}$ MO/MΦs to demonstrate the role they play in DCMi:

First, depletion of Ly6G$^-$CD11b$^+$ MO/MΦs by clodronate-loaded liposomes also lowered the ratio of Ly6C^{hi} to Ly6C^{lo} MO/MΦs in the heart. Second, PBS-loaded liposomes specifically lowered the ratio of Ly6C^{hi} to Ly6C^{lo} MO/MΦs without affecting the total number of MO/MΦs in the heart. Neither method induced any change in severity of myocarditis, but both protected mice from cardiac fibrosis and the development of severe DCMi, demonstrating that Ly6C^{hi} MO/MΦs aggravate the development of DCMi. Similarly, in a heart ischemia/reperfusion model, early recruitment of Ly6C^{hi} monocytes is associated with injury, preceding the recruitment of Ly6C^{lo} monocytes, which appear to be involved in myocardial healing (Nahrendorf, 2012). Ly6C^{lo} monocytes were shown to be able to arrest and reverse fibrosis in a model of CCl_4-induced liver damage (Ramachandran et al., 2012).

We further suggest that the M1/M2 paradigm does not perfectly overlap with Ly6C^{hi} and Ly6C^{low} subsets and does not accurately describe these two different populations in the heart during EAM. Traditionally, M1 represents a population that promotes inflammation whereas M2 is responsible for tissue repair and fibrosis (Gordon and Taylor, 2005). However, in our EAM model, Ly6C^{hi} MO/MΦs have a proinflammatory and profibrotic phenotype. They upregulate both classic M1 markers like *Tnf* and *Nos2*, as well as M2 markers like *Chi3l3*, while Ly6C^{lo} MO/MΦs produced molecules that are believed to help resolve fibrosis (Ramachandran et al., 2012; Bessich et al., 2013).

We have shown previously that MO/MΦs express receptors for IL-17A but direct stimulation of MO/MΦs with IL-17A does not induce a proinflammatory phenotype (Barin et al., 2012). Bone marrow chimeras revealed that deficiency of IL-17A/IL-17RA signaling in non-hematopoietic cells is sufficient to suppress the augmentation of immune response and protect mice from cardiac damage. In addition, IL-17A signaling to cardiac resident cells was essential for the IL-17A driven recruitment of neutrophils and Ly6C^{hi} monocytes to the inflamed heart.

A recent study found that IL-17A was able to induce apoptosis in neonatal cardiomyocytes *in vitro* (Liao et al., 2012). The authors suggested that this effect contributed to cardiomyocyte death during myocardial infarction in adult mice. Other investigators reported that IL-17A induced collagen production in neonatal cardiac fibroblasts (Liu et al., 2012). However, neonatal cells have unique properties that are not retained in adult cells and are not necessarily the appropriate model to study adult diseases. We observed that IL-17A neither induced apoptosis nor activated the NF-κB pathway in primary adult cardiomyocytes *in vitro*, indicating that cardiomyocytes are not likely to be the primary target of IL-17A in adults. In addition, IL-17A did not directly stimulate collagen production in adult cardiac fibroblasts.

In contrast, adult cardiac fibroblasts respond to IL-17A by producing high levels of chemokines and cytokines known to facilitate myeloid cell recruitment and instruct their *in situ* differentiation towards an

inflammatory phenotype. Cardiac fibroblasts isolated from *Il17ra*$^{-/-}$ mice during EAM expressed significantly lower levels of proinflammatory cytokines and chemokines. Importantly, although it was reported that endothelial cells react to IL-17A stimulation, they produced minimal amount of cytokines and chemokines compared with cardiac fibroblasts, hence endothelial cells do not appear to be the primary target o IL-17A in our model of EAM and DCMi. Thus, our study highlights the central, decisive role "non-immune" cells like fibroblasts can play in immunologic processes. Cardiac fibroblasts served as a critical mediator between adaptive and innate immune cells and actively participated in the augmentation of immune response. In response to IL-17A stimulation from adaptive T cells, cardiac fibroblasts produce granulocytic and monocytic chemokines to recruit innate effector cells and aggravate the immune response. Cardiac fibroblasts also secrete cytokines, in this case GM-CSF, to direct these recruited MO/MΦ effectors to a more proinflammatory phenotype, which further intensifies inflammation. Moreover, this mediator role played by cardiac fibroblasts proved crucial in DCMi, as deficiency of IL-17A/IL-17RA signaling in non-hematopoietic cells was sufficient to protect mice from cardiac damage.

Our studies also revealed that the main mediator of local communications between cardiac fibroblasts and MO/MΦs was cardiac fibroblast-derived GM-CSF. GM-CSF is known to elicit the expansion and differentiation of progenitors of the myeloid lineages; GM-CSF also

supports the survival and activation of effector functions of myeloid cells (Papatriantafyllou, 2011). In ischemic heart disease, although associated with poor prognosis (Maekawa et al., 2004), GM-CSF has been studied largely for its role outside of its immunologic functions. These mechanisms mostly involve angiogenesis or the mobilization of HSC-like cells (Zbinden et al., 2005). There have also been attempts to study the role of GM-CSF in myocarditis: Blyszczuk *et al.* argued that GM-CSF does not affect dendritic cell functions during the effector phase of EAM (Blyszczuk et al., 2013); however, they neglected to address the effects of GM-CSF on MO/MΦs, and their impact on cardiac damage. Our data now point to GM-CSF acting as a key mediator of IL-17A-driven autoimmunity in DCMi: IL-17A signaling induces GM-CSF production from cardiac fibroblasts. GM-CSF then drives differentiation of heart-infiltrating MO/MΦs toward a proinflammatory phenotype that in turn promotes DCMi.

In conclusion, our study demonstrates that the IL-17A/IL-17RA axis is critical in the development of DCMi, a fatal inflammatory heart disease. IL-17A induces chemokine production by cardiac fibroblasts, resulting in an infiltrate rich in neutrophils and Ly6C^{hi} MO/MΦs in the heart. Furthermore, IL-17A directs monocytic infiltrates into an even more inflammatory phenotype by inducing GM-CSF production from cardiac fibroblasts. This novel pathway provides new potential markers to identify myocarditis patients with a high risk of developing DCMI. This

pathway further suggests new targets for the prevention of DCMi. In addition, other groups have shown that IL-17A is critical in inflammatory diseases including myocardial ischemia/reperfusion injury (Liao et al., 2012), pulmonary fibrosis (Wilson et al., 2010) and liver cirrhosis (Kono et al., 2011). The pathway involving IL-17A, fibroblasts, GM-CSF, and MO/MΦs may therefore play a key role in many other diseases.

3.3 Figures and Tables

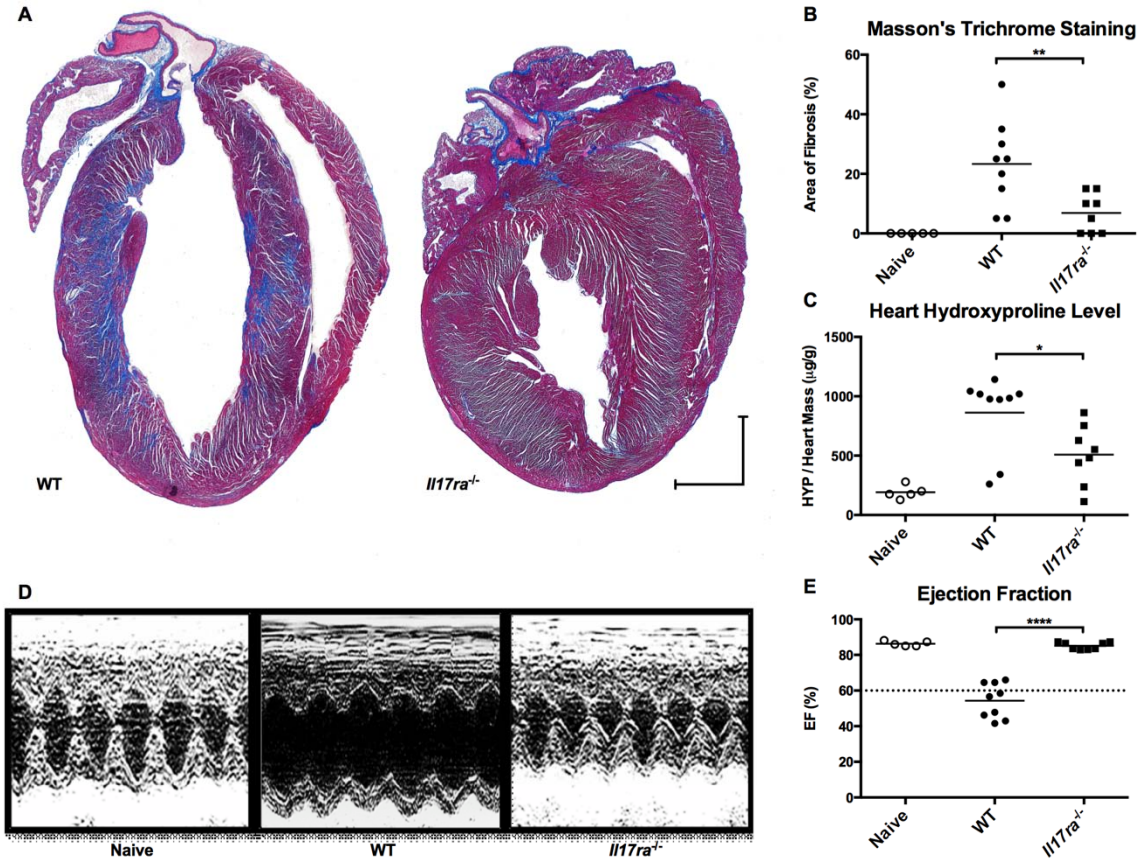

Figure 21. *Il17ra*$^{-/-}$ mice are protected from DCMi

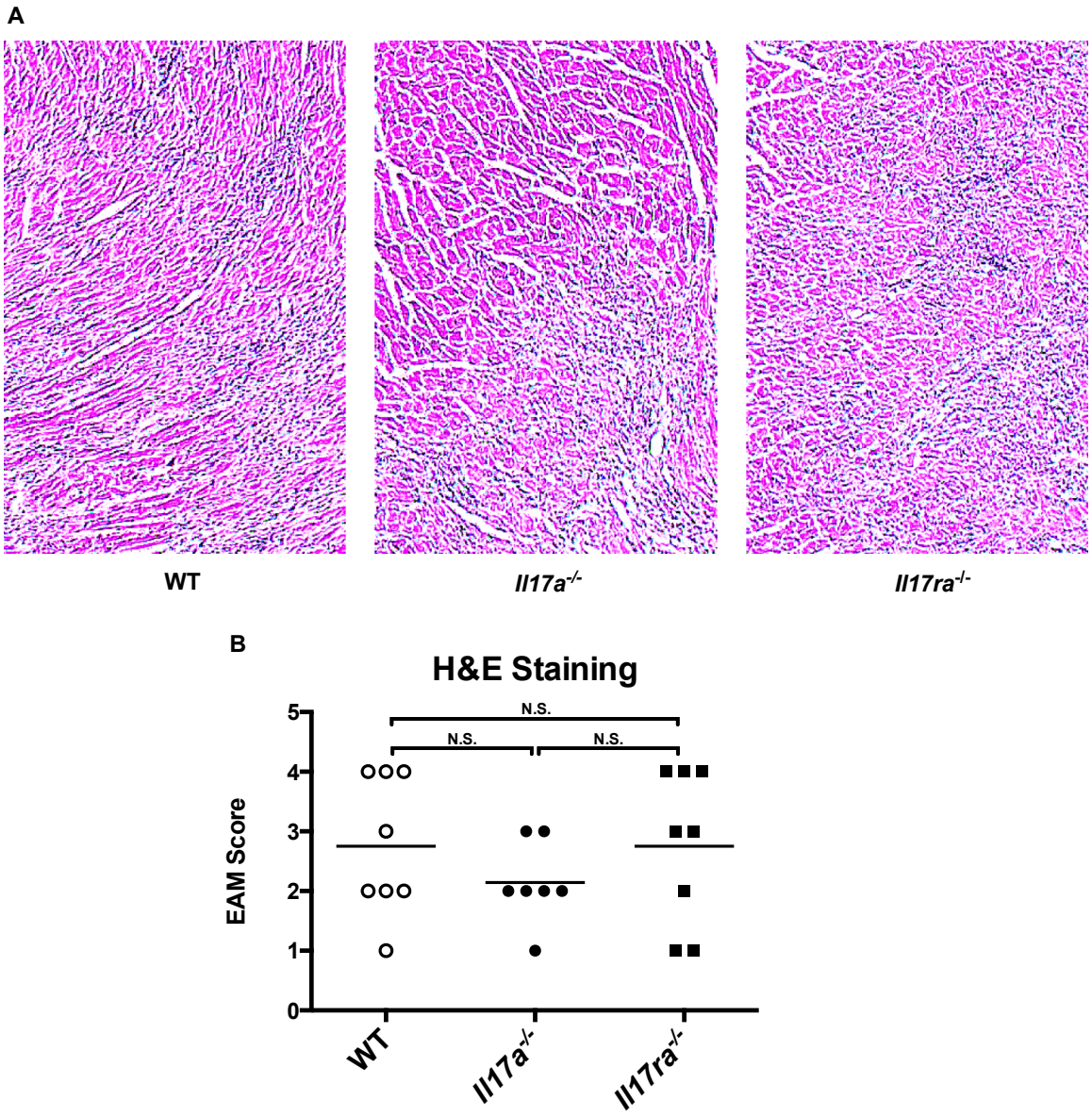

Figure 22. *Il17ra*$^{-/-}$ mice develop EAM comparable to WT and *Il17a*$^{-/-}$ mice

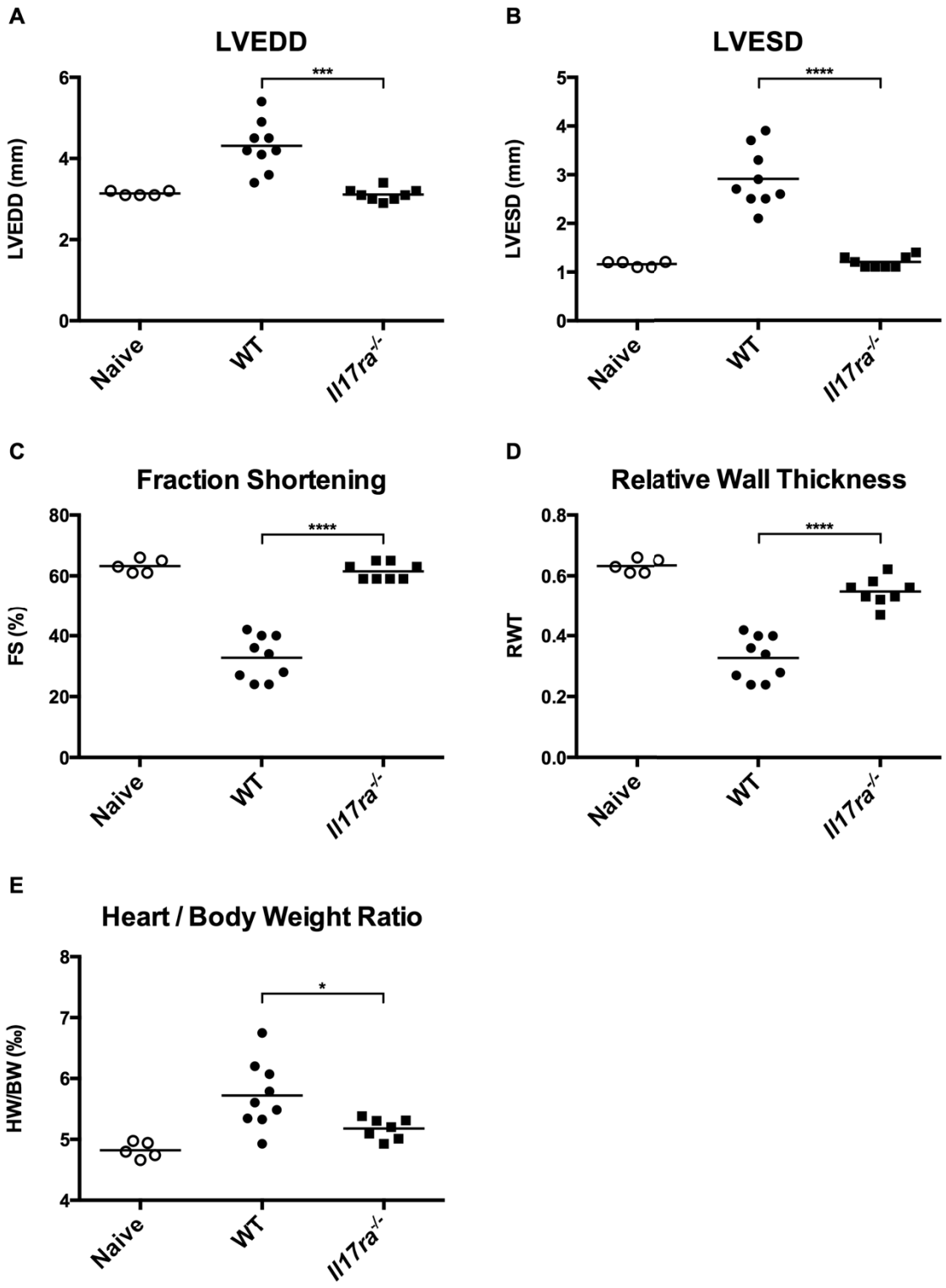

Figure 23. *Il17ra*$^{-/-}$ mice are protected from DCMi

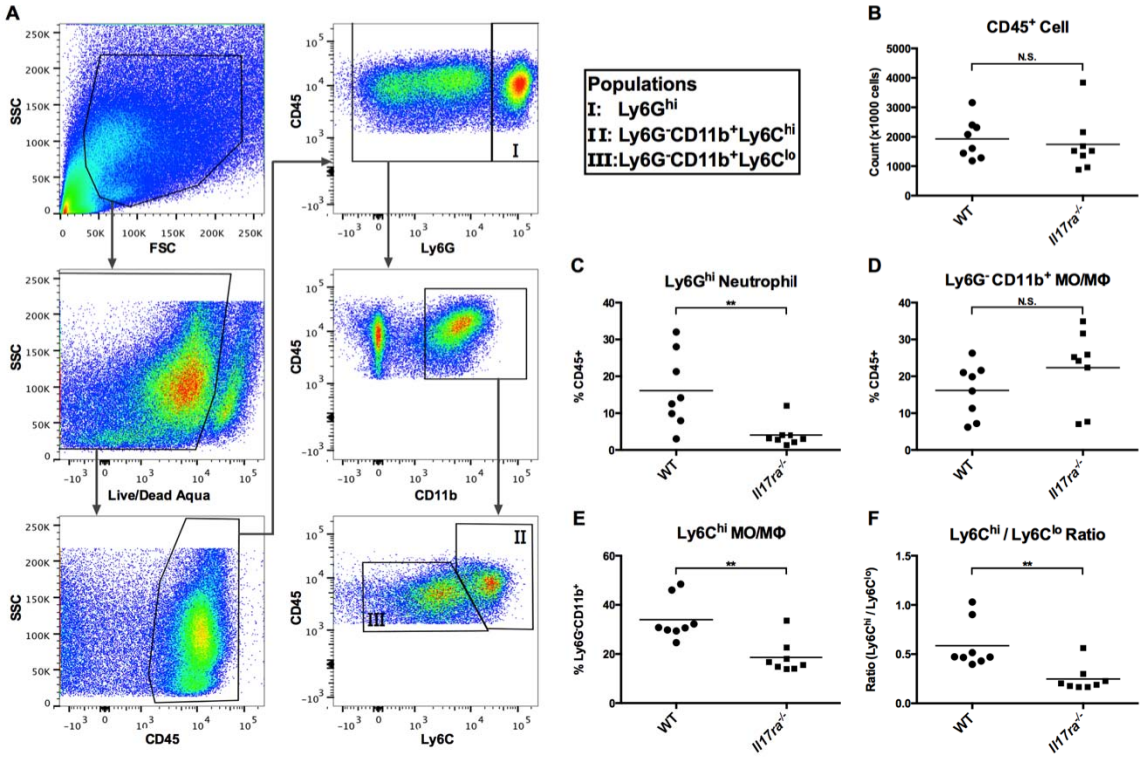

Figure 24. IL-17RA deficiency alters the composition of heart-infiltrating cells

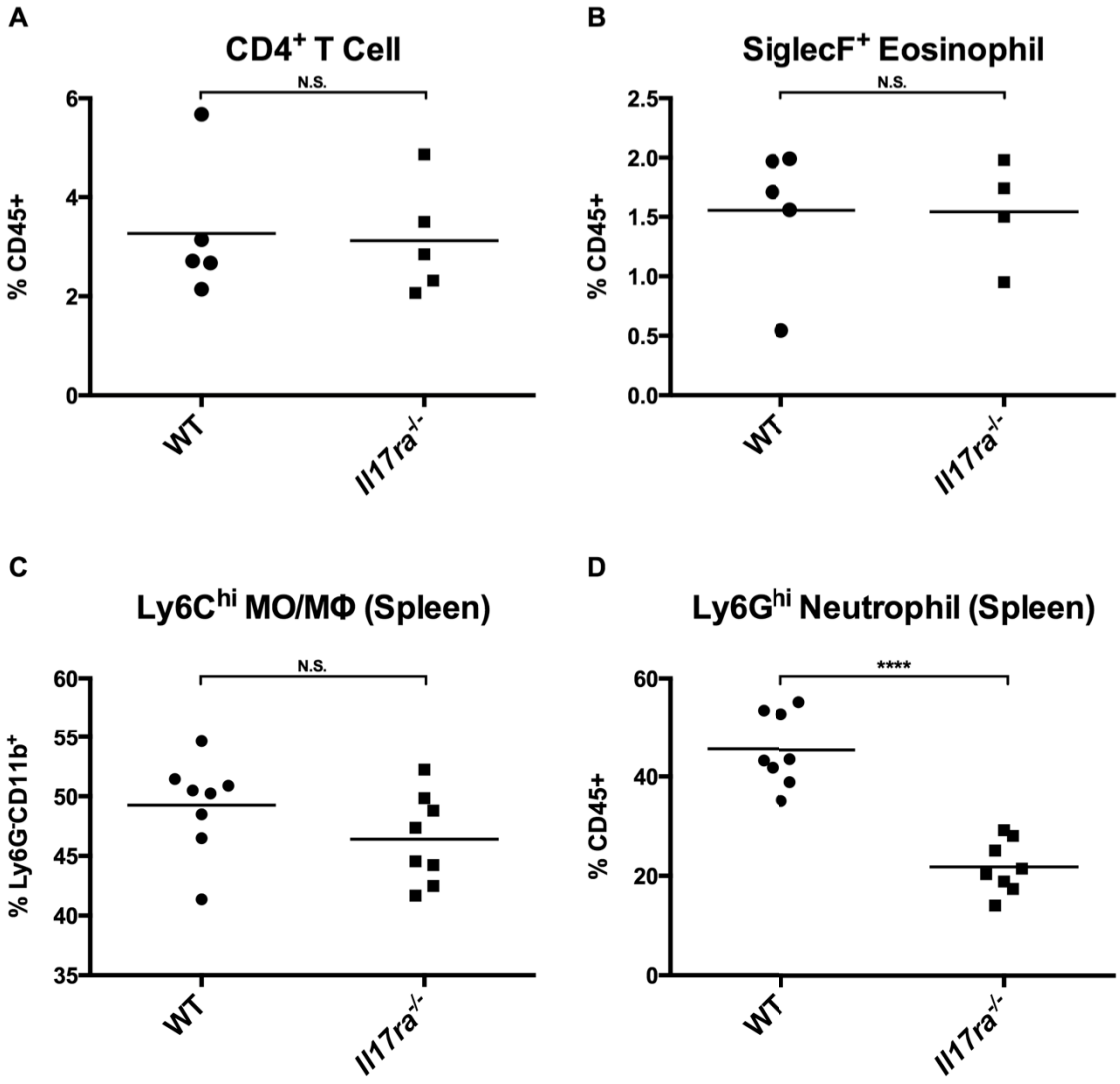

Figure 25. IL-17RA deficiency has no effects on infiltration of CD4^{+} T cell and SiglecF^{+} eosinophil in the heart or the balance of Ly6C^{hi} and Ly6C^{lo} monocytes in the spleen

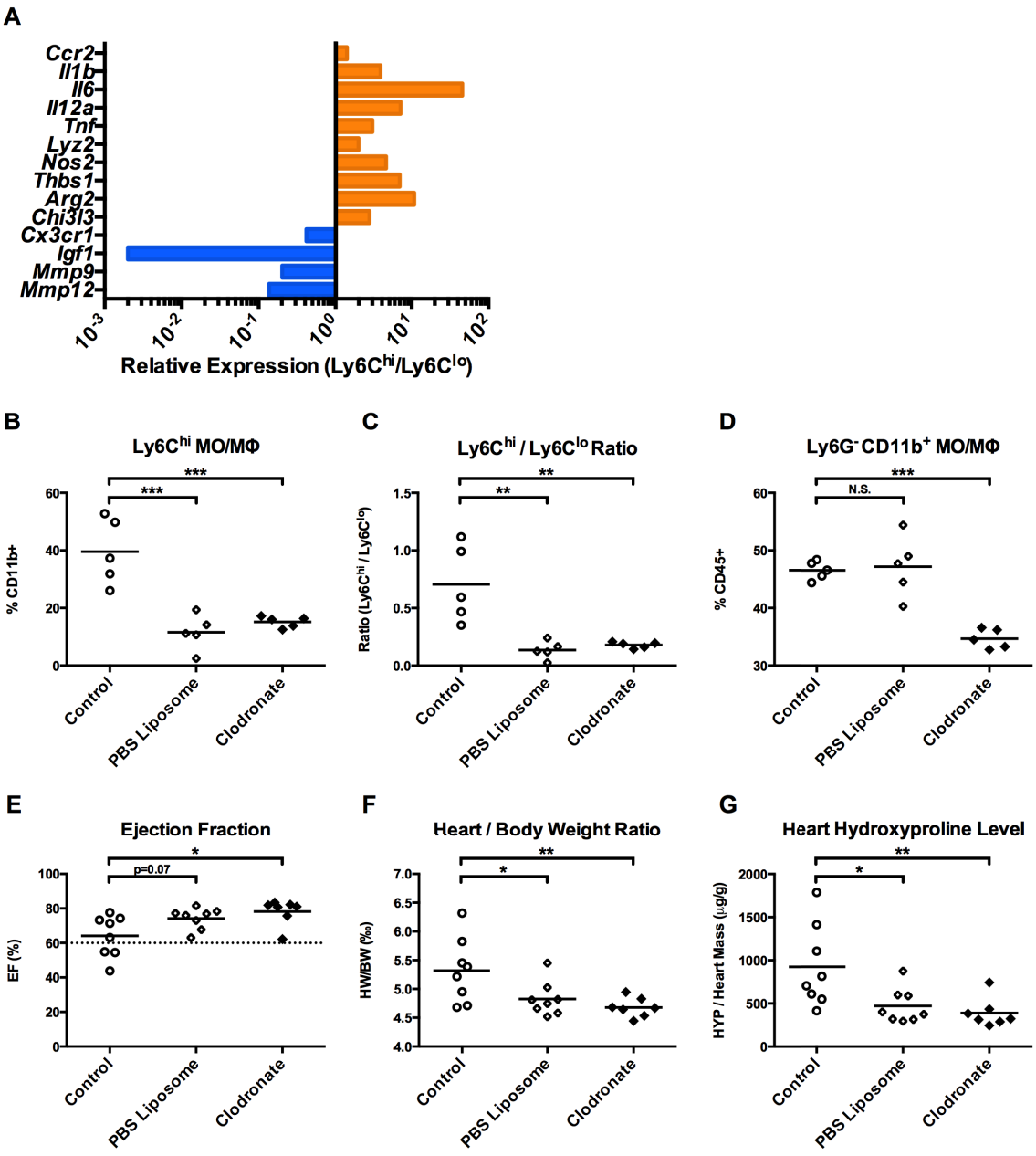

Figure 26. Transcriptomes and functions of intracardiac Ly6C^{hi} and Ly6C^{lo} MO/MΦs

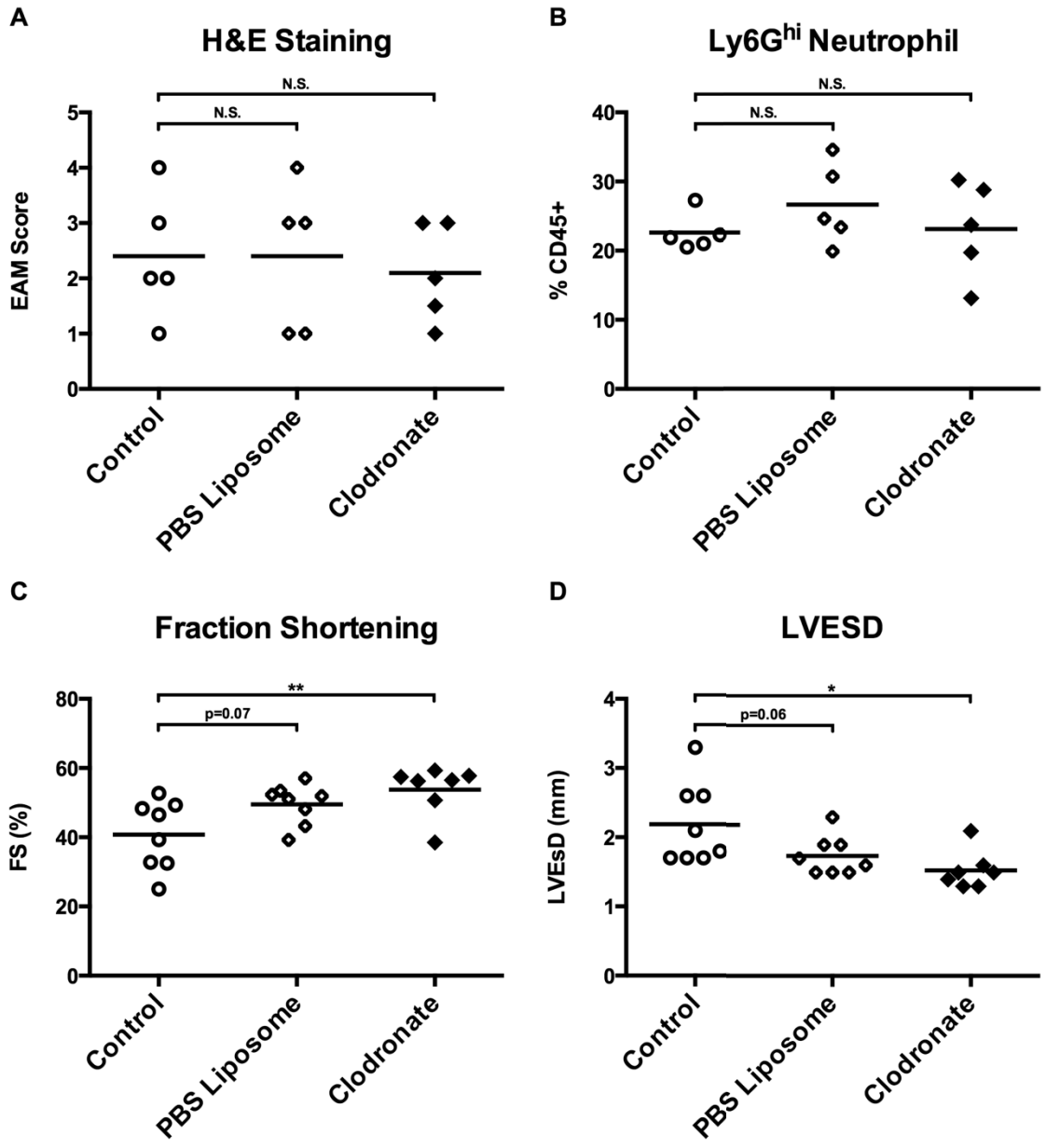

Figure 27. Manipulation of Ly6C^{hi} and Ly6C^{lo} MO/MΦs protects mice from DCMi

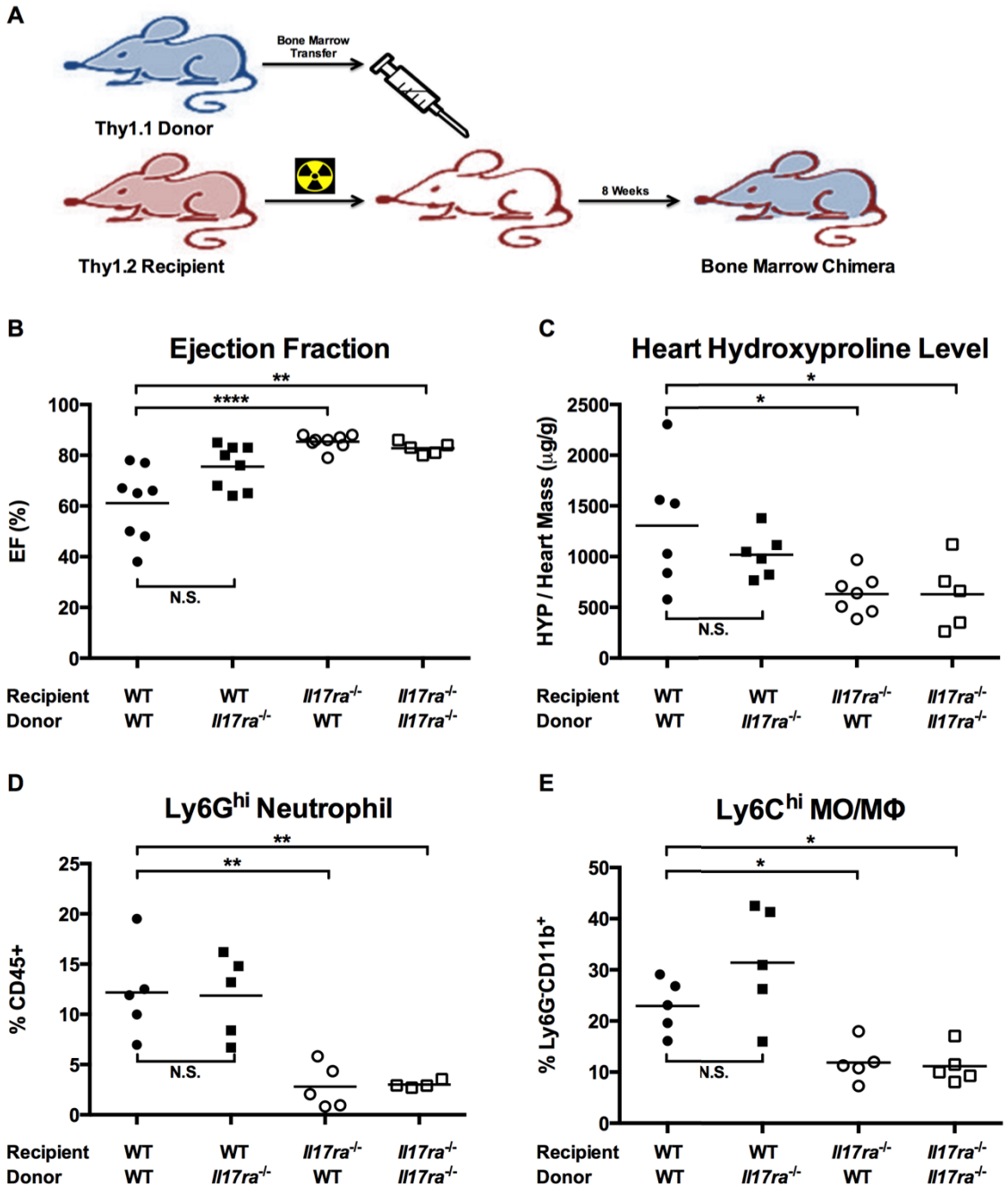

Figure 28. IL-17RA signaling to cardiac resident cells is required for the development of DCMi

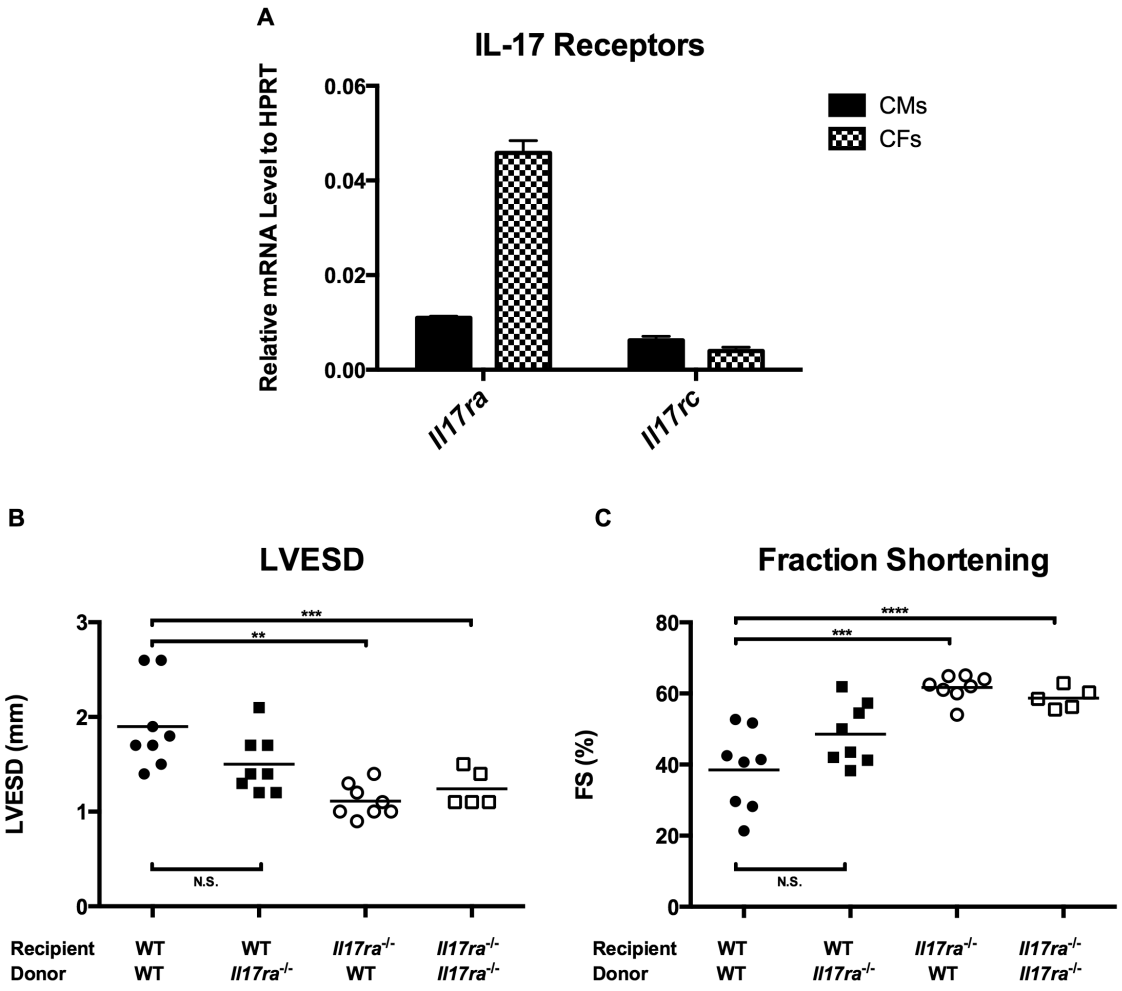

Figure 29. IL-17RA signaling to cardiac resident cells is required for the development of DCMi

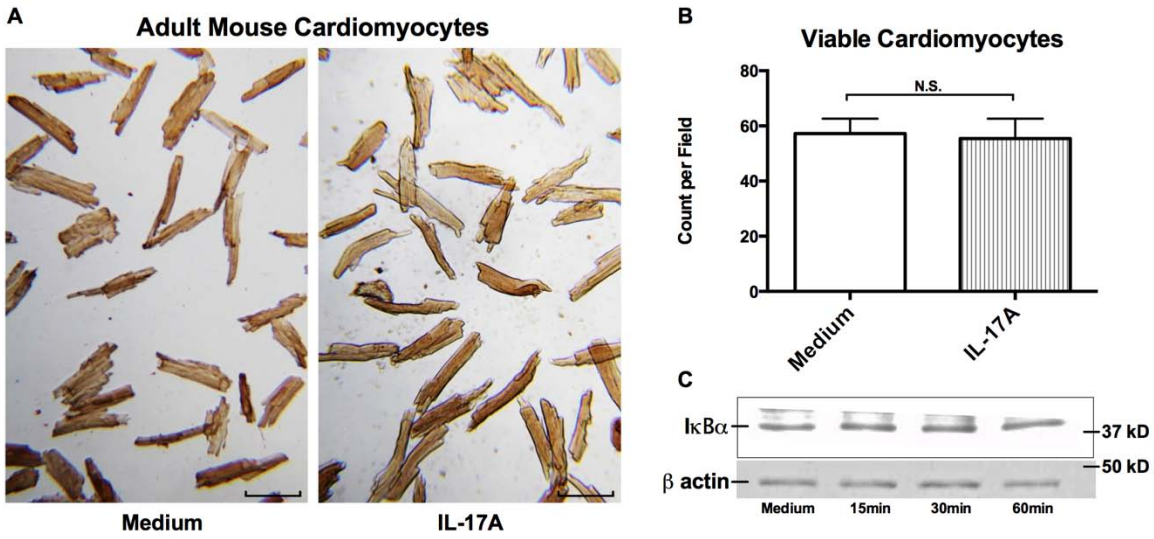

Figure 30. IL-17A has no significant effects on adult mouse cardiomyocytes *in vitro*

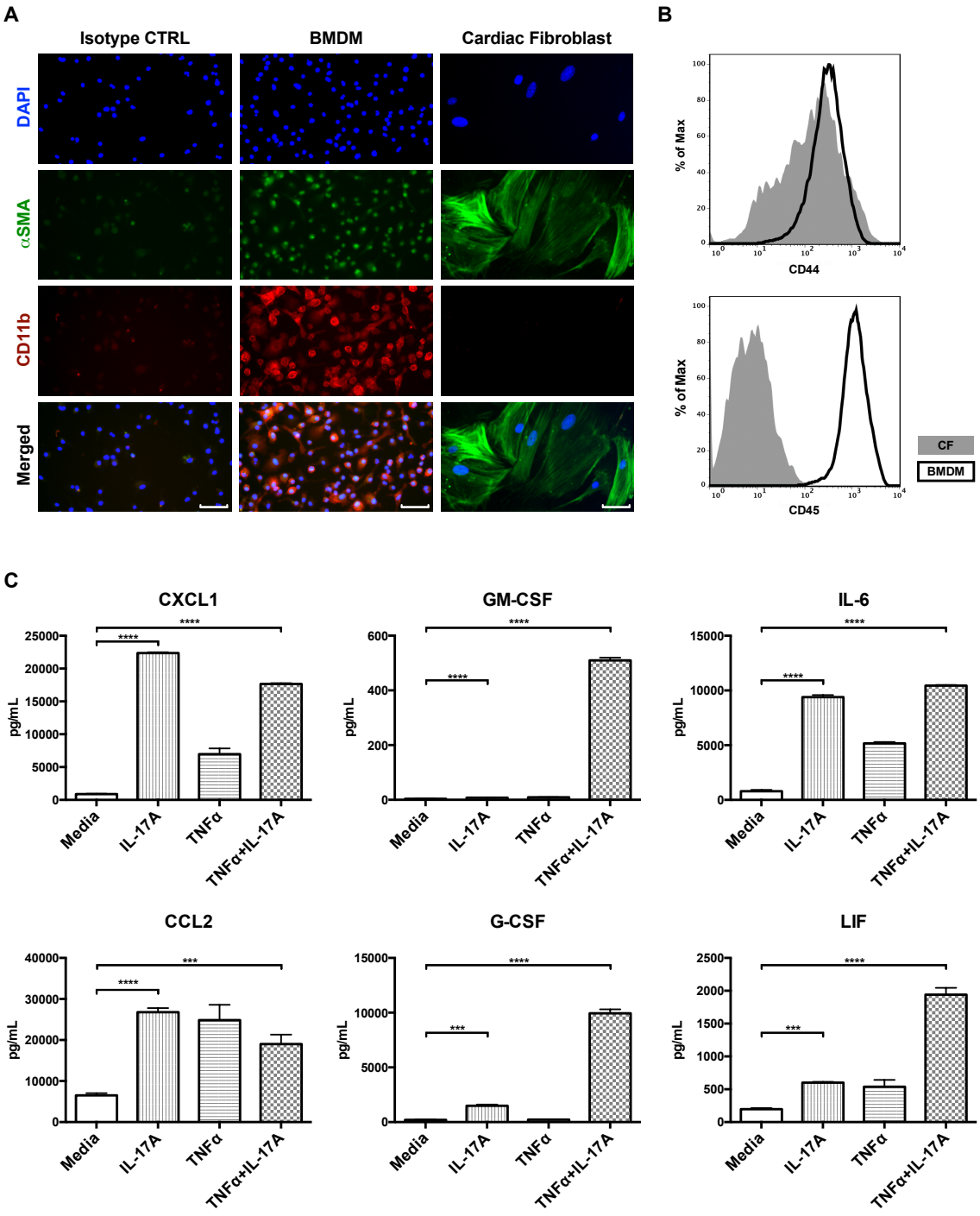

Figure 31. IL-17A stimulates the production of myeloid chemokines and cytokines in adult cardiac fibroblasts *in vitro*

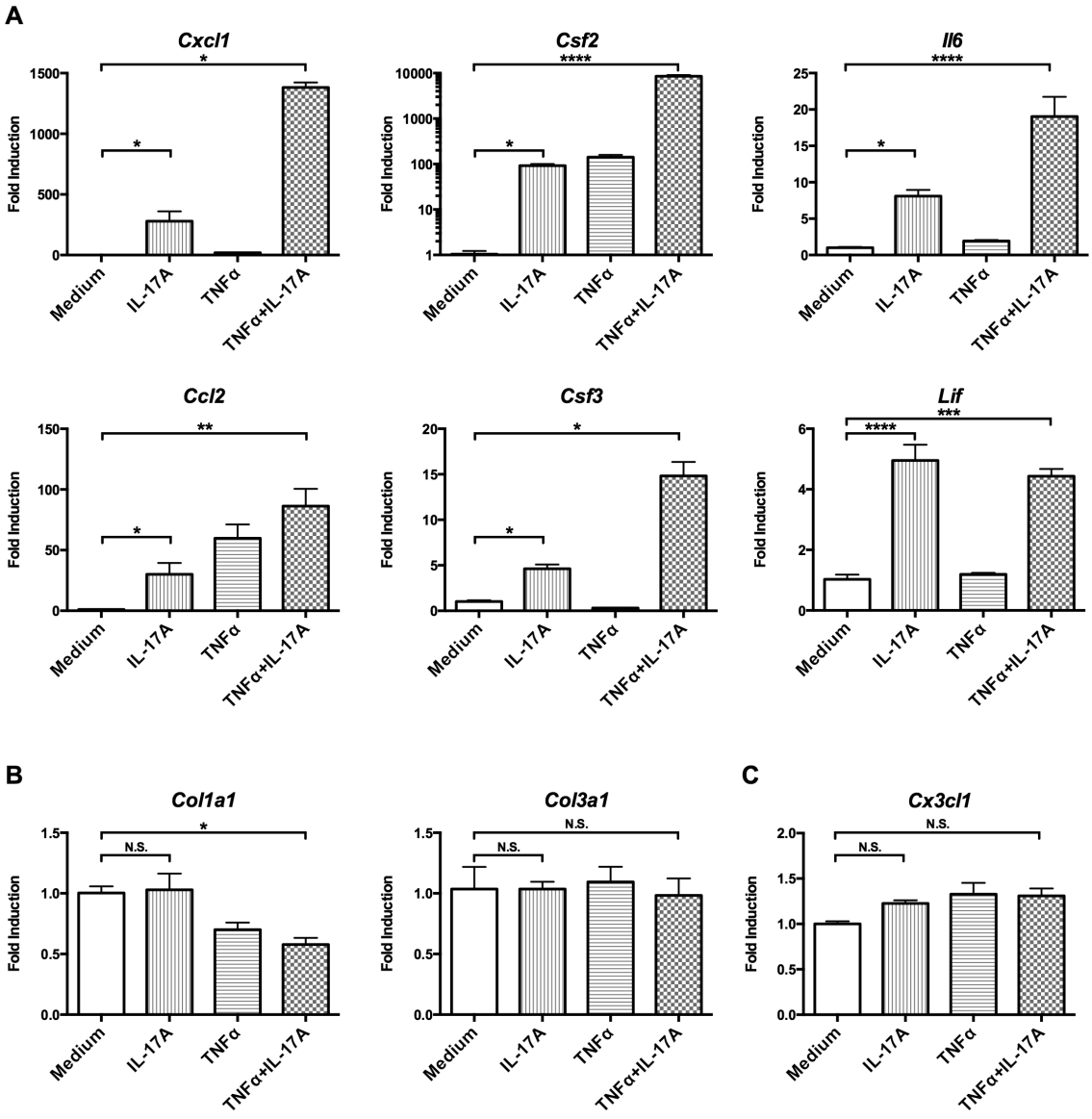

Figure 32. IL-17A stimulates the production of myeloid chemokines and cytokines in adult cardiac fibroblasts *in vitro*

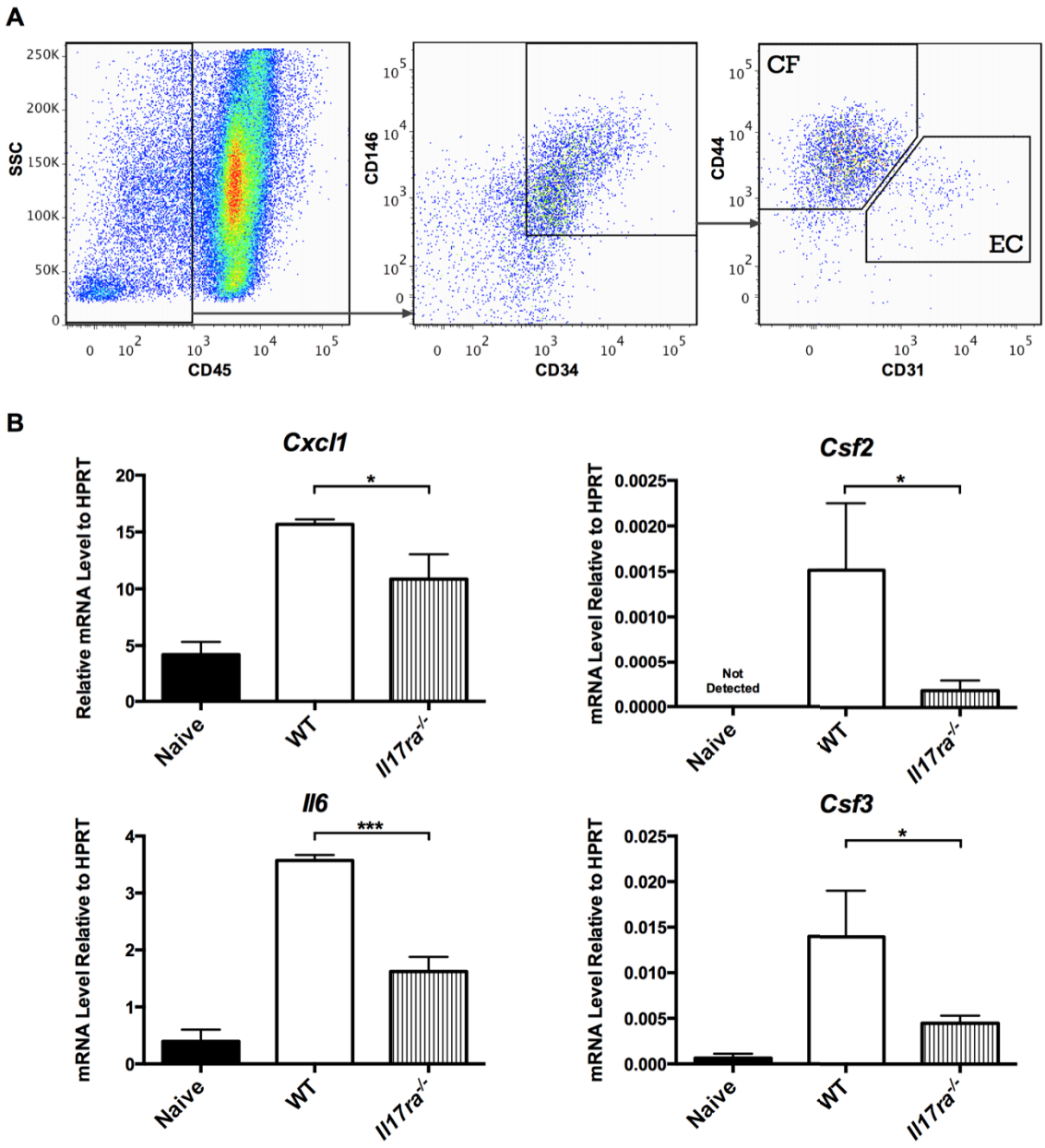

Figure 33. Cardiac fibroblasts react to IL-17A to produce proinflammatory cytokines and chemokines *in vivo*

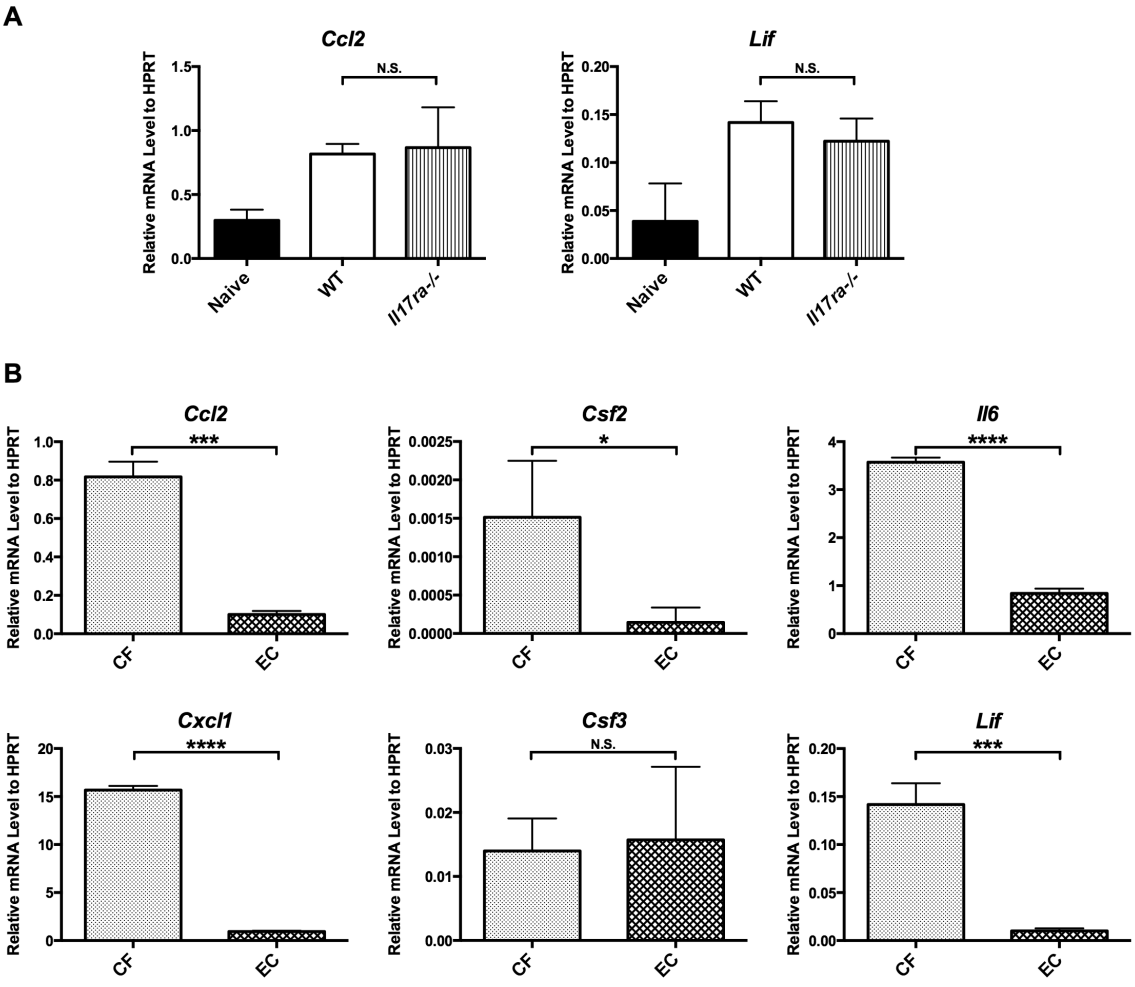

Figure 34. Cardiac fibroblasts react to IL-17A to be the dominant source of proinflammatory cytokines and chemokines *in vivo*

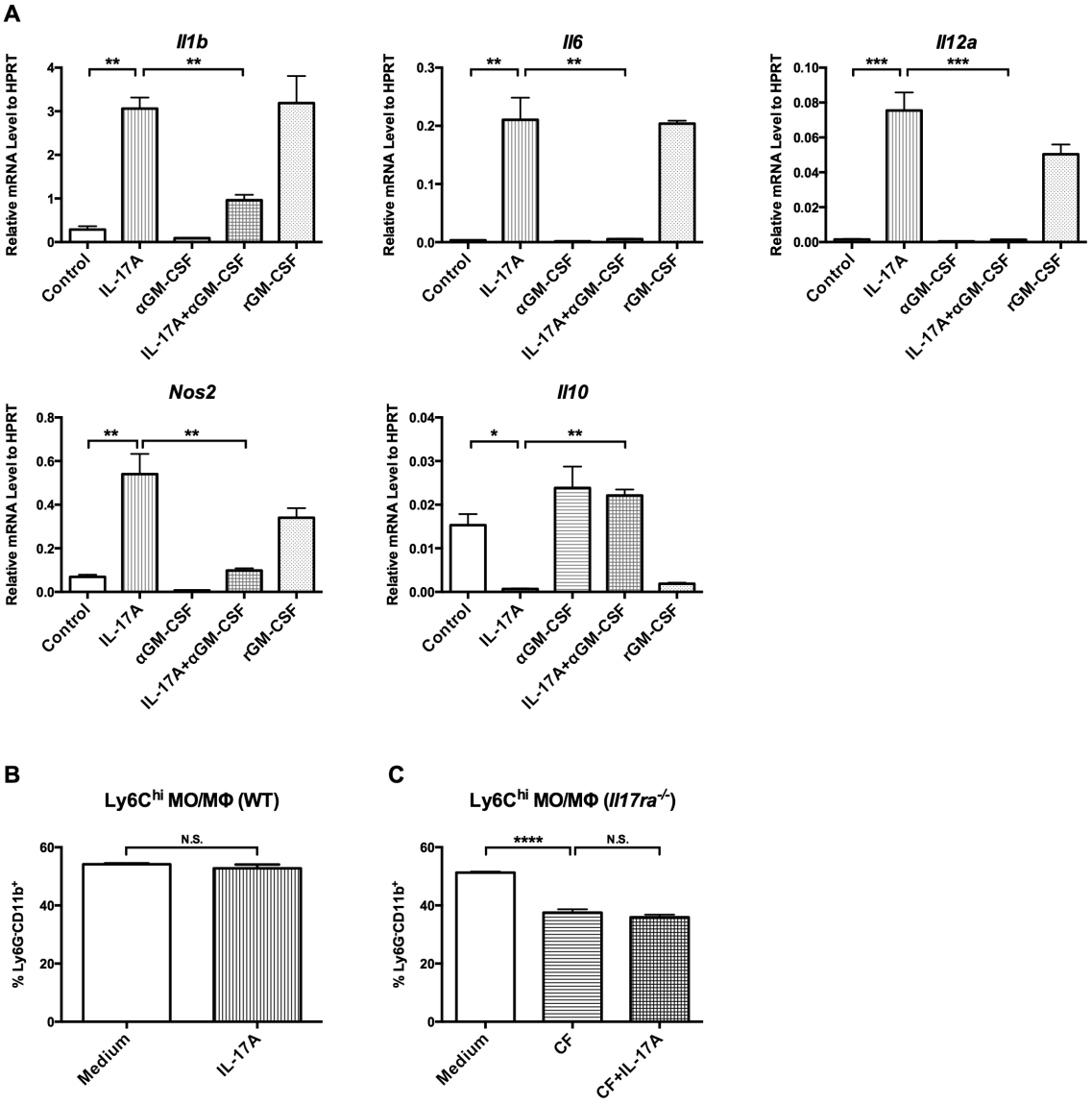

Figure 35. IL-17A drives the differentiation of monocytes *in trans* through cardiac fibroblasts and GM-CSF but has no effect in the balance of Ly6C^{hi} and Ly6C^{lo} populations

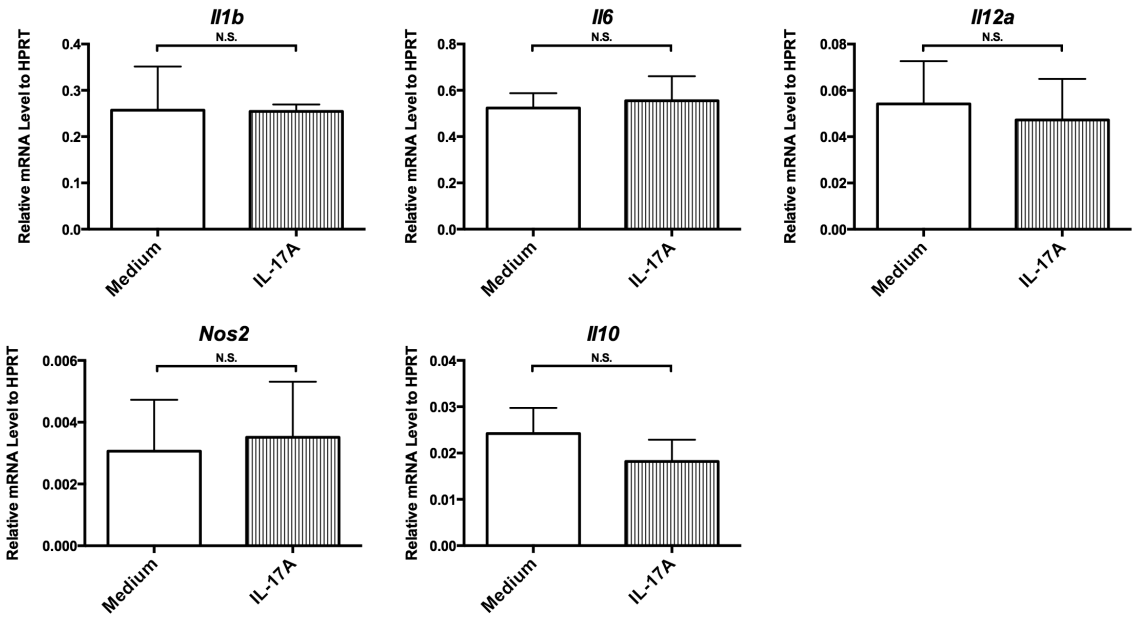

Figure 36. Specificity of IL-17A in indirectly driving the differentiation of monocytes

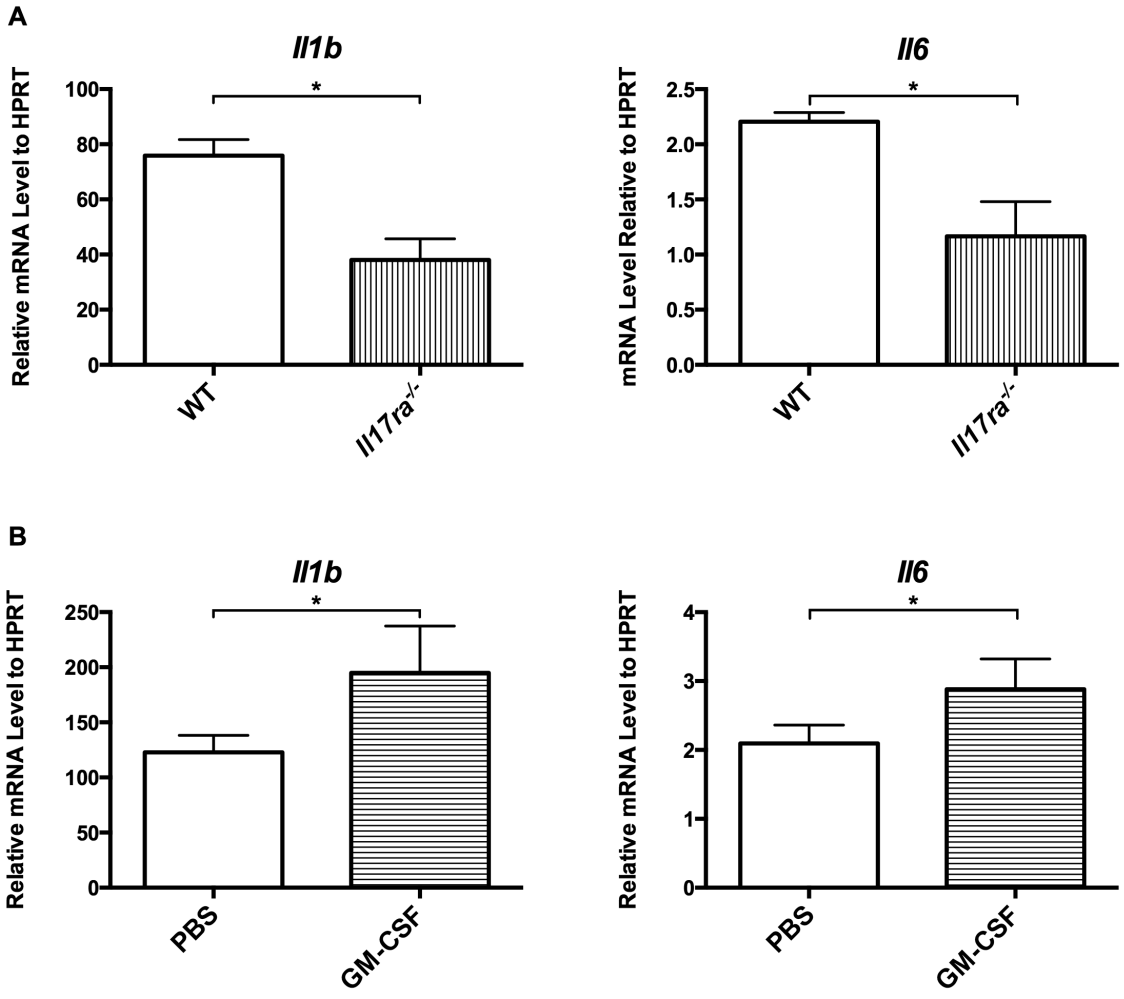

Figure 37. IL-17A and GM-CSF drive cardiac infiltration of Ly6C^{hi} MO/MΦs into proinflammatory phenotype *in vivo*

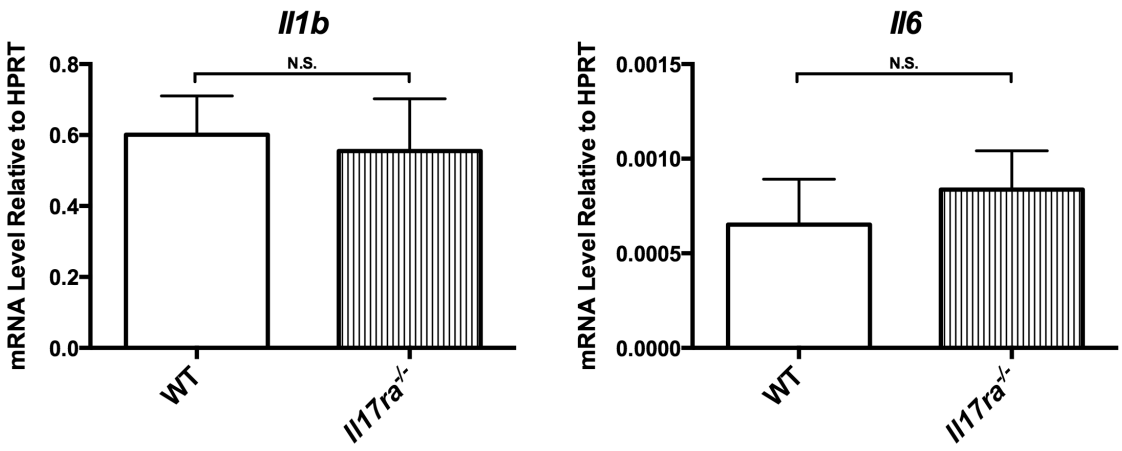

Figure 38. The effects of IL-17A in driving the polarization of Ly6C^{hi} MO/MΦs is local

Table III Transcriptomes of intracardiac Ly6C^{hi} and Ly6C^{lo} MO/MΦs

Gene	Ly6C^{hi} MO/MΦ		Ly6C^{lo} MO/MΦ		p Value	Ly6C^{hi}/Ly6C^{lo} Ratio
	GeoMean	95% CI	GeoMean	95% CI		
Ccr2	2.97E+00	(2.49E+00, 3.45E+00)	2.10E+00	(1.94E+00, 2.26E+00)	0.0270	1.41
Il1b	7.54E+01	(6.40E+01, 8.68E+01)	1.97E+01	(1.48E+01, 2.45E+01)	0.0009	3.84
Il6	1.80E+00	(1.14E+00, 2.47E+00)	2.51E-01	(1.58E-01, 3.43E-01)	0.0093	7.19
Il12a	7.55E-02	(4.03E-02, 1.11E-01)	1.65E-03	(0, 1.03E-02)	0.0170	45.78
Tnf	2.36E+00	(1.39E+00, 3.33E+00)	7.83E-01	(3.67E-01, 1.20E+00)	0.0392	3.02
Lyz2	1.42E+02	(9.97E+01, 1.85E+02)	7.17E+01	(5.03E+01, 9.30E+01)	0.0411	1.99
Nos2	7.13E-02	(3.44E-02, 1.08E-01)	1.57E-02	(1.05E-02, 2.09E-02)	0.0341	4.54
Thbs1	2.68E+00	(1.39E+00, 3.98E+00)	3.83E-01	(3.25E-01, 4.42E-01)	0.0199	7.00
Arg2	1.33E+00	(1.09E+00, 1.58E+00)	4.83E-01	(1.93E-01, 7.73E-01)	0.0136	2.76
Chi3l3	6.80E-01	(4.10E-01, 9.50E-01)	6.28E-02	(1.51E-02, 1.11E-01)	0.0105	10.83
Cx3cr1	1.00E+00	(3.84E-01, 1.63E+00)	2.39E+00	(2.09E+00, 2.70E+00)	0.0212	0.419
Igf1	6.10E-05	(8.28E-06, 1.14E-04)	2.66E-02	(1.15E-02, 4.16E-02)	0.0207	0.002
Mmp9	6.12E-03	(0, 1.49E-02)	3.01E-02	(2.34E-02, 3.68E-02)	0.0194	0.203
Mmp12	1.57E-01	(0, 3.59E-01)	1.15E+00	(7.77E-01, 1.51E+00)	0.0103	0.137

EAM and DCMi were induced in WT mice. Mice were sacrificed 21days post-immunization. Ly6G^{-}CD11b^{+}Ly6C^{hi} (Ly6C^{hi}) and Ly6G^{-}CD11b^{+}Ly6C^{lo} (Ly6C^{lo}) MO/MΦ populations were isolated from mouse hearts by FACS. mRNA levels were determined by real-time qPCR and normalized to the levels of housekeeping gene *Hprt*. Geometric mean of 3 replicates and

95% confidence interval (95% CI) are shown. The ratios of the mRNA levels in Ly6C^{hi} population to Ly6C^{lo} population are calculated. Data are analyzed by unpaired two-tailed Student's t test.

Table IV Purity of Cardiac Fibroblast Culture

Gene	Cardiac Fibroblast Culture		BMDM Culture	
	GeoMean	**95% CI**	**GeoMean**	**95% CI**
Agtr1a	4.29E-03	(2.06E-03, 6.53E-03)	Not Detected	
Ddr2	7.19E-01	(5.60E-01, 8.77E-01)	Not Detected	
Ccr2	Not Detected		1.70E-01	(2.96E-02, 3.11E-01)
Cx3cr1	Not Detected		1.47E-02	(5.26E-03, 2.42E-02)
Mpo	Not Detected		2.80E-02	(6.60E-03, 4.93E-02)
Pgcd1lg2	Not Detected		3.86E-01	(4.53E-02, 7.26E-01)

Primary adult mouse cardiac fibroblasts (CFs) and bone marrow derived macrophages (BMDMs) were isolated from WT BALB/cJ mice and cultured separately. RNA was isolated from CF and BMDM cultures of 10^5 cells. mRNA levels of fibroblast-specific genes (*Agtr1a* and *Ddr2*) and myeloid cell-specific genes (*Ccr2*, *Cx3cr1*, *Mpo* and *Pgcd1lg2*) were determined by real-time qPCR and normalized to housekeeping gene *Hprt*. Geometric mean of 3 replicates and 95% confidence interval (95% CI) are shown.

3.4 Figure Legends

Figure 21. *Il17ra*$^{-/-}$ mice are protected from DCMi

EAM and DCMi were induced in WT and *Il17ra*$^{-/-}$ mice. 63 days post-immunization, naïve and immunized mice underwent echocardiography and were sacrificed. This experiment was independently performed three times with similar results.

(A) Representative histopathology of *Il17ra*$^{-/-}$ and WT mice hearts showing Masson's trichrome blue staining. Fibrotic tissue was stained blue. 2.5X magnification. Scale bars represent 1mm.

(B) Cardiac fibrosis in *Il17ra*$^{-/-}$ and WT mice scored using Masson's trichrome blue staining.

(C) Cardiac hydroxyproline assay normalized to heart weight.

(D) Representative M-Mode echocardiography of naïve, WT and *Il17ra*$^{-/-}$ mice.

(E) Ejection fraction (%) of naïve, WT and *Il17ra*$^{-/-}$ mice by echocardiography. Dash line marks 60%, the threshold for severe DCMi.

(B), (C) and (E) Data points represent individual mice. Bars represent mean. Data were analyzed by one-way ANOVA followed by Tukey's post-test. *, $p<0.05$; **, $p<0.01$; ****, $p<0.0001$.

Figure 22. *Il17ra*$^{-/-}$ mice develop EAM comparable to WT and *Il17a*$^{-/-}$ mice

EAM and DCMi were induced in WT, *Il17a*$^{-/-}$ and *Il17ra*$^{-/-}$ mice. Mice were sacrificed 21 days post-immunization. This experiment was independently performed three times with similar results.

(A) Representative histopathology of WT, *Il17a*$^{-/-}$ and *Il17ra*$^{-/-}$ mice hearts showing H&E staining. 10X magnification.

(B) EAM in WT, *Il17a*$^{-/-}$ and *Il17ra*$^{-/-}$ mice scored using H&E staining. Data points represent individual mice. Bars represent mean. Data are analyzed by Kruskal-Wallis test followed by Dunn's procedure.

Figure 23. *Il17ra*$^{-/-}$ mice are protected from DCMi

EAM and DCMi were induced in WT and *Il17ra*$^{-/-}$ mice. 63 days post-immunization, naïve and immunized mice underwent echocardiography and were sacrificed. This experiment was independently performed three times with similar results.

(A) Left ventriclar end-diastolic dimension (LVEDD); (B) Left ventriclar end-systolic dimension (LVESD); (C) Fraction shortening (FS); (D) Relative wall thickness (RWT) ; (E) Heart weight / body weight ratio (‰) of naïve, WT and *Il17ra*$^{-/-}$ mice by echocardiography. Data points represent individual mice. Bars represent mean. Data were analyzed by one-way ANOVA followed by Tukey's post-test. *, $p<0.05$; ****, $p<0.0001$.

Figure 24. IL-17RA deficiency alters the composition of heart-infiltrating cells

EAM and DCMi were induced in WT or *Il17ra*$^{-/-}$ mice. Mice were sacrificed 21 days post-immunization. The composition of heart-infiltrating cells was analyzed by flow cytometry. This experiment was independently performed four times with similar results.

(A) Representative gating of heart-infiltrating myeloid cells.

(B) Total intracardiac CD45^{+} leukocytes in WT and *Il17ra*$^{-/-}$ mice.

(C) Intracardiac Ly6G^{hi} neutrophils as a proportion of total CD45^{+} leukocytes.

(D) Intracardiac Ly6G^{-}CD11b^{+} MO/MΦs as a proportion of total CD45^{+} leukocytes.

(E) Ly6C^{hi} MO/MΦs as a proportion of Ly6G^{-}CD11b^{+} population.

(F) Ly6C^{hi} to Ly6C^{lo} MO/MΦ ratio.

(B) ~ (F) Data points represent individual mice. Bars represent mean. Data are analyzed by unpaired two-tailed Student's t test. **, $p<0.01$.

Figure 25. IL-17RA deficiency has no effects on infiltration of CD4^{+} T cell and SiglecF^{+} eosinophil in the heart or the balance of Ly6C^{hi} and Ly6C^{lo} monocytes in the spleen

EAM and DCMi were induced in WT and *Il17ra*$^{-/-}$ mice. Mice were sacrificed 21 days post-immunization. The compositions of heart-infiltrating cells and splenocytes were analyzed by flow cytometry. This experiment was independently performed four times with similar results.

(A) Intracardiac CD4^{+} T cells as a proportion of total CD45^{+} leukocytes.

(B) Intracardiac SiglecF^{+} eosinophils as a proportion of total CD45^{+} leukocytes.

(C) Ly6C^{hi} monocytes as a proportion of total Ly6G^{-}CD11b^{+} population in the spleen.

(D) Ly6G^{hi} neutrophils as a proportion of total CD45^{+} leukocytes in the spleen.

(A) ~ (D) Data points represent individual mice. Bars represent mean. Data are analyzed by unpaired two-tailed Student's t test. ****, $p<0.0001$.

Figure 26. Transcriptomes and functions of intracardiac Ly6C^{hi} and Ly6C^{lo} MO/MΦs

(A) EAM and DCMi were induced in WT mice. Mice were sacrificed 21 days post-immunization. Ly6G^{-}CD11b^{+}Ly6C^{hi} (Ly6C^{hi}) and Ly6G^{-}CD11b^{+}Ly6C^{lo} (Ly6C^{lo}) MO/MΦ populations were isolated from mouse hearts by FACS. mRNA levels were determined by real-time quantitative PCR, normalized to housekeeping gene *Hprt*. This experiment was independently performed twice with similar results. Detailed data are shown in **Table S1**. For each individual gene, the ratio of its expression in Ly6C^{hi} population versus that in Ly6C^{lo} was calculated and plotted in log scale. Ratio greater than one indicates the gene was upregulated in Ly6C^{hi} MO/MΦs (orange), and ratio smaller than one indicates the gene was upregulated in Ly6C^{lo} MO/MΦs (blue).

(B) ~ (D) EAM and DCMi were induced in WT mice. On days 14, 16, 18 and 20, mice were injected *i.v.* with 250μL PBS (Control), PBS-loaded liposome (PBS Liposome) or clodronate-loaded liposome (Clodronate), respectively. Mice were sacrificed 21 days post-immunization. The composition of heart-infiltrating cells was analyzed by flow cytometry. This experiment was independently performed twice with similar results.

(B) $Ly6C^{hi}$ MO/MΦs as a proportion of $Ly6G^{-}CD11b^{+}$ population.

(C) $Ly6C^{hi}$ to $Ly6C^{lo}$ MO/MΦ ratio.

(D) Intracardiac $Ly6G^{-}CD11b^{+}$ MO/MΦs as a proportion of total $CD45^{+}$ leukocytes.

(E) ~ (G) EAM and DCMi were induced in WT mice. From day 14 to day 35, mice were injected *i.v.* every other day with 250μL PBS (Control), PBS-loaded liposome (PBS Liposome) or clodronate-loaded liposome (Clodronate), respectively. 63 days post-immunization, mice underwent echocardiography and were sacrificed. This experiment was independently performed twice with similar results.

(E) Ejection fraction (%) by echocardiography. Dash line marks 60%, the threshold for severe DCMi.

(F) Heart weight / body weight ratio (‰).

(G) Cardiac hydroxyproline assay normalized to heart weight.

(B) ~ (G) Data points represent individual mice. Bars represent mean. Data were analyzed by one-way ANOVA followed by Tukey's post-test. *, $p<0.05$; **, $p<0.01$; ***, $p<0.001$.

Figure 27. Manipulation of Ly6C^{hi} and Ly6C^{lo} MO/MΦs protects mice from DCMi

(A) and (B) EAM and DCMi were induced in WT mice. On days 14, 16, 18 and 20, mice were injected *i.v.* every with 250μL PBS (Control), PBS-loaded liposome (PBS Liposome) or clodronate-loaded liposome (Clodronate), respectively. Mice were sacrificed 21 days post-immunization. This experiment was independently performed twice with similar results.

(A) EAM severity in mice treated with PBS, PBS-loaded or clodronate-loaded liposomes were scored using H&E staining. Data points represent individual mice. Bars represent mean. Data are analyzed by Kruskal-Wallis test followed by Dunn's procedure.

(B) The composition of heart-infiltrating cells was analyzed by flow cytometry, showing Ly6G^{hi} neutrophils as a proportion of total CD45^{+} leukocytes.

(C) ~ (D) EAM and DCMi were induced in WT mice. From day 14 to day 35, mice were injected *i.v.* every other day with 250μL PBS, PBS-loaded liposome or clodronate-loaded liposome, respectively. 63 days post-immunization, mice underwent echocardiography. This experiment was independently performed twice with similar results. (C) Fraction shortening (FS) and (D) Left ventriclar end-systolic dimension (LVESD).

(B) ~ (D) Data points represent individual mice. Bars represent mean. Data were analyzed by one-way ANOVA followed by Tukey's post-test. *, $p<0.05$; **, $p<0.01$.

Figure 28. IL-17RA signaling to cardiac resident cells is required for the development of DCMi

(A) Schemiatic of the generation of bone marrow chimeras: bone marrows were transferred from WT or *Il17ra*$^{-/-}$ Thy1.1 donor into lethally irradiated *Il17ra*$^{-/-}$ or WT Thy1.2 recipients. EAM and DCMi were induced 8 weeks after transfer.

(B) and (C) 63 days post-immunization, mice underwent echocardiography and were sacrificed. This experiment was independently performed four times with similar results.

(B) Ejection fraction (%) of bone marrow chimeras with depicted genotypes.

(C) Cardiac hydroxyproline assay normalized to heart weight.

(D) and (E) 21 days post-immunization, mice were sacrificed, and their heart-infiltrating cells were analyzed by flow cytometry. This experiment was independently performed three times with similar results.

(D) Ly6G^{hi} neutrophil as a proportion of intracardiac CD45^{+} leukocytes in bone marrow chimeras with depicted genotype.

(E) Ly6C^{hi} MO/MΦs as a proportion of intracardiac Ly6G^{-} CD11b^{+}population.

(B) ~ (E) Data points represent individual mice. Bars represent mean. Data are analyzed by two-way ANOVA (genotype of donor vs genotype of recipient) followed by Tukey's post-test. *, $p<0.05$; **, $p<0.01$; ****, $p<0.0001$.

Figure 29. IL-17RA signaling to cardiac resident cells is required for the development of DCMi

(A) Primary adult mouse cardiomyocytes and cardiac fibroblasts were isolated from naïve WT mice. mRNA of *Il17ra* and *Il17rc* were detected by real-time qPCR. Data are shown as Mean+SEM of 3 replicates.

(B) and (C) Bone marrow chimeras were generated by transferring bone marrow from WT or *Il17ra*$^{-/-}$ Thy1.1 donor mice into lethally irradiated *Il17ra*$^{-/-}$ or WT Thy1.2 recipients. EAM and DCMi were induced 8 weeks after transfer. 63 days post-immunization, mice underwent echocardiography and were sacrificed. This experiment was independently performed four times with similar results.

(B) LVESD of bone marrow chimeras with depicted genotypes.

(C) Fraction shortening (%) of bone marrow chimeras with depicted genotypes.

(B) and (C) Data points represent individual mice. Bars represent mean. Data are analyzed by two-way ANOVA (genotype of donor vs genotype of recipient) followed by Tukey's post-test. **, $p<0.01$; ***, $p<0.001$; ****, $p<0.0001$.

Figure 30. IL-17A has no significant effects on adult mouse cardiomyocytes *in vitro*

(A) and (B) Primary adult mouse cardiomyocytes (CMs) were cultured with or without rIL-17A (100ng/mL) for 24 hours. This experiment was independently performed three times with similar results.

(A) Bright field microscopy (10X) showed cell morphology and viability of rIL-17A-treated and control CMs. Scale bars represent 100μm.

(B) Viable CMs were counted in 5 different fields (10X). Data are shown as Mean+SEM and analyzed by unpaired two-tailed Student's t test.

(C) Primary adult CMs were stimulated with rIL-17A (100ng/mL) for 15min, 30min or 60min. Western blot detected no degradation of IκBα in rIL-17A treated CMs.

Figure 31. IL-17A stimulates the production of myeloid chemokines and cytokines in adult cardiac fibroblasts *in vitro*

(A) Primary adult mouse cardiac fibroblasts (CFs) and bone marrow derived macrophages (BMDMs) were cultured on chamber slides. Immunofluorescence microscopy (20X) showed that CFs expressed α-smooth muscle actin (αSMA) (green) but not CD11b (red). BMDMs were stained with isotype-matched antibodies as isotype control. Scale bars represent 100μM.

(B) The expression of surface markers CD44 and CD45 in CF (filled) and BMDM (open) cultures were analyzed by flow cytometry. Levels of expression on all 7-AAD-negative viable cells from respective cultures were plotted on histograms.

(C) CFs were cultured with rIL-17A (100ng/mL), rTNFα (5ng/mL) or two cytokines combined for 24 hours. Supernatant were collected after culture, and the levels of CXCL1, CCL2, GM-CSF, G-CSF, IL-6 and LIF were measured by ELISA. These experiment were independently performed three times with similar results. Data are shown as Mean+SEM of 3 replicates and analyzed by one-way ANOVA followed by Tukey's post-test. ***, $p<0.001$; ****, $p<0.0001$.

Figure 32. IL-17A stimulates the production of myeloid chemokines and cytokines in adult cardiac fibroblasts *in vitro*

Primary adult mouse cardiac fibroblasts (CFs) from naïve WT mice were cultured with rIL-17A (100ng/mL), rTNFα (5ng/mL) or two cytokines combined for 6 hours. RNA were isolated from CFs and the mRNA levels of (A) *Cxcl1*, *Ccl2*, *Csf2*, *Csf3*, *Il6* and *Lif*; (B) *Col1a1* and *Col3a1*; (C) *Cx3cl1* were determined by real-time qPCR and normalized to housekeeping gene *Hprt*. These experiment were independently performed three times with similar results. Data are shown as Mean+SEM of 3 replicates and analyzed by one-way ANOVA followed by Tukey's post-test. *, $p<0.05$; **, $p<0.01$; ***, $p<0.001$; ****, $p<0.0001$.

Figure 33. Cardiac fibroblasts react to IL-17A to produce proinflammatory cytokines and chemokines *in vivo*

EAM and DCMi were induced in WT and *Il17ra*$^{-/-}$ mice. Mice were sacrificed 21 days post-immunization. CD45^{-}CD34^{+}CD146^{+}CD44^{hi}CD31^{-} cardiac fibroblasts (CFs) and CD45^{-}CD34^{+}CD146^{+}CD44^{lo}CD31^{hi} endothelial cells (ECs) were isolated from mouse hearts by FACS. This experiment was independently performed twice with similar results.

(A) Representative gating of CFs and ECs.

(B) mRNA levels of *Cxcl1*, *Csf2*, *Csf3* and *Il6* in CFs from WT and *Il17ra*$^{-/-}$ mice were determined by real-time quantitative PCR and normalized to housekeeping gene *Hprt*. Data are shown as Mean+SEM of 3 replicates and analyzed by unpaired two-tailed Student's t test. *, $p<0.05$; ***, $p<0.001$.

Figure 34. Cardiac fibroblasts react to IL-17A to be the dominant source of proinflammatory cytokines and chemokines *in vivo*

EAM and DCMi were induced in WT and *Il17ra*$^{-/-}$ mice. Mice were sacrificed 21 days post-immunization. CD45^{-}CD34^{+}CD146^{+}CD44^{hi}CD31^{-} cardiac fibroblasts (CFs) and CD45^{-}CD34^{+}CD146^{+}CD44^{lo}CD31^{hi} were isolated from mouse hearts by FACS. This experiment was independently performed twice with similar results.

(A) mRNA levels of *Ccl2* and *Lif* in CFs from WT and *Il17ra*$^{-/-}$ mice were determined by real-time quantitative PCR and normalized to housekeeping gene *Hprt*.

(B) mRNA levels of *Ccl2*, *Cxcl1*, *Csf2*, *Csf3*, *Il6* and *Lif* in CFs and ECs from WT mice were determined by real-time quantitative PCR and normalized to housekeeping gene *Hprt*.

(A) and (B) Data are shown as Mean+SEM of 3 replicates and analyzed by unpaired two-tailed Student's t test. *, $p<0.05$; ***, $p<0.001$; ****, $p<0.0001$.

Figure 35. IL-17A drives the differentiation of monocytes *in trans* through cardiac fibroblasts and GM-CSF but has no effect in the balance of Ly6C^{hi} and Ly6C^{lo} populations

(A) Ly6G^{-}CD11c^{-}CD11b^{+}F4/80^{-}Ly6C^{hi} spleen monocytes were isolated from naïve *Il17ra*$^{-/-}$ mice by FACS, and co-cultured with primary adult cardiac fibroblasts (CFs) from naïve WT mice for 48 hours under various conditions as depicted. mRNA were isolated from FACS-sorted monocytes in the end of co-culture. The mRNA levels of *Il1b*, *Il6*, *Il12*a, *Nos2* and *Il10* were measured by real-time qPCR, and normalized to *Hprt*. This experiment was independently performed three times with similar results.

(B) Ly6G^{-}CD11c^{-}CD11b^{+}F4/80^{-} splenic monocytes with mixed Ly6C^{hi} and Ly6C^{lo} populations were isolated from naïve WT mice by FACS, and

stimulated with 100ng/mL rIL-17A for 48 hours. Ly6C^{hi} monocyte as a proportion of total was analyzed by flow cytometry.

(C) Ly6G^{-}CD11c^{-}CD11b^{+}F4/80^{-} splenic monocytes with mixed Ly6C^{hi} and Ly6C^{lo} populations were isolated from naïve *Il17ra*$^{-/-}$ mice by FACS, and cultured alone (Medium), with WT CFs (CF), or with WT CF and rIL-17A (CF+IL-17A) for 48 hours. Ly6C^{hi} monocytes as a proportion of total was analyzed by flow cytometry.

(A) ~ (C) Data are shown as Mean+SEM of 3 replicates and analyzed by (A) and (C) one-way ANOVA followed by Tukey's post-test, or (B) unpaired two-tailed Student's t test. *, $p<0.05$; **, $p<0.01$; ***, $p<0.001$; ****, $p<0.0001$.

Figure 36. Specificity of IL-17A in indirectly driving the differentiation of monocytes

Ly6G^{-}CD11c^{-}CD11b^{+}F4/80^{-}Ly6C^{hi} spleen monocytes were isolated from naïve *Il17ra*$^{-/-}$ mice by FACS, and co-cultured with primary adult cardiac fibroblasts (CFs) from naïve *Il17ra*$^{-/-}$ mice for 48 hours with or without 100ng/mL rIL-17A. mRNA were isolated from FACS-sorted monocytes in the end of co-culture. The mRNA levels of *Il1b*, *Il6*, *Il12*a, *Nos2* and *Il10* were measured by real-time qPCR, and normalized to *Hprt*. Data are shown as Mean+SEM of 3 replicates and analyzed by unpaired two-tailed Student's t test.

Figure 37. IL-17A and GM-CSF drive cardiac infiltration of Ly6C^{hi} MO/MΦs into proinflammatory phenotype *in vivo*

(A) EAM and DCMi were induced in WT and *Il17ra*$^{-/-}$ mice. Mice were sacrificed 21 days post-immunization. Ly6G^{-}CD11b^{+}Ly6C^{hi} MO/MΦs were isolated from mouse hearts by FACS.

(B) EAM and DCMi were induced in WT mice. Mice were injected *i.p.* with PBS or 0.5μg rGM-CSF 36 hours and 12 hours before day 21 sacrifice. Ly6G^{-}CD11b^{+}Ly6C^{hi} MO/MΦs were isolated from mouse hearts by FACS.

(A) and (B) mRNA levels of *Il1b* and *Il6* were determined by real-time quantitative PCR and normalized to housekeeping gene *Hprt*. This experiment was independently performed twice with similar results. Data are shown as Mean+SEM of 3 replicates and analyzed by unpaired two-tailed Student's t test. *, $p<0.05$.

Figure 38. The effects of IL-17A in driving the polarization of Ly6C^{hi} MO/MΦs is local

EAM and DCMi were induced in WT and *Il17ra*$^{-/-}$ mice. Mice were sacrificed 21 days post-immunization. Ly6G^{-}CD11b^{+}Ly6C^{hi} MO/MΦs were isolated from mouse spleen by FACS. mRNA levels of *Il1b*, *Il6* were determined by real-time quantitative PCR and normalized to housekeeping gene *Hprt*. Data are shown as Mean+SEM of 3 replicates and analyzed by unpaired two-tailed Student's t test.

3.5 Materials and Methods

Mice

Il17ra$^{-/-}$ founder mice backcrossed 10 generations from C57BL/6 to BALB/c background were provided by Amgen Inc. and Dr. Jay Kolls. WT BALB/cJ and CBy.PL(B6)-Thy1a/ScrJ (Thy1.1) founder mice were purchased from the Jackson Laboratory. *Il17ra*$^{-/-}$ mice were crossed to Thy1.1 mice and bred to homozygosity at both loci for the generation of bone marrow chimeras. All mice were maintained in the Johns Hopkins University School of Medicine specific-pathogen free vivarium. Age-matched WT, Thy1.1 and *Il17ra*$^{-/-}$ mice bred separately in the Johns Hopkins vivarium were used for experiments involving multiple gene backgrounds. For experiments conducted exclusively on WT background, WT BALB/cJ (000651) mice were purchased from the Jackson Laboratory and housed in the Johns Hopkins vivarium for a week before immunization. Experiments were conducted on 6-10 week old male mice, and in compliance with the Animal Welfare Act and the principles set forth in the Guide for the Care and Use of Laboratory Animals. All methods and protocols are approved by the Animal Care and Use Committee of The Johns Hopkins University.

Induction of EAM and DCMi

We employed the myocarditogenic peptide MyHC$\alpha_{614\text{-}629}$ (Ac-SLKLMATLFSTYASAD) commercially synthesized by fMOC chemistry and purified to a minimum of 90% by HPLC (Genscript). On days 0 and 7,

mice received axillary *s.c.* immunizations of 100 μg of MyHC$\alpha_{614\text{-}629}$ peptide emulsified in CFA (Sigma) supplemented to 5 mg/mL of heat-killed *M. tb* strain H37Ra (Difco). On day 0, mice also received 500 ng of pertussis toxin *i.p.* (List Biologicals).

Assessment of EAM and DCMi Histopathology

Mice were evaluated for the development of EAM and DCMi on day 21 and day 63 respectively. Heart tissues were fixed in SafeFix solution (Fisher Scientific). Tissues were embedded longitudinally, and 5 μm serial sections were cut and stained with H&E or Masson's Trichrome Blue (HistoServ, Gaithersburg, MD). Myocarditis severity was evaluated by H&E staining of myocardium area infiltrated with hematopoietic cells, according to the following scoring system: grade 0, no inflammation; grade 1, less than 10% of the heart section is involved; grade 2, 10-25%; grade 3, 25-50%; grade 4, 50-75%; grade 5, more than 75%. Grading was performed by grading five sections per heart by two independent, blinded investigators and averaged. Cardiac fibrosis was evaluated by measuring the area of blue staining of fibrosis as a proportion of heart cross section.

Echocardiography

Trans-thoracic echocardiography was performed using the Acuson Sequoia C256 ultrasonic imaging system (Siemens). Conscious, depilated mice were held in supine position. The heart was imaged in two-dimensional (2-D) mode in the parasternal short axis view. From this mode, an M-mode cursor was positioned perpendicular to the

interventricular septum (IVS) and the left ventricular posterior wall (LVPW) at the level of the papillary muscles. From M-mode, the wall thicknesses and chamber dimensions were measured. For each mouse, three to five values for each measurement were obtained and averaged for evaluation. The left ventricular end-diastolic dimension (LVEdD), LV end-systolic dimension (LVEsD), interventricular septal wall thickness at end-diastole (IVSD), and LV posterior wall thickness at end diastole (LVPWTED) were measured from a frozen M-mode tracing. Fractional shortening (FS), ejection fraction (EF) and relative wall thickness (RWT) were calculated from these parameters as previously described (Baldeviano et al., 2010).

Hydroxyproline Assay

Heart samples were weighed, homogenized in de-ionized water, and then hydrolyzed in 6N HCl overnight at 120°C. Lysates are transferred and desiccated in 96-well plates, and reconstituted in de-ionized water. After incubation with 50 mM Chloramine T (Sigma), followed by 1M dimethylaminobenzaldehyde (Sigma), the OD values are read at 570 nm. The concentration of hydroxyproline is determined by a 1-100 μg/mL standard curve of hydroxyproline (Sigma) and normalized to starting heart sample mass.

Flow Cytometry Analysis and FACS Isolation of Heart Infiltrating Cells, CFs and ECs

For flow cytometry analysis, single cell suspension were made from mouse spleen by gentle dissociation or from mouse hearts by perfusing for 3 min with 1x PBS + 0.5% FBS, and digested in GentleMACS C Tubes according to manufacturer's instructions (Miltenyi Biotec). Viability was determined by LIVE/DEAD staining according to manufacturer's instructions (Life Techonologies). Cells were blocked with αCD16/32 (eBiosciences), and surface markers were stained with fluorochrome-conjugated mAbs (eBioscience, BD Pharmingen, BioLegend). Samples were acquired on the LSR II cytometer running FACSDiva 6 (BD Immunocytometry). Data were analyzed with FlowJo 7.6 (Treestar Software). For FACS isolation, single cell suspension from mouse heart or spleen was first purified with a 20% - 80% Percoll (GE Healthcare) gradient to eliminate dead cells and debris. Cells were then stained with fluorochrome-conjugated mAbs (eBioscience, BD Pharmingen, BioLegend) and sorted with Beckman Coulter MoFlo Cell Sorter.

Treatment of PBS-loaded or clodronate-loaded liposomes and rGM-CSF during EAM and DCMi

PBS-loaded and clodronate-loaded liposomes were purchased from ClodLip BV (Haalem, the Netherlands). Recombinant mouse GM-CSF was purchased from R&D Systems. For liposome treatment, 250μL of PBS, PBS-loaded or clodronate-loaded liposomes were injected intravenously via the tail vein every other day. For rGM-CSF treatment, PBS or 0.5μg rGM-CSF in 200μL PBS were injected *i.p.*.

Real-Time Quantitative PCR

Tissue total RNA was extracted in TRIZOL (Life Technologies). cDNA were synthesized with High Capacity cDNA Reverse Transcription Kit (Life Technologies) and amplified with Power SYBR Green Mastermix (Life Technologies) in MyiQ2 thermocycler (Bio-Rad) running iQ5 software (Bio-Rad). Primer sequences are detailed in Supplemental Data. Data were analyzed by the $2^{-\Delta\Delta Ct}$ method of Livak, et al., comparing threshold cycles first to *Hprt* expression, then ΔCt of target genes in controls.

Generation of Bone Marrow Chimera Mice

Thy1.2$^+$ WT or *Il17ra*$^{-/-}$ recipient mice were irradiated with two doses of 600 rad irradiation within 4 hours. 24 hours later they were reconstituted with 10×10^6 Thy1.1$^+$ WT or *Il17ra*$^{-/-}$ donor bone marrow cells *i.v.*. Animals were allowed to reconstitute for a minimum of 8 weeks prior to EAM induction.

Isolation of Primary Adult Mouse CM and CF

Hearts were dissected from 6-8 week old male mice pre-treated with heparin, aorta were cannulated, and hearts were perfused with calcium-free perfusion buffer, and digested by type II collagenase (Worthington). Cardiomyocytes were separated from resulting suspensions by their rapid spontaneous precipitation. Isolated cardiomyocytes were cultured in mouse laminin-coated plates or chamber slides and used for experiments after 24 hours. Cardiac fibroblasts and other cell

populations remain in supernatant, and were seeded on uncoated plates in DMEM with 4.5g/L glucose, 2mM L-glutamine, 1mM sodium pyruvate, 25mM HEPES, 100U/mL penicillin G, 100μg/mL streptomycin, 250ng/mL amphotericin B and 20% FBS. Non-adherent cells were washed off after 45 min. Infiltrating hematopoietic cells die off in high FBS media due to cytokine exhaustion, resulting in cardiac fibroblast culture.

Western Blot

Cells were collected in RIPA buffer (Sigma), and total protein was quantified by BCA assay (Thermo Scientific). 20μg of sample were separated with 10% SDS-PAGE with Mini-Protean precast gels (Bio-Rad). After transferred to PVDF membrane (Bio-Rad), IκBα was blotted with mAb clone L35A5 (Cell Signaling), and β-actin was blotted with mAb clone 13E5 (Cell Signaling). HRP-conjugated secondary antibodies (Jackson ImmunoResearch) and Amersham ECL Prime detection system (GE Healthcare) was used to visualize the bands.

Bone Marrow Derived Macrophage

Bone marrow cells from femur and tibia were isolated from adult WT BALB/cJ mice and cultured in DMEM with 4.5g/L glucose, 2mM L-Glutamine, 1mM sodium pyruvate, 25mM HEPES, 100U/mL penicillin G, 100μg/mL streptomycin, 55μM 2-mercaptoethanol and 10% FBS supplemented with 10ng/mL recombinant M-CSF (R&D Systems) for 8 days.

Immunofluorescence Microscopy

Cardiac fibroblasts and bone marrow derived macrophages were grown on chamber slides (Thermo Scientific). Cells were fixed with 4% paraformaldehyde and permeabilized with 0.1% Triton X-100 (Sigma). After blocking with donkey serum, cells were incubated with anti-α smooth muscle actin (Abcam ab5694) and anti-mouse CD11b (ebioscience clone M1/70) antibodies. FITC-conjugated donkey anti-rabbit and TexasRed-conjugated donkey anti-rat secondary antibodies with minimal cross reactivity (Jackson Immunoresearch) were then used. Cells were counterstained by DAPI. Images were acquired by Nikon Eclipse 90i microscope at 20X magnification and Volocity image analysis software (Perkin Elmer).

ELISA

Quantitative sandwich ELISA for cell culture supernatants were determined by colorimetric ELISA kits according to manufacturers' recommended protocols (R&D Systems).

Statistics

Normally distributed data were analyzed by two-tailed Student's t-test (up to two groups), one-way ANOVA followed by Tukey's post-test or two-way ANOVA (multiple factor analysis) followed by Tukey's post-test. EAM severity scores were analyzed by Kruskal-Wallis test followed by Dunn's procedure. Values of $p < 0.05$ were considered statistically significant.

Chapter IV Conclusion

IL-23 Drives the Pathogenicity of Autoreactive CD4+ T Cells

Early studies have established that mouse EAM is a CD4+ T cell – dependent disease. As demonstrated in Chapter II, deficiency of IL-23 resulted in complete resistance to EAM in *Il23a*$^{-/-}$ mice. Yet, with a BMDC transfer model, we showed that even transient IL-23 stimulation from a small number of WT antigen presenting cells was sufficient to generate pathogenic CD4+ T cells in otherwise resistant *Il23a*$^{-/-}$ recipients. Moreover, IL-23 was dispensable in EAM once a pathogenic autoreactive CD4+ T cell population was established, as pathogenic CD4+ T cells induced myocarditis in *IL23a*$^{-/-}$ recipients comparable to WT counterparts. To summarize these results, IL-23 stimulation is indispensable in generating the pathogenicity of CD4+ T cells in EAM; however, once pathogenicity is established in CD4+ T cells, IL-23 is no longer required for its maintenance.

The Pathogenicity of Th17 Polarized CD4+ T Cells Rests on Factors apart from IL-17A

Our results confirmed previous findings in other models that IL-23 deficiency directly impaired Th17 polarization in CD4+ T cells. However, it is still unclear what factors produced by Th17 – polarized CD4+ T cells are responsible for their pathogenicity. The CD4+ T cell transfer experiments illustrated that IL-23 was essential in maintaining IL-17A

production in CD4+ T cells, as the lack of IL-23 in recipients significantly impaired the ability of transferred CD4+ T cells to continue producing IL-17A. However, the reduction in IL-17A production had no significant effect on the pathogenicity of CD4+ T cells, as *Il23a*$^{-/-}$ recipients developed disease comparable to WT controls. In Chapter III of this dissertation, using *Il17ra*$^{-/-}$ mice, we further demonstrated that the pathogenicity of EAM does not rely on the IL-17A signal.

Resent studies using mouse EAE model indicated that GM-CSF production by Th17 polarized CD4+ T cells is crucial in their pathogenicity (El-Behi et al., 2011a). The results shown in Chapter II indicated that GM-CSF production determines the pathogenicity of CD4+ T cells in EAM model as well. First, in the active immunization model, IL-23 deficiency significantly reduced GM-CSF production in CD4+ T cells, concurrent with protection from EAM. Second, in the CD4+ T cell transfer experiments, although the lack of IL-23 in recipients reduced IL-17A production in CD4+ T cells, GM-CSF production remained the same, consistent with the disease outcome.

Plasticity of Autoreactive CD4+ T Cells

As suggested by CD4+ T cell transfer experiments, instead of being rigidly committed to a solitarily defined phenotype, Th17 polarized cells may convert from a IL-17A-producing phenotype towards a IFN γ -

producing phenotype, and their pathogenicity was not significantly affected during the conversion. Recent studies in the mouse EAE model discovered similar pattern (Annunziato and Romagnani, 2010). With the help of YFP reporter mice, the investigators reported that the majority of IFN γ -producing CD4+ T cells arise from IL-17A producers (Hirota et al., 2011).

Although IL-23 is not required once pathogenicity of autoreactive CD4+ T cells is established, IL-23 is indispensable in establishing pathogenicity. Therefore, it is possible that in order for CD4+ T cells to become a GM-CSF producer and gain pathogenicity, they first have to undergo a IL-23-dependent Th17 polarization program. Once GM-CSF production is established, IL-23 signaling is no longer required for pathogenicity.

Composition of Heart – Infiltrating Cells Determines the Prognosis of Myocarditis

According to the Dallas criteria, the definitive diagnosis of myocarditis depends upon a biopsy of the myocardium, in which the heart is evaluated based on the presence and density of inflammatory infiltration and cardiomyocyte death (Aretz et al., 1987). However, our study clearly shows that not only the quantity, but also the quality of these infiltrating cells is critical in predicting the development of DCMi. *Il17ra*$^{-/-}$ mice developed myocarditis and had overall inflammatory infiltration

comparable to WT, but were nonetheless protected from DCMi. This protection is associated with a different profile of infiltrating cells. *Il17ra*$^{-/-}$ mice had diminished infiltration of neutrophils and proinflammatory monocytes, and lower ratio of Ly6C^{hi} to Ly6C^{lo} MO/MΦ evident locally in the heart. These differences provide potentially useful biomarkers to help identify myocarditis patients with high risk of developing DCMi.

Monocytes and Macrophages Are Key Effector Cells during Cardiac Inflammation

MO/MΦs are not a homogeneous population (Hashimoto et al., 2011). In mouse, monocytes form two major subsets in blood, CCR2^{hi}CX3CR1^{lo}Ly6C^{hi} (resembling human CD14^{hi}CD16^{-} monocytes) and CCR2^{lo}CX3CR1^{hi}Ly6C^{lo} (resembling human CD14^{lo}CD16^{+} monocytes) (Geissmann et al., 2003; Shi and Pamer, 2011). In our study, the balance of these two MO/MΦs subsets in the heart determines the outcome of inflammation. We observed that heart-infiltrating Ly6C^{hi} MO/MΦs had a proinflammatory and profibrotic phenotype, whereas Ly6C^{lo} monocytes in heart produced high levels of MMPs and IGF-1, which have been described as protective against fibrosis (Ramachandran et al., 2012; Bessich et al., 2013). We used two methods to specifically manipulate the balance of Ly6C^{hi} and Ly6C^{lo} MO/MΦs, and demonstrated the role they play in DCMi: First, depletion of Ly6G^{-}CD11b^{+} MO/MΦs by clodronate-loaded liposomes also lowered the ratio of Ly6C^{hi} to Ly6C^{lo} MO/MΦs in

the heart. Second, PBS-loaded liposomes specifically lowered the ratio of Ly6C^{hi} to Ly6C^{lo} MO/MΦs without affecting the total number of MO/MΦs in the heart. Both manipulations protected mice from cardiac fibrosis and the development of severe DCMi, demonstrating that Ly6C^{hi} MO/MΦs aggravate the development of DCMi.

We further suggest that the M1/M2 paradigm does not perfectly overlap with Ly6C^{hi} and Ly6C^{low} subsets and does not accurately describe these two different populations in the heart during EAM. Traditionally, M1 represents a population that promotes inflammation whereas M2 is responsible for tissue repair and fibrosis (Gordon and Taylor, 2005). However, in our EAM model, Ly6C^{hi} MO/MΦs have a proinflammatory and profibrotic phenotype. They upregulate both classic M1 markers like *Tnf* and *Nos2*, as well as M2 markers like *Chi3l3*, while Ly6C^{lo} MO/MΦs produced molecules that are believed to help resolve fibrosis (Ramachandran et al., 2012; Bessich et al., 2013).

Cardiac Fibroblasts Mediate the Effects of IL-17A

Bone marrow chimera experiments revealed that IL-17A/IL-17RA signaling in non-hematopoietic cells is required for the development of DCMi. We observed that IL-17A neither induced apoptosis nor activated the NF-κB pathway in primary adult cardiomyocytes *in vitro*, indicating that cardiomyocytes are not likely to be the primary target of IL-17A in adults. In contrast, adult cardiac fibroblasts respond to IL-17A by

producing chemokines and cytokines known to facilitate myeloid cell recruitment and instruct their *in situ* differentiation towards an inflammatory phenotype. Cardiac fibroblasts isolated from *Il17ra*$^{-/-}$ mice during EAM expressed significantly lower levels of proinflammatory cytokines and chemokines. Importantly, although it was reported that endothelial cells react to IL-17A stimulation, they produced minimal amount of cytokines and chemokines compared with cardiac fibroblasts. Thus, our study highlights the central, decisive role "non-immune" cells like fibroblasts can play in immunologic processes. Cardiac fibroblasts served as a critical mediator between adaptive and innate immune cells and actively participated in the augmentation of immune response.

In response to IL-17A stimulation from adaptive T cells, cardiac fibroblasts produce granulocytic and monocytic chemokines to recruit innate effector cells and aggravate the immune response. Cardiac fibroblasts also secrete cytokines, in this case GM-CSF, to direct these recruited MO/MΦ effectors to a more proinflammatory phenotype, which thereby intensifing inflammation.

GM-CSF from Cardiac Fibroblasts Drives Macrophages into Proinflammatory Phenotype

Our studies also revealed that the main mediator of local communications between cardiac fibroblasts and MO/MΦs was cardiac fibroblast-derived GM-CSF. GM-CSF is known to elicit the expansion and

differentiation of progenitors of the myeloid lineages; GM-CSF also supports the survival and activation of effector functions of myeloid cells (Papatriantafyllou, 2011). In ischemic heart disease, although associated with poor prognosis (Maekawa et al., 2004), GM-CSF has been studied largely for its role outside of its immunologic functions. These mechanisms mostly involve angiogenesis or the mobilization of HSC-like cells (Zbinden et al., 2005). Our data point to GM-CSF acting as a key mediator of IL-17A-driven autoimmunity in DCMi: IL-17A signaling induces GM-CSF production from cardiac fibroblasts. GM-CSF then drives differentiation of heart-infiltrating MO/MΦs toward a proinflammatory phenotype, which in turn promotes DCMi (Figure 39).

The Sign of Four

In conclusion, the work presented in this dissertation investigated the interactions between CD4+ T lymphocyte and three cytokines, IL-23, IL-17A and GM-CSF, and demonstrates that the IL-23 – CD4+ T cell – IL-17A – GM-CSF axis is critical in the pathogenesis of myocarditis and DCMi. IL-23 drives the pathogenicity of CD4+ T cells and maintains their IL-17A production. IL-17A induces chemokine production by cardiac fibroblasts, resulting in an infiltrate rich in neutrophils and Ly6C^{hi} MO/MΦs in the heart. Furthermore, IL-17A directs monocytic infiltrates into an even more inflammatory phenotype by inducing GM-CSF production from cardiac fibroblasts. This novel pathway provides new

potential markers to identify myocarditis patients with a high risk of developing DCMI, and further suggests new targets for the prevention of DCMi.

Figures

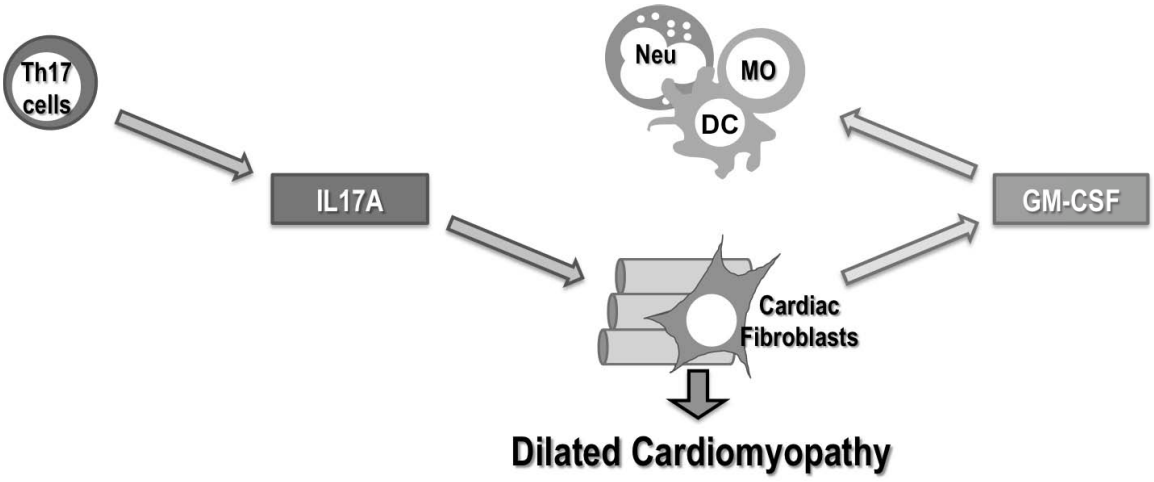

Figure 39 Cardiac Fibroblasts Mediate IL-17A-Driven Inflammatory Dilated Cardiomyopathy

References

Abdel-Aty, H., P. Boyé, A. Zagrosek, R. Wassmuth, A. Kumar, D. Messroghli, P. Bock, R. Dietz, M.G. Friedrich, and J. Schulz-Menger. 2005. Diagnostic performance of cardiovascular magnetic resonance in patients with suspected acute myocarditis: comparison of different approaches. *J. Am. Coll. Cardiol.* 45:1815–22. doi:10.1016/j.jacc.2004.11.069.

Abraham, C., and J.H. Cho. 2009. IL-23 and autoimmunity: new insights into the pathogenesis of inflammatory bowel disease. *Annu. Rev. Med.* 60:97–110. doi:10.1146/annurev.med.60.051407.123757.

Afanasyeva, M., D. Georgakopoulos, D. Fairweather, P. Caturegli, D. a Kass, and N.R. Rose. 2004. Novel model of constrictive pericarditis associated with autoimmune heart disease in interferon-gamma-knockout mice. *Circulation.* 110:2910–7. doi:10.1161/01.CIR.0000147538.92263.3A.

Afanasyeva, M., Y. Wang, Z. Kaya, S. Park, M.J. Zilliox, B.H. Schofield, S.L. Hill, and N.R. Rose. 2001a. Experimental autoimmune myocarditis in A/J mice is an interleukin-4-dependent disease with a Th2 phenotype. *Am. J. Pathol.* 159:193–203. doi:10.1016/S0002-9440(10)61685-9.

Afanasyeva, M., Y. Wang, Z. Kaya, E.A. Stafford, K.M. Dohmen, A.A. Sadighi Akha, and N.R. Rose. 2001b. Interleukin-12 receptor/STAT4 signaling is required for the development of autoimmune myocarditis in mice by an interferon-gamma-independent pathway. *Circulation.* 104:3145–51.

Annunziato, F., and S. Romagnani. 2010. The transient nature of the Th17 phenotype. *Eur. J. Immunol.* 40:3312–6. doi:10.1002/eji.201041145.

Aretz, H.T., M.E. Billingham, W.D. Edwards, S.M. Factor, J.T. Fallon, J.J. Fenoglio, E.G. Olsen, and F.J. Schoen. 1987. Myocarditis. A histopathologic definition and classification. *Am. J. Cardiovasc. Pathol.* 1:3–14.

Auffray, C., M.H. Sieweke, and F. Geissmann. 2009. Blood monocytes: development, heterogeneity, and relationship with dendritic cells. *Annu. Rev. Immunol.* 27:669–92. doi:10.1146/annurev.immunol.021908.132557.

Baldeviano, G.C., J.G. Barin, M.V. Talor, S. Srinivasan, D. Bedja, D. Zheng, K. Gabrielson, Y. Iwakura, N.R. Rose, and D. Cihakova. 2010. Interleukin-17A is dispensable for myocarditis but essential for the progression to dilated cardiomyopathy. *Circ. Res.* 106:1646. doi:10.1161/CIRCRESAHA.109.213157.

Barin, J.G., N.R. Rose, and D. Cihákova. 2012. Macrophage diversity in cardiac inflammation: a review. *Immunobiology*. 217:468–75. doi:10.1016/j.imbio.2011.06.009.

Becher, B., B.G. Durell, and R.J. Noelle. 2003. IL-23 produced by CNS-resident cells controls T cell encephalitogenicity during the effector phase of experimental autoimmune encephalomyelitis. *J. Clin. Invest.* 112:1186–91. doi:10.1172/JCI19079.

Bessich, J.L., A.B. Nymon, L.A. Moulton, D. Dorman, and A. Ashare. 2013. Low levels of insulin-like growth factor-1 contribute to alveolar macrophage dysfunction in cystic fibrosis. *J. Immunol.* 191:378–85. doi:10.4049/jimmunol.1300221.

Blyszczuk, P., S. Behnke, T.F. Lüscher, U. Eriksson, and G. Kania. 2013. GM-CSF promotes inflammatory dendritic cell formation but does not contribute to disease progression in experimental autoimmune myocarditis. *Biochim. Biophys. Acta.* 1833:934–44. doi:10.1016/j.bbamcr.2012.10.008.

Bocchi, E.A., A. Arias, H. Verdejo, M. Diez, E. Gómez, and P. Castro. 2013. The reality of heart failure in Latin America. *J. Am. Coll. Cardiol.* 62:949–58. doi:10.1016/j.jacc.2013.06.013.

Bonney, K.M., and D.M. Engman. 2008. Chagas heart disease pathogenesis: one mechanism or many? *Curr. Mol. Med.* 8:510–8.

Breinholt, J.P., M. Moulik, W.J. Dreyer, S.W. Denfield, J.J. Kim, J.L. Jefferies, J.W. Rossano, C.M. Gates, S.K. Clunie, K.R. Bowles, D.L. Kearney, N.E. Bowles, and J.A. Towbin. 2010. Viral epidemiologic shift in inflammatory heart disease: the increasing involvement of parvovirus B19 in the myocardium of pediatric cardiac transplant patients. *J. Heart Lung Transplant.* 29:739–46. doi:10.1016/j.healun.2010.03.003.

Caforio, A.L.P., F. Tona, S. Bottaro, A. Vinci, G. Dequal, L. Daliento, G. Thiene, and S. Iliceto. 2008. Clinical implications of anti-heart autoantibodies in myocarditis and dilated cardiomyopathy. *Autoimmunity*. 41:35–45. doi:10.1080/08916930701619235.

Cho, J.S., E.M. Pietras, N.C. Garcia, R.I. Ramos, D.M. Farzam, H.R. Monroe, J.E. Magorien, A. Blauvelt, J.K. Kolls, A.L. Cheung, G. Cheng, R.L. Modlin, and L.S. Miller. 2010. IL-17 is essential for host defense against cutaneous Staphylococcus aureus infection in mice. *J. Clin. Invest.* 120:1762–73. doi:10.1172/JCI40891.

Chung, L., G.J. Berry, and E.F. Chakravarty. 2005. Giant cell myocarditis: a rare cardiovascular manifestation in a patient with systemic lupus erythematosus. *Lupus*. 14:166–9.

Cihakova, D., J.G. Barin, M. Afanasyeva, M. Kimura, D. Fairweather, M. Berg, M. V Talor, G.C. Baldeviano, S. Frisancho, K. Gabrielson, D. Bedja, and N.R. Rose. 2008. Interleukin-13 protects against experimental autoimmune myocarditis by regulating macrophage differentiation. *Am. J. Pathol.* 172:1195–208. doi:10.2353/ajpath.2008.070207.

Cihakova, D., and N.R. Rose. 2008. Pathogenesis of myocarditis and dilated cardiomyopathy. 99. Elsevier Inc.

Cihákova, D., R.B. Sharma, D. Fairweather, M. Afanasyeva, and N.R. Rose. 2004. Animal models for autoimmune myocarditis and autoimmune thyroiditis. *Methods Mol. Med.* 102:175–194.

Cooper, L.T., K.L. Baughman, A.M. Feldman, A. Frustaci, M. Jessup, U. Kuhl, G.N. Levine, J. Narula, R.C. Starling, J. Towbin, and R. Virmani. 2007. The role of endomyocardial biopsy in the management of cardiovascular disease: a scientific statement from the American Heart Association, the American College of Cardiology, and the European Society of Cardiology Endorsed by the Heart Failure Society of . *Eur. Heart J.* 28:3076–93. doi:10.1093/eurheartj/ehm456.

Cooper, L.T., J.M. Hare, H.D. Tazelaar, W.D. Edwards, R.C. Starling, M.C. Deng, S. Menon, G.M. Mullen, B. Jaski, K.R. Bailey, M.W. Cunningham, and G.W. Dec. 2008. Usefulness of immunosuppression for giant cell myocarditis. *Am. J. Cardiol.* 102:1535–9. doi:10.1016/j.amjcard.2008.07.041.

Cooper, Leslie T., J. 2009. Myocarditis. *N. Engl. J. Med.* 360:1526 – 1538.

Cunha-Neto, E., A.M. Bilate, K. V Hyland, S.G. Fonseca, J. Kalil, and D.M. Engman. 2006. Induction of cardiac autoimmunity in Chagas heart disease: a case for molecular mimicry. *Autoimmunity*. 39:41–54. doi:10.1080/08916930500485002.

D'Ambrosio, A., G. Patti, A. Manzoli, G. Sinagra, A. Di Lenarda, F. Silvestri, and G. Di Sciascio. 2001. The fate of acute myocarditis between spontaneous improvement and evolution to dilated cardiomyopathy: a review. *Heart*. 85:499–504.

Dimas, V.V., S.W. Denfield, R.A. Friedman, B.C. Cannon, J.J. Kim, E.O. 'brian Smith, S.K. Clunie, J.F. Price, J.A. Towbin, W.J. Dreyer, and N.J. Kertesz. 2009. Frequency of cardiac death in children with idiopathic dilated cardiomyopathy. *Am. J. Cardiol.* 104:1574–7. doi:10.1016/j.amjcard.2009.07.034.

Ding, L., H. Hanawa, Y. Ota, G. Hasegawa, K. Hao, F. Asami, R. Watanabe, T. Yoshida, K. Toba, K. Yoshida, M. Ogura, M. Kodama, and Y. Aizawa. 2010. Lipocalin-

2/neutrophil gelatinase-B associated lipocalin is strongly induced in hearts of rats with autoimmune myocarditis and in human myocarditis. *Circ. J.* 74:523–30.

El-Behi, M., B. Ciric, H. Dai, Y. Yan, M. Cullimore, F. Safavi, G.-X. Zhang, B.N. Dittel, and A. Rostami. 2011a. The encephalitogenicity of T(H)17 cells is dependent on IL-1- and IL-23-induced production of the cytokine GM-CSF. *Nat. Immunol.* 12:568–75. doi:10.1038/ni.2031.

El-Behi, M., B. Ciric, H. Dai, Y. Yan, M. Cullimore, F. Safavi, G.-X. Zhang, B.N. Dittel, and A. Rostami. 2011b. The encephalitogenicity of T(H)17 cells is dependent on IL-1- and IL-23-induced production of the cytokine GM-CSF. *Nat. Immunol.* 12:568–75. doi:10.1038/ni.2031.

Epelman, S., K.J. Lavine, A.E. Beaudin, D.K. Sojka, J.A. Carrero, B. Calderon, T. Brija, E.L. Gautier, S. Ivanov, A.T. Satpathy, J.D. Schilling, R. Schwendener, I. Sergin, B. Razani, E.C. Forsberg, W.M. Yokoyama, E.R. Unanue, M. Colonna, G.J. Randolph, and D.L. Mann. 2014. Embryonic and Adult-Derived Resident Cardiac Macrophages Are Maintained through Distinct Mechanisms at Steady State and during Inflammation. *Immunity*. 40:91–104. doi:10.1016/j.immuni.2013.11.019.

Frangogiannis, N.G. 2012. Matricellular proteins in cardiac adaptation and disease. *Physiol. Rev.* 92:635–88. doi:10.1152/physrev.00008.2011.

Frustaci, A., L. Cuoco, C. Chimenti, M. Pieroni, G. Fioravanti, N. Gentiloni, A. Maseri, and G. Gasbarrini. 2002. Celiac disease associated with autoimmune myocarditis. *Circulation*. 105:2611–8.

Gaffen, S.L. 2009. Structure and signalling in the IL-17 receptor family. *Nat. Rev. Immunol.* 9:556–567. doi:10.1038/nri2586.

Gaffen, S.L. 2011. Recent advances in the IL-17 cytokine family. *Curr. Opin. Immunol.* 3:1–7. doi:10.1016/j.coi.2011.07.006.

Geissmann, F., S. Jung, and D.R. Littman. 2003. Blood monocytes consist of two principal subsets with distinct migratory properties. *Immunity*. 19:71–82.

Ginhoux, F., M. Greter, M. Leboeuf, S. Nandi, P. See, S. Gokhan, M.F. Mehler, S.J. Conway, L.G. Ng, E.R. Stanley, I.M. Samokhvalov, and M. Merad. 2010. Fate mapping analysis reveals that adult microglia derive from primitive macrophages. *Science*. 330:841–5. doi:10.1126/science.1194637.

Gordon, S., and P.R. Taylor. 2005. Monocyte and macrophage heterogeneity. *Nat. Rev. Immunol.* 5:953–64. doi:10.1038/nri1733.

Guilliams, M., I. De Kleer, S. Henri, S. Post, L. Vanhoutte, S. De Prijck, K. Deswarte, B. Malissen, H. Hammad, and B.N. Lambrecht. 2013. Alveolar macrophages develop from fetal monocytes that differentiate into long-lived cells in the first week of life via GM-CSF. *J. Exp. Med.* 210:1977–92. doi:10.1084/jem.20131199.

Hashimoto, D., A. Chow, C. Noizat, P. Teo, M.B. Beasley, M. Leboeuf, C.D. Becker, P. See, J. Price, D. Lucas, M. Greter, A. Mortha, S.W. Boyer, E.C. Forsberg, M. Tanaka, N. van Rooijen, A. García-Sastre, E.R. Stanley, F. Ginhoux, P.S. Frenette, and M. Merad. 2013. Tissue-Resident Macrophages Self-Maintain Locally throughout Adult Life with Minimal Contribution from Circulating Monocytes. *Immunity*. 38:792–804. doi:10.1016/j.immuni.2013.04.004.

Hashimoto, D., J. Miller, and M. Merad. 2011. Dendritic Cell and Macrophage Heterogeneity In Vivo. *Immunity*. 35:323–335. doi:10.1016/j.immuni.2011.09.007.

Herskowitz, A., S. Campbell, J. Deckers, E.K. Kasper, J. Boehmer, D. Hadian, D.A. Neumann, and K.L. Baughman. 1993. Demographic features and prevalence of idiopathic myocarditis in patients undergoing endomyocardial biopsy. *Am. J. Cardiol.* 71:982–6.

Hiroi, T., T. Wajima, T. Negoro, M. Ishii, Y. Nakano, Y. Kiuchi, Y. Mori, and S. Shimizu. 2013. Neutrophil TRPM2 channels are implicated in the exacerbation of myocardial ischaemia/reperfusion injury. *Cardiovasc. Res.* 97:271–81. doi:10.1093/cvr/cvs332.

Hirota, K., J.H. Duarte, M. Veldhoen, E. Hornsby, Y. Li, D.J. Cua, H. Ahlfors, C. Wilhelm, M. Tolaini, U. Menzel, A. Garefalaki, A.J. Potocnik, and B. Stockinger. 2011. Fate mapping of IL-17-producing T cells in inflammatory responses. *Nat. Immunol.* 12:255–263. doi:10.1038/ni.1993.

Ho, A.W., F. Shen, H.R. Conti, N. Patel, E.E. Childs, A.C. Peterson, N. Hernández-Santos, J.K. Kolls, L.P. Kane, W. Ouyang, and S.L. Gaffen. 2010. IL-17RC is required for immune signaling via an extended SEF/IL-17R signaling domain in the cytoplasmic tail. *J. Immunol.* 185:1063–70. doi:10.4049/jimmunol.0903739.

Izcue, A., S. Hue, S. Buonocore, C. V Arancibia-Cárcamo, P.P. Ahern, Y. Iwakura, K.J. Maloy, and F. Powrie. 2008. Interleukin-23 restrains regulatory T cell activity to drive T cell-dependent colitis. *Immunity*. 28:559–70. doi:10.1016/j.immuni.2008.02.019.

Kallwellis-Opara, A., A. Dörner, W.-C. Poller, M. Noutsias, U. Kühl, H.-P. Schultheiss, and M. Pauschinger. 2007. Autoimmunological features in inflammatory cardiomyopathy. *Clin. Res. Cardiol.* 96:469–80. doi:10.1007/s00392-007-0524-x.

Kandolin, R., J. Lehtonen, K. Salmenkivi, A. Räisänen-Sokolowski, J. Lommi, and M. Kupari. 2013. Diagnosis, treatment, and outcome of giant-cell myocarditis in the era of combined immunosuppression. *Circ. Heart Fail.* 6:15–22. doi:10.1161/CIRCHEARTFAILURE.112.969261.

Kindermann, I., C. Barth, F. Mahfoud, C. Ukena, M. Lenski, A. Yilmaz, K. Klingel, R. Kandolf, U. Sechtem, L.T. Cooper, and M. Böhm. 2012. Update on Myocarditis. *J. Am. Coll. Cardiol.* 59:779–792. doi:10.1016/j.jacc.2011.09.074.

Kinnebrew, M. a, C.G. Buffie, G.E. Diehl, L. a Zenewicz, I. Leiner, T.M. Hohl, R. a Flavell, D.R. Littman, and E.G. Pamer. 2012. Interleukin 23 Production by Intestinal

CD103(+)CD11b(+) Dendritic Cells in Response to Bacterial Flagellin Enhances Mucosal Innate Immune Defense. *Immunity*. 36:276–87. doi:10.1016/j.immuni.2011.12.011.

Kono, H., H. Fujii, M. Ogiku, N. Hosomura, H. Amemiya, M. Tsuchiya, and M. Hara. 2011. Role of IL-17A in neutrophil recruitment and hepatic injury after warm ischemia-reperfusion mice. *J. Immunol.* 187:4818–25. doi:10.4049/jimmunol.1100490.

Korn, T., E. Bettelli, M. Oukka, and V.K. Kuchroo. 2009. IL-17 and Th17 Cells. *Annu. Rev. Immunol.* 27:485–517. doi:10.1146/annurev.immunol.021908.132710.

Kurschus, F.C., A.L. Croxford, A. P Heinen, S. Wörtge, D. Ielo, and A. Waisman. 2010. Genetic proof for the transient nature of the Th17 phenotype. *Eur. J. Immunol.* 40:3336–46. doi:10.1002/eji.201040755.

Lan, R.Y.Z., T.L. Salunga, K. Tsuneyama, Z.-X. Lian, G.-X. Yang, W. Hsu, Y. Moritoki, A.A. Ansari, C. Kemper, J. Price, J.P. Atkinson, R.L. Coppel, and M.E. Gershwin. 2009. Hepatic IL-17 responses in human and murine primary biliary cirrhosis. *J. Autoimmun.* 32:43–51. doi:10.1016/j.jaut.2008.11.001.

Leuschner, F., P.J. Rauch, T. Ueno, R. Gorbatov, B. Marinelli, W.W. Lee, P. Dutta, Y. Wei, C. Robbins, Y. Iwamoto, B. Sena, A. Chudnovskiy, P. Panizzi, E. Keliher, J.M. Higgins, P. Libby, M. a Moskowitz, M.J. Pittet, F.K. Swirski, R. Weissleder, and M. Nahrendorf. 2012. Rapid monocyte kinetics in acute myocardial infarction are sustained by extramedullary monocytopoiesis. *J. Exp. Med.* doi:10.1084/jem.20111009.

Liao, Y.-H., N. Xia, S.-F. Zhou, T.-T. Tang, X.-X. Yan, B.-J. Lv, S.-F. Nie, J. Wang, Y. Iwakura, H. Xiao, J. Yuan, H. Jevallee, F. Wei, G.-P. Shi, and X. Cheng. 2012. Interleukin-17A Contributes to Myocardial Ischemia/Reperfusion Injury by Regulating Cardiomyocyte Apoptosis and Neutrophil Infiltration. *J. Am. Coll. Cardiol.* 59:420–9. doi:10.1016/j.jacc.2011.10.863.

Liu, Y., H. Zhu, Z. Su, C. Sun, J. Yin, H. Yuan, S. Sandoghchian, Z. Jiao, S. Wang, and H. Xu. 2012. IL-17 contributes to cardiac fibrosis following experimental autoimmune

myocarditis by a PKCβ/Erk1/2/NF-κB-dependent signaling pathway. *Int. Immunol.* 24:605–12. doi:10.1093/intimm/dxs056.

Maddur, M.S., P. Miossec, S. V Kaveri, and J. Bayry. 2012. Th17 Cells: Biology, Pathogenesis of Autoimmune and Inflammatory Diseases, and Therapeutic Strategies. *Am. J. Pathol.* 181:8–18. doi:10.1016/j.ajpath.2012.03.044.

Maekawa, Y., T. Anzai, T. Yoshikawa, Y. Sugano, K. Mahara, T. Kohno, T. Takahashi, and S. Ogawa. 2004. Effect of granulocyte-macrophage colony-stimulating factor inducer on left ventricular remodeling after acute myocardial infarction. *J. Am. Coll. Cardiol.* 44:1510–20. doi:10.1016/j.jacc.2004.05.083.

Maruyama, T., J. Li, J. Vaque, and J. Konkel. 2010. Control of the differentiation of regulatory T cells and TH17 cells by the DNA-binding inhibitor Id3. *Nature*. 12:86–95. doi:10.1038/ni.1965.

McAleer, J.P., and J.K. Kolls. 2011. Mechanisms controlling Th17 cytokine expression and host defense. *J. Leukoc. Biol.* 90:263–270. doi:10.1189/jlb.0211099.

Mukasa, R., A. Balasubramani, Y.K. Lee, S.K. Whitley, B.T. Weaver, Y. Shibata, G.E. Crawford, R.D. Hatton, and C.T. Weaver. 2010. Epigenetic Instability of Cytokine and Transcription Factor Gene Loci Underlies Plasticity of the T Helper 17 Cell Lineage. *Immunity*. 32:616–627. doi:10.1016/j.immuni.2010.04.016.

Nahrendorf, M. 2012. Macrophages in the infarct: Fiery friends or friendly fire? *J. Mol. Cell. Cardiol.* 9–10. doi:10.1016/j.yjmcc.2012.09.001.

Ng, W.-F., A. von Delwig, A.J. Carmichael, P.D. Arkwright, M. Abinun, A.J. Cant, S. Jolles, and D. Lilic. 2010. Impaired T(H)17 responses in patients with chronic mucocutaneous candidiasis with and without autoimmune polyendocrinopathy-candidiasis-ectodermal dystrophy. *J. Allergy Clin. Immunol.* 126:1006–15, 1015.e1–4. doi:10.1016/j.jaci.2010.08.027.

Nishii, M., T. Inomata, H. Takehana, I. Takeuchi, H. Nakano, T. Koitabashi, J. Nakahata, N. Aoyama, and T. Izumi. 2004. Serum levels of interleukin-10 on admission as a prognostic predictor of human fulminant myocarditis. *J. Am. Coll. Cardiol.* 44:1292–7. doi:10.1016/j.jacc.2004.01.055.

Nunes, M.C.P., W. Dones, C.A. Morillo, J.J. Encina, and A.L. Ribeiro. 2013. Chagas disease: an overview of clinical and epidemiological aspects. *J. Am. Coll. Cardiol.* 62:767–76. doi:10.1016/j.jacc.2013.05.046.

Papatriantafyllou, M. 2011. Cytokines: GM-CSF in focus. *Nat. Rev. Immunol.* 11:370–1. doi:10.1038/nri2996.

Pietra, B.A., P.F. Kantor, H.L. Bartlett, C. Chin, C.E. Canter, R.L. Larsen, R.E. Edens, S.D. Colan, J.A. Towbin, S.E. Lipshultz, J.K. Kirklin, D.C. Naftel, and D.T. Hsu. 2012. Early predictors of survival to and after heart transplantation in children with dilated cardiomyopathy. *Circulation*. 126:1079–86. doi:10.1161/CIRCULATIONAHA.110.011999.

Poppensieker, K., D.-M. Otte, B. Schürmann, A. Limmer, P. Dresing, E. Drews, B. Schumak, L. Klotz, J. Raasch, A. Mildner, A. Waisman, S. Scheu, P. Knolle, I. Förster, M. Prinz, W. Maier, A. Zimmer, and J. Alferink. 2012. CC chemokine receptor 4 is required for experimental autoimmune encephalomyelitis by regulating GM-CSF and IL-23 production in dendritic cells. *Proc. Natl. Acad. Sci. U. S. A.* 109:3897–902. doi:10.1073/pnas.1114153109.

Puel, A., S. Cypowyj, J. Bustamante, J.F. Wright, L. Liu, H.K. Lim, M. Migaud, L. Israel, M. Chrabieh, M. Audry, M. Gumbleton, A. Toulon, C. Bodemer, J. El-Baghdadi, M. Whitters, T. Paradis, J. Brooks, M. Collins, N.M. Wolfman, S. Al-Muhsen, M. Galicchio, L. Abel, C. Picard, and J.-L. Casanova. 2011. Chronic mucocutaneous candidiasis in humans with inborn errors of interleukin-17 immunity. *Science*. 332:65–8. doi:10.1126/science.1200439.

RABIN, E.R., S.A. HASSAN, A.B. JENSON, and J.L. MELNICK. 1964. COXSACKIE VIRUS B3 MYOCARDITIS IN MICE. AN ELECTRON MICROSCOPIC, IMMUNOFLUORESCENT AND VIRUS-ASSAY STUDY. *Am. J. Pathol.* 44:775–97.

Ramachandran, P., A. Pellicoro, M. a Vernon, L. Boulter, R.L. Aucott, A. Ali, S.N. Hartland, V.K. Snowdon, A. Cappon, T.T. Gordon-Walker, M.J. Williams, D.R. Dunbar, J.R. Manning, N. van Rooijen, J. a Fallowfield, S.J. Forbes, and J.P. Iredale. 2012. Differential Ly-6C expression identifies the recruited macrophage phenotype, which orchestrates the regression of murine liver fibrosis. *Proc. Natl. Acad. Sci. U. S. A.* 109:E3186–95. doi:10.1073/pnas.1119964109.

Rangachari, M., N. Mauermann, R.R. Marty, S. Dirnhofer, M.O. Kurrer, V. Komnenovic, J.M. Penninger, and U. Eriksson. 2006. T-bet negatively regulates autoimmune myocarditis by suppressing local production of interleukin 17. *J. Exp. Med.* 203:2009–19. doi:10.1084/jem.20052222.

Ruddy, M.J., G.C. Wong, X.K. Liu, H. Yamamoto, S. Kasayama, K.L. Kirkwood, and S.L. Gaffen. 2004. Functional cooperation between interleukin-17 and tumor necrosis factor-alpha is mediated by CCAAT/enhancer-binding protein family members. *J. Biol. Chem.* 279:2559–67. doi:10.1074/jbc.M308809200.

Sagar, S., P.P. Liu, and L.T. Cooper. 2011. Myocarditis. *Lancet.* 6736. doi:10.1016/S0140-6736(11)60648-X.

Schultheiss, H.-P., U. Kühl, and L.T. Cooper. 2011. The management of myocarditis. *Eur. Heart J.* 32:2616–25. doi:10.1093/eurheartj/ehr165.

Sheppard, R., M. Bedi, T. Kubota, M.J. Semigran, W. Dec, R. Holubkov, A.M. Feldman, W.D. Rosenblum, C.F. McTiernan, and D.M. McNamara. 2005. Myocardial expression of fas and recovery of left ventricular function in patients with recent-onset cardiomyopathy. *J. Am. Coll. Cardiol.* 46:1036–42. doi:10.1016/j.jacc.2005.05.067.

Shi, C., and E.G. Pamer. 2011. Monocyte recruitment during infection and inflammation. *Nat. Rev. Immunol.* 11:762–774. doi:10.1038/nri3070.

Sica, A., and A. Mantovani. 2012. Macrophage plasticity and polarization : in vivo veritas. *J. Clin. Invest.* 122:787. doi:10.1172/JCI59643DS1.

Smith, S.C., and P.M. Allen. 1991. Myosin-induced acute myocarditis is a T cell-mediated disease. *J. Immunol.* 147:2141–7.

Smith, S.C., and P.M. Allen. 1993. The role of T cells in myosin-induced autoimmune myocarditis. *Clin. Immunol. Immunopathol.* 68:100–106.

Swirski, F.K.F.K., M. Nahrendorf, M. Etzrodt, M. Wildgruber, V. Cortez-Retamozo, P. Panizzi, J.L.J.-L. Figueiredo, R.H.R.H. Kohler, A. Chudnovskiy, P. Waterman, E. Aikawa, T.R. Mempel, P. Libby, R. Weissleder, M.J. Pittet, and others. 2009. Identification of splenic reservoir monocytes and their deployment to inflammatory sites. *Science (80-.).* 325:612. doi:10.1126/science.1175202.

Vinten-Johansen, J. 2004. Involvement of neutrophils in the pathogenesis of lethal myocardial reperfusion injury. *Cardiovasc. Res.* 61:481–97. doi:10.1016/j.cardiores.2003.10.011.

Wilson, M.S., S.K. Madala, T.R. Ramalingam, B.R. Gochuico, I.O. Rosas, A.W. Cheever, and T. a Wynn. 2010. Bleomycin and IL-1beta-mediated pulmonary fibrosis is IL-17A dependent. *J. Exp. Med.* 207:535–52. doi:10.1084/jem.20092121.

Yang, X.O., B.P. Pappu, R. Nurieva, A. Akimzhanov, H.S. Kang, Y. Chung, L. Ma, B. Shah, A.D. Panopoulos, K.S. Schluns, S.S. Watowich, Q. Tian, A.M. Jetten, and C. Dong. 2008. T helper 17 lineage differentiation is programmed by orphan nuclear receptors ROR alpha and ROR gamma. *Immunity*. 28:29–39.

Yona, S., K.-W. Kim, Y. Wolf, A. Mildner, D. Varol, M. Breker, D. Strauss-Ayali, S. Viukov, M. Guilliams, A. Misharin, D. a Hume, H. Perlman, B. Malissen, E. Zelzer, and S. Jung. 2013. Fate Mapping Reveals Origins and Dynamics of Monocytes and Tissue

Macrophages under Homeostasis. *Immunity*. 38:79–91. doi:10.1016/j.immuni.2012.12.001.

Yuan, J., A.-L. Cao, M. Yu, Q.-W. Lin, X. Yu, J.-H. Zhang, M. Wang, H.-P. Guo, and Y.-H. Liao. 2010. Th17 cells facilitate the humoral immune response in patients with acute viral myocarditis. *J. Clin. Immunol.* 30:226–34. doi:10.1007/s10875-009-9355-z.

Zbinden, S., R. Zbinden, P. Meier, S. Windecker, and C. Seiler. 2005. Safety and efficacy of subcutaneous-only granulocyte-macrophage colony-stimulating factor for collateral growth promotion in patients with coronary artery disease. *J. Am. Coll. Cardiol.* 46:1636–42. doi:10.1016/j.jacc.2005.01.068.

Zúñiga, L. a, R. Jain, C. Haines, and D.J. Cua. 2013. Th17 cell development: from the cradle to the grave. *Immunol. Rev.* 252:78–88. doi:10.1111/imr.12036.

Curriculum Vitae

Lei Wu
1101 N Calvert St. Apt 1707
Baltimore, MD 21202
(443) 286 - 3007
lwu26@jhmi.edu

Date and Place of Birth

Jan 27th, 1987, Beijing, China

Education

Ph.D., Molecular Microbiology and Immunology

Johns Hopkins University, April 2014

Dissertation: Pathogenesis of Myocarditis and Inflammatory Dilated Cardiomyopathy: the Sign of Four

Adviser: Noel R. Rose, M.D., Ph.D.

B.S., Biology

Peking University, July 2009

Dissertation: Regulation of Retinoic Acid - Inducible Gene 1 (RIG-I)

Adviser: Jun Gu, Ph.D.

B.S., Psychology

Peking University, July 2009

Working Experience

Research Intern, HBV-induced Hepatocellular Carcinoma

Novartis Institutes for Biomedical Research, June ~ August 2008, Shanghai, China

Awards and Honors

Association of Medical Laboratory Immunologists (AMLI) Doctorate Award, August 2013, Savannah, Georgia

O'Leary – Wilson Fellowship in Autoimmune Disease Research, Johns Hopkins Center for Autoimmune Disease Research, January 2013, Baltimore, Maryland

The Katharine E. Welsh Fellowship in Immunology & Infectious Disease, Johns Hopkins University School of Public Health, May 2011, Baltimore, Maryland

The Carlton and Estelle Herman Award, Johns Hopkins University School of Public Health, May 2010, Baltimore, Maryland

YKM Undergraduate Research Fellowship, Peking University, May 2008 ~ May 2009, Beijing, China

WUSI Scholarship, Peking University, June 2007, Beijing, China

Publications

Lei Wu, SuFey Ong, Monica V. Talor, Jobert G. Barin, G. Christian Baldeviano, David A. Kass, Djahida Bedja, Hao Zhang, Asfandyar Sheikh, Joseph B. Margolick, Yoichiro Iwakura, Noel R. Rose, and Daniela

Čiháková (Revised and Resubmitted) *Cardiac Fibroblasts Mediate IL-17A-Driven Inflammatory Dilated Cardiomyopathy.* Journal of Experimental Medicine

Barin JG, Baldeviano GC, Talor MV, **Wu L**, Ong S, Fairweather D, Bedja D, Stickel NR, Fontes JA, Cardamone AB, Zheng D, Gabrielson KL, Rose NR, Cihákova D. (2013) *Fatal eosinophilic myocarditis develops in the absence of IFN-γ and IL-17A.* Journal of Immunology

Barin JG, Baldeviano GC, Talor MV, **Wu L**, Ong S, Quader F, Chen P, Zheng D, Caturegli P, Rose NR, Cihákova D. (2012) *Macrophages participate in IL-17-mediated inflammation.* European Journal of Immunology

Poster Presentations

Association of Medical Laboratory Immunologists (AMLI) Annual Meeting, August 2013, Savannah, Georgia

Gordon Research Conferences: Phagocytes, June 2013, Waterville Valley, New Hampshire

Cold Spring Harbor Symposium: Immunity & Tolerance, May 2013, Cold Spring Harbor, New York

Johns Hopkins Pathology Young Investigator Day, April 2013, Baltimore, Maryland